nature immunology

TANK is a negative regulator of Toll-like receptor signaling and is critical for the prevention of autoimmune nephritis

Tatsukata Kawagoe[1,2,6], Osamu Takeuchi[1,2,6], Yoshitsugu Takabatake[3], Hiroki Kato[1,2], Yoshitaka Isaka[4], Tohru Tsujimura[5] & Shizuo Akira[1,2]

The intensity and duration of immune responses are controlled by many proteins that modulate Toll-like receptor (TLR) signaling. TANK has been linked to positive regulation of the transcription factors IRF3 and NF-κB. Here we demonstrate that TANK is not involved in interferon responses and is a negative regulator of proinflammatory cytokine production induced by TLR signaling. TLR-induced polyubiquitination of the ubiquitin ligase TRAF6 was upregulated in *Tank*$^{-/-}$ macrophages. Notably, *Tank*$^{-/-}$ mice spontaneously developed fatal glomerulonephritis owing to deposition of immune complexes. Autoantibody production in *Tank*$^{-/-}$ mice was abrogated by antibiotic treatment or the absence of interleukin 6 (IL-6) or the adaptor MyD88. Our results demonstrate that constitutive TLR signaling by intestinal commensal microflora is suppressed by TANK.

Toll-like receptors (TLRs) recognize microbial components and elicit innate as well as adaptive immune responses. Stimulation with TLR ligands induces the production of proinflammatory cytokines and type I interferons in cells of the innate immune system through intracellular signaling cascades[1–3]. After stimulation, TLRs trigger the recruitment of adaptor molecules containing Toll–interleukin 1 receptor (IL-1R) homology domains. One adaptor, MyD88, is essential for the 'downstream' signaling of various TLRs, except for TLR3 (refs. 4–6). MyD88 interacts with the kinase IRAK4, which activates IRAK1 and IRAK2 (ref. 7). In turn, the IRAKs dissociate from MyD88 and interact with TRAF6 (A002312), which acts as a ubiquitin protein ligase. Together with an E2 ubiquitin-conjugating enzyme complex composed of Ubc13 and Uev1A, TRAF6 catalyzes formation of a lysine 63–linked polyubiquitin chain on TRAF6 itself and on the transcription factor NF-κB modulator NEMO (also called IKKγ). The kinase TAK1 is also recruited to TRAF6 and phosphorylates the kinases IKKβ and MEKK6 (ref. 8). Subsequently, the inhibitor of NF-κB (IκB) kinase (IKK) complex, composed of IKKα, IKKβ and NEMO, is formed. NF-κB binds to IκBα in resting cells and is sequestered in the cytoplasm. Phosphorylation of IκB by the IKK complex leads to its degradation by the ubiquitin-proteasome system, thereby freeing NF-κB to translocate to the nucleus and activate the expression of genes encoding proinflammatory cytokines. Activation of the mitogen-activated protein kinase cascade is responsible for gene expression induced by the transcription activator AP-1. In plasmacytoid dendritic cells (DCs), MyD88-dependent signaling activates the production of type I interferons through the transcription factor IRF7 (refs. 1,9).

Many proteins control TLR signaling to ensure that the strength and duration of TLR signals is appropriate for any given immune response. TLRs have been linked to the development of autoimmune diseases, and aberrant activation of innate immunity may contribute to rheumatoid arthritis, inflammatory bowel disease and systemic lupus erythematosus[10,11]. Endogenous RNA molecules such as U1snRNP can activate autoreactive B cells and DCs through TLR7 (ref. 12). Furthermore, duplication of the *Tlr7* gene accounts for the autoimmune phenotypes associated with Yaa mice (Y chromosome–linked autoimmune accelerator)[13]. TLR9 is also involved in the recognition of immune complexes of DNA and anti–double-stranded DNA (anti-dsDNA) antibodies together with the B cell antigen receptor (BCR)[14]. Signaling proteins that inhibit TLR signaling include IRAKM, ST2, SIGIRR, SOCS1, the tumor suppressor CYLD and A20 (refs. 15–21). Cells lacking any one of those proteins produce more proinflammatory cytokines in response to TLR stimulation. Furthermore, mice lacking SOCS1 or A20 have immune disorders that lead to premature death. In addition, the immunosuppressive cytokine IL-10 suppresses colitis development by inhibiting TLR responses[22–24]. Such studies indicate that negative regulation of TLR signaling is important for coordinated innate immune responses.

TANK (also known as I-TRAF) has been identified as a TRAF-binding protein[25,26]. Among the six reported TRAF family members, TRAF1, TRAF2, TRAF3, TRAF5 and TRAF6 interact with TANK[25–28].

[1]Laboratory of Host Defense, World Premier International Immunology Frontier Research Center, and [2]Research Institute for Microbial Diseases, Osaka University, Osaka, Japan. [3]Department of Nephrology and [4]Department of Advanced Technology for Transplantation, Osaka University Graduate School of Medicine, Osaka, Japan. [5]Department of Pathology, Hyogo College of Medicine, Hyogo, Japan. [6]These authors contributed equally to this work. Correspondence should be addressed to S.A. (sakira@biken.osaka-u.ac.jp).

Received 10 February; accepted 16 June; published online 9 August 2009; doi:10.1038/ni.1771

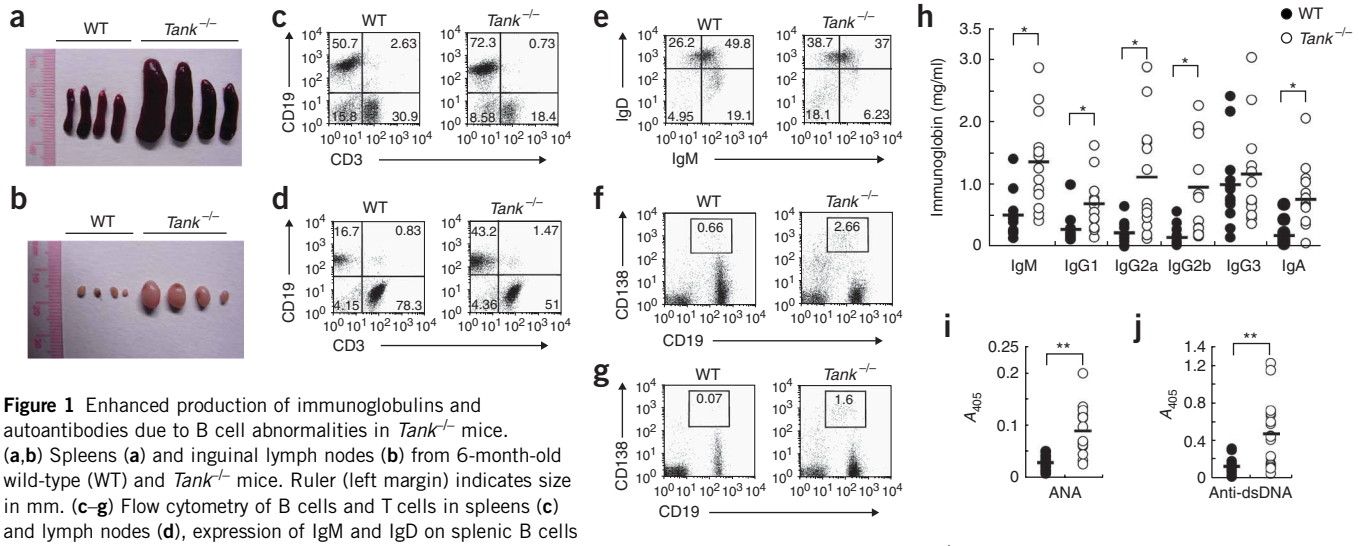

Figure 1 Enhanced production of immunoglobulins and autoantibodies due to B cell abnormalities in *Tank*$^{-/-}$ mice. (**a**,**b**) Spleens (**a**) and inguinal lymph nodes (**b**) from 6-month-old wild-type (WT) and *Tank*$^{-/-}$ mice. Ruler (left margin) indicates size in mm. (**c**–**g**) Flow cytometry of B cells and T cells in spleens (**c**) and lymph nodes (**d**), expression of IgM and IgD on splenic B cells (**e**), and expression of CD138 and CD19 on cells in spleens (**f**) and lymph nodes (**g**) from wild-type and *Tank*$^{-/-}$ mice. Numbers in quadrants and outlined areas indicate percent cells in each. (**h**) Enzyme-linked immunosorbent assay (ELISA) of basal titers of immunoglobulin isotypes in serum from unimmunized 3-month-old wild-type and *Tank*$^{-/-}$ mice. (**i**,**j**) ELISA of antinuclear antibodies (ANA; **i**) and anti-dsDNA antibodies (**j**) in serum from 12-month-old wild-type and *Tank*$^{-/-}$ mice. A_{405}, absorbance at 405 nm. Each symbol represents an individual mouse; small horizontal lines indicate the mean (**h**–**j**). $*P < 0.005$ and $**P < 0.001$, versus *Tank*$^{-/-}$ cells (**h**–**j**;). Data are representative of at least five experiments (**a**,**b**); three independent experiments (**c**–**g**); or single experiments with a total of 13 (**h**) or 12 (**i**,**j**) mice per genotype (**h**–**j**).

TANK has been linked to the positive regulation of NF-κB activation. In addition to TRAF family members, Ikki and TBK1 are TANK-binding partners[29,30]. These proteins phosphorylate IRF3 and IRF7, which are transcription factors essential for the expression of type I interferon and interferon-inducible genes[31,32]. TBK1 and Ikki are activated in response to recognition of viruses through TLRs and RNA helicase RIG-I–like receptors (RLRs)[33,34]. TRAF3 is required for the activation of TBK1 and Ikki downstream of TLRs and RLRs[35,36]. It has been reported that TANK functions as an adaptor that bridges TRAF3 and TBK1-Ikki and that TANK is required for the production of type I interferon in response to viral infection or TLR stimulation[37]. However, the functions of TANK *in vivo* have not yet been clarified.

Here we used *Tank*-deficient (*Tank*$^{-/-}$) mice to demonstrate that TANK is not involved in interferon responses but is a negative regulator of TLR and BCR signaling. Macrophages and B cells from *Tank*$^{-/-}$ mice had more canonical NF-κB activation in response to stimulation of TLRs and the BCR. TLR-induced polyubiquitination of TRAF6 was upregulated in *Tank*$^{-/-}$ macrophages, which indicates that TANK suppresses TLR signaling by controlling TRAF ubiquitination. *Tank*$^{-/-}$ mice spontaneously developed lupus-like autoimmune nephritis. Autoantibody production in *Tank*$^{-/-}$ mice was abolished in the absence of IL-6 or MyD88 but not in the absence of tumor necrosis factor (TNF). Furthermore, treatment of *Tank*$^{-/-}$ mice with antibiotics resulted in lower autoantibody production, which indicates that IL-6 produced by constitutive TLR stimulation resulting from intestinal commensal microflora is important for the development of disease.

RESULTS

Tank$^{-/-}$ mice develop lupus-like nephritis

To investigate the physiological functions of TANK *in vivo*, we generated *Tank*$^{-/-}$ mice by homologous recombination in embryonic stem cells. We targeted exons 3 and 4 of mouse *Tank* with a neomycin-resistance cassette in embryonic stem cells and established *Tank*$^{-/-}$ mice (**Supplementary Fig. 1a**). We confirmed homologous recombination of the *Tank* locus by Southern blot analysis (**Supplementary Fig. 1b**). Expression of *Tank* mRNA and TANK protein was abrogated in *Tank*$^{-/-}$ macrophages (**Supplementary Fig. 1c**,**d**). *Tank*$^{-/-}$ mice were born from interbred *Tank*$^{+/-}$ mice at the expected mendelian ratios and grew normally.

Tank$^{-/-}$ mice had splenomegaly and lymphadenopathy (**Fig. 1a**,**b**). Flow cytometry showed a higher percentage of CD19^{+} B cells in the spleen and lymph nodes of *Tank*$^{-/-}$ mice (**Fig. 1c**,**d**). Immunoglobulin M–low (IgM^{lo}) IgD^{hi} mature B cells accumulated in the spleen of *Tank*$^{-/-}$ mice (**Fig. 1e**). The percentage of CD19^{+}CD138^{+} plasma cells was also much higher in the spleen and lymph nodes of *Tank*$^{-/-}$ mice (**Fig. 1f**,**g**). In contrast, the percentage of Foxp3^{+}CD4^{+} regulatory T cells did not differ between wild-type and *Tank*$^{-/-}$ mice (**Supplementary Fig. 2a**). Consistent with the larger B cell populations, basal serum concentrations of IgM, IgG1, IgG2a, IgG2b and IgA were significantly higher, by 1.2-fold to 6.2-fold, in *Tank*$^{-/-}$ mice than in wild-type mice (**Fig. 1h**). Notably, we detected antinuclear antibodies and anti-dsDNA antibodies in the serum of *Tank*$^{-/-}$ mice (**Fig. 1i**,**j**).

Tank$^{-/-}$ mice began to spontaneously die at 3 months after birth, and about 50% had died by 12 months after birth (**Fig. 2a**). Histological studies showed that 24-week-old *Tank*$^{-/-}$ mice had glomerulonephritis with mesangial cell proliferation and expansion of the mesangial matrix (**Fig. 2b**,**c**). The glomerular structure was devastated in terminally ill *Tank*$^{-/-}$ mice (data not shown), which suggested that renal failure was the cause of death. Although we found infiltration of lymphocytes in the liver and lungs of *Tank*$^{-/-}$ mice, we detected no histological changes in their intestine, heart or joints (data not shown). In addition, we found deposition of IgG, IgM and complement components C3 and C1q in the glomeruli of *Tank*$^{-/-}$ mice (**Fig. 2d**). Such depositions are characteristic of lupus-like nephritis and suggest that deposition of immune complexes of autoantibodies was the cause of the glomerulonephritis in *Tank*$^{-/-}$ mice.

TANK is a negative regulator of TLR responses

Next we examined the type I interferon responses of *Tank*$^{-/-}$ cells to virus infection. In contrast to the results obtained by *in vitro* studies, interferon-β (IFN-β) production in response to infection with

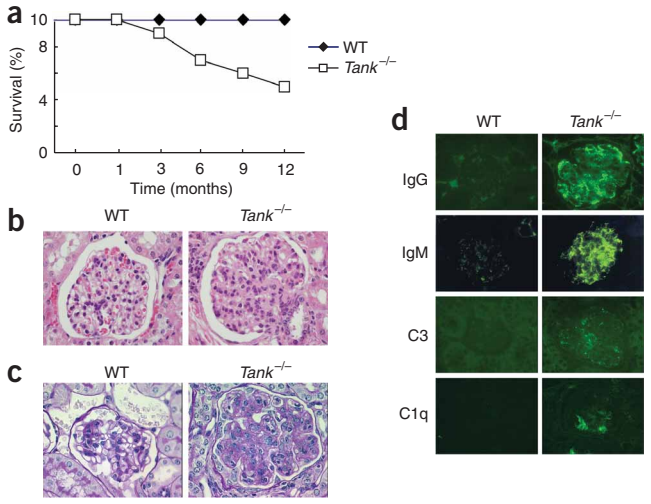

Figure 2 Development of lethal glomerulonephritis in *Tank*$^{-/-}$ mice. (**a**) Survival of wild-type and *Tank*$^{-/-}$ mice monitored for 1 year. (**b**,**c**) Kidney sections from 6-month-old wild-type and *Tank*$^{-/-}$ mice, stained with hematoxylin and eosin (**b**) or periodic acid–Schiff (**c**). (**d**) Kidney sections from 6-month-old wild-type and *Tank*$^{-/-}$ mice, stained with fluorescein isothiocyanate (FITC)-labeled anti–mouse IgG, IgM, C3 and C1q. Original magnification, ×100 (**b**–**d**). Data are representative of single experiments with a total of ten mice per genotype (**a**), or five (**b**,**c**) or two (**d**) experiments.

Newcastle disease virus did not differ between wild-type and *Tank*$^{-/-}$ conventional DCs derived from bone marrow cells (**Fig. 3a**). Wild-type and *Tank*$^{-/-}$ conventional DCs also produced similar amounts of IL-6 (**Fig. 3b**). Newcastle disease virus is recognized by the RNA helicase RIG-I in conventional DCs, which indicates that TANK is not essential for the activation of signaling pathways by RLRs. TRAF3 has been shown to be activated downstream of TLR7 and TLR9 in plasmacytoid DCs. However, bone marrow plasmacytoid DCs induced by the cytokine Flt3L from *Tank*$^{-/-}$ mice produced more rather than less IFN-α and IL-6 in response to A- or D-type CpG DNA (**Fig. 3c**,**d**). Collectively these results indicate that TANK is not essential for type I interferon responses.

Next we examined the production of proinflammatory cytokines in macrophages in response to a set of TLR ligands, including MALP-2 (TLR6-TLR2), polyinosinic-polycytidylic acid (poly(I:C); TLR3), lipopolysaccharide (LPS; TLR4), the synthetic imidazoquinoline resiquimod (R-848; TLR7) and CpG DNA (TLR9). The production of IL-6 and TNF in response to these TLR ligands, except poly(I:C), was much higher in *Tank*$^{-/-}$ peritoneal macrophages than in wild-type cells (**Fig. 3e**,**f**). Of note, the enhanced cytokine production in response to LPS stimulation in *Tank*$^{-/-}$ macrophages was less substantial than that induced by other TLR ligands. Conventional DCs from *Tank*$^{-/-}$ mice also showed excessive cytokine production in response to these TLR ligands (data not shown).

We subsequently assessed the function of TANK in cytokine responses to stimulation with TLR ligands *in vivo*. We chose R-848, because the enhancement in cytokine production in *Tank*$^{-/-}$ macrophages was most pronounced after stimulation with R-848. We injected R-848 into the peritoneum of 8-week-old mice and measured serum concentrations of IL-6 and IFN-α 1 and 3 h later. *Tank*$^{-/-}$ mice had significantly more of these serum cytokines at both time points than did wild-type mice (**Fig. 3g**,**h**). Together these results indicate that TANK is a negative regulator of TLR-mediated responses but is not an essential positive regulator of type I interferon responses *in vivo*.

TANK controls TRAF6 ubiquitination

We examined whether the enhanced cytokine production in *Tank*$^{-/-}$ macrophages was evident at the level of transcription. In response to R-848 stimulation, wild-type macrophages showed induction of the expression of *Il6*, *Tnf*, *Il12b*, *Ptgs2* (encoding cyclooxygenase 2), *Nfkbiz* (encoding IκBζ) and *Nos2* (encoding nitric oxide synthase 2). The expression of these genes was enhanced in *Tank*$^{-/-}$ macrophages in response to R-848 stimulation (**Fig. 4a**), which indicated that initial TLR-induced gene expression was enhanced in *Tank*$^{-/-}$ macrophages. Next we analyzed activation of the transcription factors NF-κB and AP-1 by electrophoretic mobility-shift assay (EMSA). In response to R-848 stimulation, activation of NF-κB and AP-1 was enhanced in *Tank*$^{-/-}$ macrophages compared with that in wild-type macrophages (**Fig. 4b**,**c**).

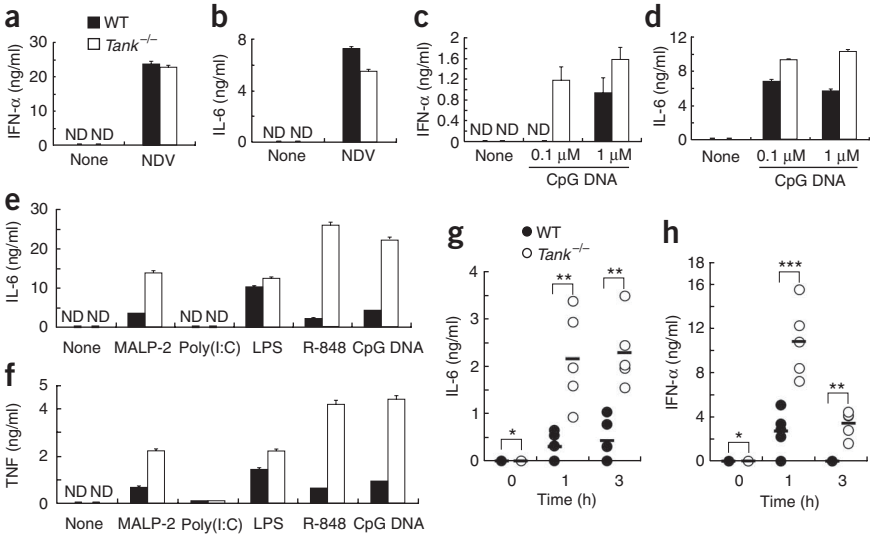

Figure 3 Enhanced proinflammatory cytokine production in response to TLR stimulation in *Tank*$^{-/-}$ mice. (**a**,**b**) ELISA of IFN-α (**a**) and IL-6 (**b**) in culture supernatants of wild-type and *Tank*$^{-/-}$ bone marrow–derived DCs infected for 24 h with Newcastle disease virus (NDV). (**c**,**d**) ELISA of IFN-α (**c**) and IL-6 (**d**) in culture supernatants of wild-type and *Tank*$^{-/-}$ Flt3L-induced DCs stimulated for 24 h with 0.1 or 1 μM CpG DNA. (**e**,**f**) ELISA of IL-6 (**e**) and TNF (**f**) in culture supernatants of wild-type and *Tank*$^{-/-}$ peritoneal macrophages stimulated for 24 h with MALP-2 (10 ng/ml), poly(I:C) (100 μg/ml), LPS (100 ng/ml), R-848 (10 nM) or CpG DNA (1 μM). ND, not detectable. Data are representative of three (**a**–**d**) or five (**e**,**f**) experiments (error bars, s.d.). (**g**,**h**) ELISA of IL-6 (**g**) and IFN-α (**h**) in serum from wild-type mice ($n = 5$) and *Tank*$^{-/-}$ mice ($n = 5$) injected intraperitoneally with 30 nmol R-848. Each symbol represents an individual mouse; small horizontal lines indicate the mean. $^{*}P < 0.05$, $^{**}P < 0.01$ and $^{***}P < 0.005$, versus *Tank*$^{-/-}$ mice (two-tailed Student's *t*-test). Data are representative of a single experiment.

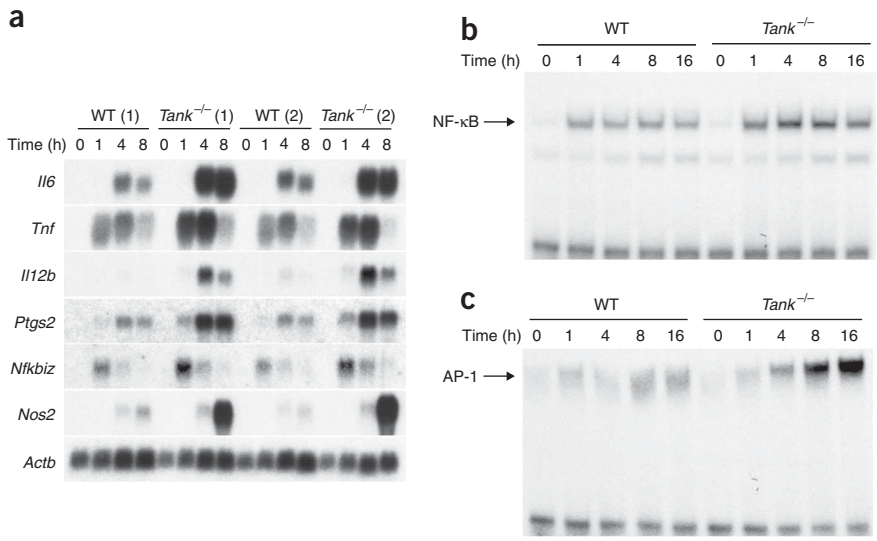

Figure 4 TANK negatively regulates the activation of NF-κB and AP-1 as well as gene expression in response to TLR7 stimulation in macrophages. (**a**) RNA blot analysis of the expression of *Il6*, *Tnf*, *Il12b*, *Ptgs2*, *Nfkbiz* and *Nos2* among total RNA extracted from wild-type and *Tank*$^{-/-}$ peritoneal macrophages stimulated for various times (above lanes) with 10 nM R-848. Bottom, rehybridization of the same membrane with an *Actb* probe (encoding β-actin). Data are from two independent experiments (1 and 2). (**b**,**c**) EMSA of the DNA-binding activity of NF-κB (**b**) and AP-1 (**c**) in nuclear extracts of wild-type and *Tank*$^{-/-}$ macrophages stimulated for various times (above lanes) with 10 μM R-848, assessed with NF-κB- and AP-1-specific probes. Arrows indicate induced NF-κB and AP-1 complexes. Data are representative of three independent experiments.

The results described above indicated that TANK negatively regulates the TLR-induced activation of NF-κB and AP-1. Activation of IRAK1 in response to R-848 was not enhanced in *Tank*$^{-/-}$ macrophages (**Fig. 5a**). Furthermore, IRAK1 was degraded after R-848 stimulation with similar kinetics in wild-type and *Tank*$^{-/-}$ macrophages (**Fig. 5b**), which indicated that TANK regulates signaling downstream of IRAKs. TANK has been reported to interact with the TRAF family members TRAF1, TRAF2, TRAF3, TRAF5 and TRAF6. Among these, TRAF6 is needed for TLR signaling. As TRAF6 is ubiquitinated in response to TLR stimulation, we examined whether TANK modifies the ubiquitination of TRAF6. We found that induction of TRAF6 ubiquitination in response to R-848 stimulation was enhanced in *Tank*$^{-/-}$ macrophages compared with that in wild-type cells (**Fig. 5c**). Reciprocally, overexpression of TANK in human embryonic kidney (HEK293) cells inhibited the ubiquitination of TRAF6 (**Fig. 5d**). Together these results indicate that TANK inhibits TLR-induced activation of NF-κB and AP-1 by suppressing TRAF6 ubiquitination.

TANK is involved in BCR and CD40 signaling

Next we investigated the responses of *Tank*$^{-/-}$ B cells to mitogens such as TLR ligands and crosslinking of the BCR and CD40. After stimulation with R-848, CpG DNA, antibody to IgM (anti-IgM) or anti-CD40, *Tank*$^{-/-}$ B cells proliferated much more than did wild-type B cells (**Fig. 6a**). In contrast, splenic B cell death after culture without mitogen was similar in wild-type and *Tank*$^{-/-}$ mice (**Fig. 6b**), which indicates that TANK is not involved in the control of B cell apoptosis. In response to anti-CD40, B cells activate both canonical and noncanonical NF-κB. The noncanonical pathway is characterized by processing of the NF-κB2 precursor protein p100 to generate p52. We found that activation of noncanonical NF-κB in response to CD40 stimulation was similar in wild-type and *Tank*$^{-/-}$ B cells (**Fig. 6c**). In contrast, NF-κB DNA-binding activity was enhanced in *Tank*$^{-/-}$ B cells compared with that in wild-type B cells (**Fig. 6d**), and the band was supershifted by anti-p65 and anti-p50 (data not shown). Ubiquitination of TRAF6 after stimulation with anti-CD40 was also enhanced in *Tank*$^{-/-}$ B cells (**Fig. 6e**). Furthermore, BCR stimulation also induced enhanced activation of NF-κB and ubiquitination of TRAF6 in *Tank*$^{-/-}$ B cells (**Supplementary Fig. 3a**,**b**). Furthermore, expression of cyclin D2, an NF-κB-inducible protein, was higher in *Tank*$^{-/-}$ B cells than in wild-type B cells after stimulation with anti-CD40 or anti-IgM (**Supplementary Fig. 4**). These data suggest that TANK is involved in canonical but not noncanonical NF-κB-activation pathways in B cells.

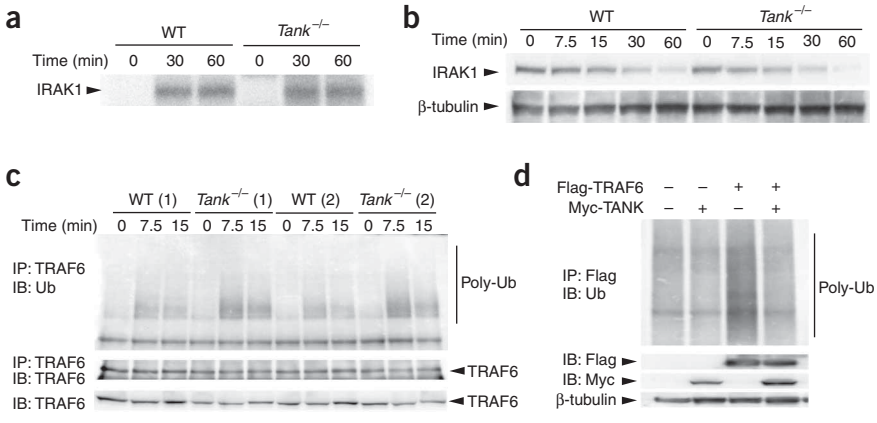

Figure 5 TANK controls TRAF6 ubiquitination in response to TLR7 stimulation in macrophages. (**a**) *In vitro* kinase assay of anti-IRAK1 immunoprecipitates from lysates of wild-type and *Tank*$^{-/-}$ peritoneal macrophages stimulated for various times (above lanes) with 10 μM R-848. Data are representative of two experiments. (**b**) Immunoblot analysis of whole-cell lysates of wild-type and *Tank*$^{-/-}$ macrophages stimulated for various times (above lanes) with 10 μM R-848, probed with anti-IRAK1. Below, immunoblot analysis of β-tubulin (loading control). Data are representative of two experiments. (**c**) Immunoblot (IB) analysis of anti-TRAF6 immunoprecipitates (IP) from lysates of macrophages treated for various times (above lanes) with R-848, probed with antibody to ubiquitin (Ub). Poly-Ub, polyubiquitin. Below, immunoblot analysis of TRAF6 (loading control), with (middle) and without (bottom) anti-TRAF6 immunoprecipitation. Data are from two independent experiments (1 and 2). (**d**) Immunoblot analysis of anti-Flag immunoprecipitates from lysates of HEK293 cells cotransfected with Flag-tagged TRAF6 and Myc-tagged TANK, probed with anti-ubiquitin. Below, immunoblot analysis of lysates without immunoprecipitation; β-tubulin, loading control. Data are representative of three independent experiments.

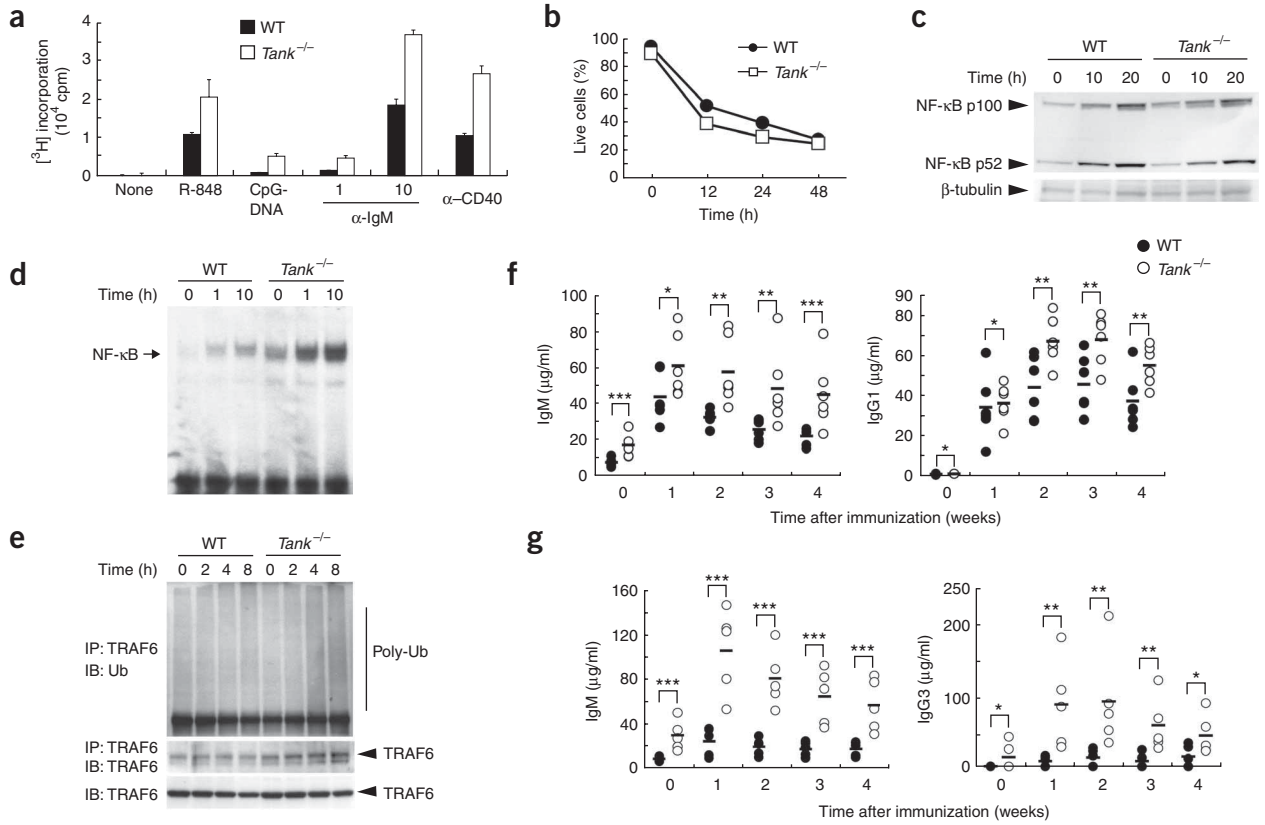

Figure 6 Enhanced activation of B cells in *Tank*$^{-/-}$ mice. (**a**) [^{3}H]thymidine incorporation by purified splenic B cells cultured for 48 h with R-848 (10 nM), CpG DNA (10 nM), anti-IgM (1 or 10 μg/ml) or anti-CD40 (1 μg/ml) and then pulsed with [^{3}H]thymidine (1 μCi) for the final 16 h, measured in a β-scintillation counter. (**b**) Viability of splenic B cells cultured for various times (horizontal axis) in the absence of cytokines, assessed by annexin V staining followed by flow cytometry. (**c**) Immunoblot analysis of the processing of p100 to p52 in whole-cell lysates of wild-type and *Tank*$^{-/-}$ B cells stimulated for various times (above lanes) with anti-CD40 (5 μg/ml). Bottom, immunoblot analysis of β-tubulin (loading control). (**d**) EMSA of NF-κB DNA-binding activity in nuclear extracts of wild-type and *Tank*$^{-/-}$ B cells stimulated for various times (above lanes) with anti-CD40 (5 μg/ml). Arrow indicates the induced NF-κB complex. (**e**) Immunoblot analysis of anti-TRAF6 immunoprecipitates from lysates of splenic B cells treated various times (above lanes) with anti-CD40 (5 μg/ml), probed with anti-ubiquitin. Bottom, immunoblot analysis of TRAF6 (loading control). (**f**) ELISA of the production of NP-specific IgM and IgG1 by mice immunized with NP-CGG, measured 1, 2, 3 and 4 weeks after immunization. (**g**) ELISA of the production of TNP-specific IgM and IgG3 by mice immunized with TNP-Ficoll, measured at 1, 2, 3 and 4 weeks after immunization. Each symbol represents an individual mouse; small horizontal lines indicate the mean (**f**,**g**). $^*P > 0.05$, $^{**}P < 0.05$ and $^{***}P < 0.01$, versus *Tank*$^{-/-}$ mice (two-tailed Student's *t*-test). Data are representative of three (**a** (error bars, s.d.) and **c**–**e**) or two (**b**) independent experiments, or single experiments with a total of five mice per genotype (**f**,**g**).

In contrast to B cells, wild-type and *Tank*$^{-/-}$ T cells proliferated to a similar degree after stimulation with anti-CD3 or anti-CD3 together with anti-CD28 (**Supplementary Fig. 2b**). When stimulated with phorbol 12-myristate 13-acetate and ionomycin *in vitro*, similar proportions of wild-type and *Tank*$^{-/-}$ CD4$^+$ T cells produced IFN-γ or IL-17 (**Supplementary Fig. 2c**). This suggests that TANK is not involved in the development of T helper type 1 or IL-17-producing T helper cells.

To explore the influence of TANK deficiency on antibody responses *in vivo*, we immunized wild-type and *Tank*$^{-/-}$ mice with the T cell–dependent antigen nitrophenol–chicken γ-globulin (NP-CGG) or the T cell–independent antigen trinitrophenyl-Ficoll (TNP-Ficoll). NP-specific IgG1 and IgM titers were higher in *Tank*$^{-/-}$ mice than in wild-type mice (**Fig. 6f**). TNP-specific IgG3 and IgM titers were also higher in *Tank*$^{-/-}$ mice than in wild-type mice (**Fig. 6g**). The difference between wild-type and *Tank*$^{-/-}$ mice was greater in response to immunization with TNP-Ficoll, which suggests that TANK may be more critical for T cell–independent immune responses than for T cell–dependent immune responses *in vivo*.

Intestinal microflora in the autoimmunity of *Tank*$^{-/-}$ mice

Proinflammatory cytokines are critical in the development of autoimmune disease. Overproduction of IL-6 and TNF in mice results in the development of mesangioproliferative glomerulonephritis and chronic polyarthritis, respectively. To investigate whether IL-6 or TNF is involved in disease pathogenesis in *Tank*$^{-/-}$ mice, we generated mice lacking IL-6 or TNF on the *Tank*$^{-/-}$ genetic background. The titers of anti-dsDNA antibodies were significantly lower in 5-month-old *Tank*$^{-/-}$*Il6*$^{-/-}$ mice than in 5-month-old *Tank*$^{-/-}$ mice (**Fig. 7a**). Moreover, IL-6 deficiency 'rescued' the glomerulonephritis that developed in *Tank*$^{-/-}$ mice (**Fig. 7b**). In contrast, TNF deficiency did not significantly alter the amount of anti-dsDNA antibody production in *Tank*$^{-/-}$ mice (**Fig. 7c**). To determine whether MyD88 deficiency protects against the disease progress, we crossed *Tank*$^{-/-}$ mice with *MyD88*$^{-/-}$ mice. Anti-dsDNA antibody titers were significantly lower in 5-month-old *Tank*$^{-/-}$*MyD88*$^{-/-}$ mice than in *Tank*$^{-/-}$ mice (**Fig. 7d**), which indicates that TLR and/or IL-1R family members are critical for the autoimmunity caused by TANK deficiency. The next question we addressed was how TLR and/or IL-1R signaling was activated to cause IL-6 production. Intestinal microflora has been shown to be involved

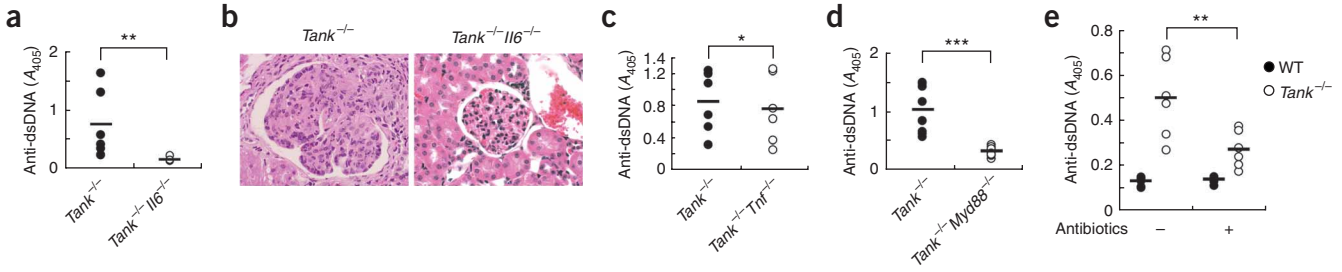

Figure 7 Antibiotic treatment, as well as deficiency of MyD88 or IL-6, ameliorates autoantibody production in *Tank*$^{-/-}$ mice. (**a**) Anti-dsDNA antibodies in serum from 5-month-old *Tank*$^{-/-}$and *Tank*$^{-/-}$*Il6*$^{-/-}$ mice. (**b**) Hematoxylin and eosin staining of kidney sections from *Tank*$^{-/-}$ mice and *Tank*$^{-/-}$*Il6*$^{-/-}$ mice. Original magnification, ×100. (**c**,**d**) ELISA of anti-dsDNA antibodies in *Tank*$^{-/-}$ and *Tank*$^{-/-}$*Tnf*$^{-/-}$ mice (**c**) or *Tank*$^{-/-}$ and *Tank*$^{-/-}$*MyD88*$^{-/-}$ mice (**d**). (**e**) ELISA of serum anti-dsDNA antibodies in 16-week-old wild-type and *Tank*$^{-/-}$ mice given drinking water (from birth onward) containing ampicillin (1 g/l), neomycin (1 g/l), vancomycin (0.5 g/l) and metronidazole (1 g/l); control wild-type and *Tank*$^{-/-}$ mice received untreated drinking water (–). Each symbol represents an individual mouse; small horizontal lines indicate the mean (**a**,**c**–**e**). $*P > 0.05$, $**P < 0.05$ and $***P < 0.01$, versus *Tank*$^{-/-}$ mice (two-tailed Student's *t*-test). Data are representative of single experiments with a total of six mice per genotype (**a**,**c**–**e**) or are representative of three experiments (**b**).

in the pathogenesis of autoimmune diseases, such as colitis in IL-10-deficient mice. Therefore, we treated *Tank*$^{-/-}$ mice orally with a combination of antibiotics to clear the intestinal microflora. The antibiotic treatment significantly ameliorated the production of anti-dsDNA antibodies (**Fig. 7e**), which suggests that continuous stimulation of TLRs by intestinal microflora contributes to the generation of autoantibodies in the absence of TANK.

DISCUSSION

Here we generated *Tank*$^{-/-}$ mice and have shown that TANK is essential for the negative regulation of canonical NF-κB signaling. *Tank*$^{-/-}$ mice had enhanced activation of macrophages and B cells in response to TLR ligands and antigens, which culminated in the development of fatal immune complex–mediated renal failure. Although TANK has been shown to positively regulate TBK1- and Ikki-mediated production of type I interferon by *in vitro* studies, analysis of *Tank*$^{-/-}$ mice showed that TANK was not needed for activation of the type I interferon pathway downstream of RLRs or TRIF. TANK forms a family with the adaptor proteins NAP1 and SINTBAD[38,39], which are composed of an amino-terminal coiled-coil domain and a TBK1-binding domain. NAP1 and SINTBAD have also been linked to the activation of TBK1 and Ikki downstream of virus sensors. Knockdown of NAP1, SINTBAD or TANK by small interfering RNA has been associated with impaired interferon responses. Hence, it is possible that these three proteins function redundantly in the activation of TBK1 and Ikki.

Although published studies have shown that TANK is a positive regulator of NF-κB, our results have shown that TANK is critical for the negative regulation of canonical NF-κB through suppression of TRAF6 ubiquitination. Lysine 63–type ubiquitination is important for the activation of TAK1 with the binding partners TAB2 and TAB3 in TLR signaling, and TANK may inhibit TRAF6 ubiquitination by directly binding to TRAF6 in response to TLR stimulation. Although A20 and CYLD have been identified as deubiquitinases[40–42], TANK does not contain a deubiquitination enzyme domain. Immunoprecipitation experiments showed that overexpressed A20 or CYLD failed to immunoprecipitate together with overexpressed TANK, which suggests that TANK may suppress ubiquitination of TRAF6 independently of A20 or CYLD (data not shown). Further studies are needed to assess the precise mechanism through which TANK modifies TRAF6. In addition, activation of canonical NF-κB in response to BCR and CD40 stimulation was augmented in *Tank*$^{-/-}$ B cells. Consistent with that, proliferation of B cells in response to TLR and BCR stimulation was much higher in *Tank*$^{-/-}$ mice. In TCR signaling, TRAF2 and TRAF6 are reported to participate in NF-κB activation downstream of the adaptors Bcl-10 and MALT1 (ref. 43). Given that TANK suppresses the polyubiquitination of TRAF6 in response to TLR stimulation in macrophages, it is possible that TANK suppresses BCR and CD40 signaling by regulating the activation of TRAF proteins in B cells. However, activation of non-canonical NF-κB was not enhanced in *Tank*$^{-/-}$ B cells, and it has been reported that TRAF3 controls mainly that activation in B cells[44]. Hence, these observations suggest that TANK is not involved in signaling downstream of TRAF3. Furthermore, TRAF2 can control noncanonical NF-κB as well as the development of marginal zone B cells. The relationship between TANK and TRAF2 needs to be explored further.

The disease caused by the absence of TANK was characterized by glomerulonephritis due to deposition of immune complexes in the glomeruli. In addition, anti-dsDNA antibodies and antinuclear antibodies were present in high concentrations in *Tank*$^{-/-}$ mice. These observations indicate that *Tank*$^{-/-}$ mice may represent a mouse model of lupus-like immune diseases. The phenotype of *Tank*$^{-/-}$ mice is reminiscent of that of mice that overexpress IL-6 in B cells[45], which is characterized by lymphadenopathy and plasmacytosis culminating in the development of severe glomerular nephritis. IL-6 is a pleiotropic cytokine responsible for fever, acute-phase protein expression, osteoclast activation and the development of IL-17-producing T helper cells and plasma cells. Indeed, *Tank*$^{-/-}$ macrophages showed enhanced production of proinflammatory cytokines, including IL-6 and TNF, in response to TLR stimulation. Furthermore, *Tank*$^{-/-}$ mice failed to produce autoantibodies and did not develop glomerulonephritis in the absence of IL-6. These results indicate that IL-6 is essential for the development of the *Tank*$^{-/-}$ B cells that are responsible for the production of autoantibodies. In contrast, *Tank*$^{-/-}$ T cells responded normally to TCR stimulation. Given that TANK is critical for inhibiting BCR-induced B cell activation, it is possible that the lack of TANK in B cells is important for the generation of autoimmune nephritis through aberrant activation of B cells in response to antigen stimulation.

The generation of anti-dsDNA antibodies in *Tank*$^{-/-}$ mice was significantly lower in response to oral treatment with antibiotics or in the absence of MyD88, which suggests that TLR signaling is critical for the development of autoimmune disease in *Tank*$^{-/-}$ mice. Although various proteins have been identified as negative regulators of TLR signaling, few mice lacking any a single one of these proteins

spontaneously develop autoimmune disease, with the exception of mice lacking A20. A20-deficient mice spontaneously develop multiorgan inflammation and premature death, which can be 'rescued' by MyD88 deficiency[46,47]. Unlike *Tank*$^{-/-}$ mice, A20-deficient mice do not develop immune complex–mediated glomerulonephritis. A20 controls TNF receptor signaling in addition to TLR signaling, yet the responses to TNF were not altered in *Tank*$^{-/-}$ cells. TNF is involved in the pathogenesis of organ-specific autoimmune diseases, such as rheumatoid arthritis and Crohn's disease[48]. Hence, the differences in the signaling pathways regulated by A20 and TANK may explain the differences in the types of autoimmune disease caused by A20 or TANK deficiency.

As oral treatment with antibiotics ameliorated autoantibody production in *Tank*$^{-/-}$ mice, constitutive stimulation of TLRs by intestinal microflora seems to be responsible for the generation of autoimmunity in the absence of TANK. Bone marrow–transfer experiments showed that hematopoietic cells were responsible for the death of *Tank*$^{-/-}$ mice (data not shown). Intestinal microflora contribute to the pathogenesis of inflammatory bowel disease[48,49], and the colitis observed in IL-10-deficient mice was 'rescued' by the absence of MyD88 (ref. 24), which suggests that TLR signaling is involved in the pathogenesis of inflammatory bowel disease. As TLRs are expressed on intestinal DCs and are responsible for sensing microbes in the intestine, it is possible that TANK controls the production of certain cytokines in intestinal tissues. Further studies are needed to understand why TANK deficiency causes autoimmune nephritis but not colitis.

In addition, the antigen-specific humoral immune responses to haptens were enhanced in *Tank*$^{-/-}$ mice. This may have been due to the enhanced DC and B cell activation in response to antigens and the adjuvant in *Tank*$^{-/-}$ mice. It will be useful to explore whether inhibition of TANK expression in certain cell types is beneficial for inducing antigen-specific immune responses *in vivo*. Modification of TANK may be helpful in vaccines administered together with an adjuvant. In summary, our results here have shown that TANK is a negative regulator of TLR and BCR responses. Future studies involving cell type–specific deletion of TANK will clarify the complex interaction between cells of the immune system needed to prevent the development of autoimmune disease.

METHODS

Methods and any associated references are available in the online version of the paper at http://www.nature.com/natureimmunology/.

Accession code. UCSD-Nature Signaling Gateway (http://www.signaling-gateway.org): A002312.

Note: Supplementary information is available on the Nature Immunology website.

ACKNOWLEDGMENTS

We thank T. Yasui (Osaka University) for *Il6*$^{-/-}$ mice and plasmids; colleagues in our laboratories; E. Kamada for secretarial assistance; Y. Fujiwara, M. Kumagai and R. Abe for technical assistance; and S. Sato for discussions. Supported by the Special Coordination Funds of the Japanese Ministry of Education, Culture, Sports, Science and Technology, and grants from the Ministry of Health, Labour and Welfare in Japan, the Global Center of Excellence Program of Japan, and the US National Institutes of Health (P01 AI070167).

AUTHOR CONTRIBUTIONS

T.K., O.T. and S.A. designed the research and analyzed data; T.K. generated *Tank*$^{-/-}$ mice and did most of the experiments; Y.T., Y.I. and T.T. did histological examination of kidneys; H.K. provided advice; and T.K., O.T. and S.A. prepared the manuscript.

Published online at http://www.nature.com/natureimmunology/.
Reprints and permissions information is available online at http://npg.nature.com/reprintsandpermissions/.

1. Akira, S., Uematsu, S. & Takeuchi, O. Pathogen recognition and innate immunity. *Cell* **124**, 783–801 (2006).
2. Beutler, B. Inferences, questions and possibilities in Toll-like receptor signalling. *Nature* **430**, 257–263 (2004).
3. Medzhitov, R. Recognition of microorganisms and activation of the immune response. *Nature* **449**, 819–826 (2007).
4. Kawai, T., Adachi, O., Ogawa, T., Takeda, K. & Akira, S. Unresponsiveness of MyD88-deficient mice to endotoxin. *Immunity* **11**, 115–122 (1999).
5. Yamamoto, M. *et al.* Role of adaptor TRIF in the MyD88-independent toll-like receptor signaling pathway. *Science* **301**, 640–643 (2003).
6. O'Neill, L.A. & Bowie, A.G. The family of five: TIR-domain-containing adaptors in Toll-like receptor signalling. *Nat. Rev. Immunol.* **7**, 353–364 (2007).
7. Kawagoe, T. *et al.* Sequential control of Toll-like receptor-dependent responses by IRAK1 and IRAK2. *Nat. Immunol.* **9**, 684–691 (2008).
8. Wang, C. *et al.* TAK1 is a ubiquitin-dependent kinase of MKK and IKK. *Nature* **412**, 346–351 (2001).
9. Honda, K., Takaoka, A. & Taniguchi, T. Type I interferon gene induction by the interferon regulatory factor family of transcription factors. *Immunity* **25**, 349–360 (2006).
10. Marshak-Rothstein, A. Toll-like receptors in systemic autoimmune disease. *Nat. Rev. Immunol.* **6**, 823–835 (2006).
11. Christensen, S.R. & Shlomchik, M.J. Regulation of lupus-related autoantibody production and clinical disease by Toll-like receptors. *Semin. Immunol.* **19**, 11–23 (2007).
12. Lau, C.M. *et al.* RNA-associated autoantigens activate B cells by combined B cell antigen receptor/Toll-like receptor 7 engagement. *J. Exp. Med.* **202**, 1171–1177 (2005).
13. Pisitkun, P. *et al.* Autoreactive B cell responses to RNA-related antigens due to TLR7 gene duplication. *Science* **312**, 1669–1672 (2006).
14. Viglianti, G.A. *et al.* Activation of autoreactive B cells by CpG dsDNA. *Immunity* **19**, 837–847 (2003).
15. Liew, F.Y., Xu, D., Brint, E.K. & O'Neill, L.A. Negative regulation of toll-like receptor-mediated immune responses. *Nat. Rev. Immunol.* **5**, 446–458 (2005).
16. Kobayashi, K. *et al.* IRAK-M is a negative regulator of Toll-like receptor signaling. *Cell* **110**, 191–202 (2002).
17. Brint, E.K. *et al.* ST2 is an inhibitor of interleukin 1 receptor and Toll-like receptor 4 signaling and maintains endotoxin tolerance. *Nat. Immunol.* **5**, 373–379 (2004).
18. Wald, D. *et al.* SIGIRR, a negative regulator of Toll-like receptor-interleukin 1 receptor signaling. *Nat. Immunol.* **4**, 920–927 (2003).
19. Nakagawa, R. *et al.* SOCS1 participates in negative regulation of LPS responses. *Immunity* **17**, 677–687 (2002).
20. Reiley, W.W. *et al.* Regulation of T cell development by the deubiquitinating enzyme CYLD. *Nat. Immunol.* **7**, 411–417 (2006).
21. Lee, E.G. *et al.* Failure to regulate TNF-induced NF-κB and cell death responses in A20-deficient mice. *Science* **289**, 2350–2354 (2000).
22. Kuhn, R., Lohler, J., Rennick, D., Rajewsky, K. & Muller, W. Interleukin-10-deficient mice develop chronic enterocolitis. *Cell* **75**, 263–274 (1993).
23. Kobayashi, M. *et al.* Toll-like receptor-dependent production of IL-12p40 causes chronic enterocolitis in myeloid cell-specific Stat3-deficient mice. *J. Clin. Invest.* **111**, 1297–1308 (2003).
24. Rakoff-Nahoum, S., Hao, L. & Medzhitov, R. Role of toll-like receptors in spontaneous commensal-dependent colitis. *Immunity* **25**, 319–329 (2006).
25. Cheng, G. & Baltimore, D. TANK, a co-inducer with TRAF2 of TNF- and CD 40L-mediated NF-κB activation. *Genes Dev.* **10**, 963–973 (1996).
26. Rothe, M. *et al.* I-TRAF is a novel TRAF-interacting protein that regulates TRAF-mediated signal transduction. *Proc. Natl. Acad. Sci. USA* **93**, 8241–8246 (1996).
27. Chin, A.I. *et al.* TANK potentiates tumor necrosis factor receptor-associated factor-mediated c-Jun N-terminal kinase/stress-activated protein kinase activation through the germinal center kinase pathway. *Mol. Cell. Biol.* **19**, 6665–6672 (1999).
28. Li, C. *et al.* Downstream regulator TANK binds to the CD40 recognition site on TRAF3. *Structure* **10**, 403–411 (2002).
29. Pomerantz, J.L. & Baltimore, D. NF-κB activation by a signaling complex containing TRAF2, TANK and TBK1, a novel IKK-related kinase. *EMBO J.* **18**, 6694–6704 (1999).
30. Nomura, F., Kawai, T., Nakanishi, K. & Akira, S. NF-κB activation through IKK-i-dependent I-TRAF/TANK phosphorylation. *Genes Cells* **5**, 191–202 (2000).
31. Fitzgerald, K.A. *et al.* IKKε and TBK1 are essential components of the IRF3 signaling pathway. *Nat. Immunol.* **4**, 491–496 (2003).
32. Sharma, S. *et al.* Triggering the interferon antiviral response through an IKK-related pathway. *Science* **300**, 1148–1151 (2003).
33. Hemmi, H. *et al.* The roles of two IκB kinase-related kinases in lipopolysaccharide and double stranded RNA signaling and viral infection. *J. Exp. Med.* **199**, 1641–1650 (2004).
34. Kato, H. *et al.* Cell type-specific involvement of RIG-I in antiviral response. *Immunity* **23**, 19–28 (2005).
35. Hacker, H. *et al.* Specificity in Toll-like receptor signalling through distinct effector functions of TRAF3 and TRAF6. *Nature* **439**, 204–207 (2006).
36. Oganesyan, G. *et al.* Critical role of TRAF3 in the Toll-like receptor-dependent and -independent antiviral response. *Nature* **439**, 208–211 (2006).

37. Guo, B. & Cheng, G. Modulation of the interferon antiviral response by the TBK1/IKKi adaptor protein TANK. *J. Biol. Chem.* **282**, 11817–11826 (2007).
38. Sasai, M. *et al.* Cutting edge: NF-κB-activating kinase-associated protein 1 participates in TLR3/Toll-IL-1 homology domain-containing adapter molecule-1-mediated IFN regulatory factor 3 activation. *J. Immunol.* **174**, 27–30 (2005).
39. Ryzhakov, G. & Randow, F. SINTBAD, a novel component of innate antiviral immunity, shares a TBK1-binding domain with NAP1 and TANK. *EMBO J.* **26**, 3180–3190 (2007).
40. Wertz, I.E. *et al.* De-ubiquitination and ubiquitin ligase domains of A20 downregulate NF-kappaB signalling. *Nature* **430**, 694–699 (2004).
41. Brummelkamp, T.R., Nijman, S.M., Dirac, A.M. & Bernards, R. Loss of the cylindromatosis tumour suppressor inhibits apoptosis by activating NF-κB. *Nature* **424**, 797–801 (2003).
42. Trompouki, E. *et al.* CYLD is a deubiquitinating enzyme that negatively regulates NF-κB activation by TNFR family members. *Nature* **424**, 793–796 (2003).
43. Sun, L., Deng, L., Ea, C.K., Xia, Z.P. & Chen, Z.J. The TRAF6 ubiquitin ligase and TAK1 kinase mediate IKK activation by BCL10 and MALT1 in T lymphocytes. *Mol. Cell* **14**, 289–301 (2004).
44. He, J.Q. *et al.* Rescue of TRAF3-null mice by p100 NF-κB deficiency. *J. Exp. Med.* **203**, 2413–2418 (2006).
45. Suematsu, S. *et al.* IgG1 plasmacytosis in interleukin 6 transgenic mice. *Proc. Natl. Acad. Sci. USA* **86**, 7547–7551 (1989).
46. Boone, D.L. *et al.* The ubiquitin-modifying enzyme A20 is required for termination of Toll-like receptor responses. *Nat. Immunol.* **5**, 1052–1060 (2004).
47. Turer, E.E. *et al.* Homeostatic MyD88-dependent signals cause lethal inflamMation in the absence of A20. *J. Exp. Med.* **205**, 451–464 (2008).
48. Xavier, R.J. & Podolsky, D.K. Unravelling the pathogenesis of inflammatory bowel disease. *Nature* **448**, 427–434 (2007).
49. Elson, C.O. *et al.* Experimental models of inflammatory bowel disease reveal innate, adaptive, and regulatory mechanisms of host dialogue with the microbiota. *Immunol. Rev.* **206**, 260–276 (2005).

ONLINE METHODS

Generation of *Tank*$^{-/-}$ mice. *Tank* was isolated from genomic DNA extracted from embryonic stem cells (GSI-I) by PCR. The targeting vector was constructed by replacement of a 2.0-kilobase fragment encoding the *Tank* open reading frame with a neomycin-resistance gene cassette; the gene encoding herpes simplex virus thymidine kinase driven by the promoter of the gene encoding phosphoglycerate kinase was inserted into the genomic fragment to facilitate negative selection. After transfection of the targeting vector into embryonic stem cells, colonies doubly resistant to the aminoglycoside G418 and gancyclovir were selected, screened by PCR and further confirmed by Southern blot analysis. Homologous recombinants were microinjected into blastocysts from C57BL/6 female mice, and heterozygous F_1 progenies were intercrossed to obtain *Tank*$^{-/-}$ mice. *Tank*$^{-/-}$ mice on the 129Sv × C57BL/6 background and their littermate controls were used.

Mice and cells. *MyD88*$^{-/-}$ and *Tnf*$^{-/-}$ mice have been described[4,23]. *Il6*$^{-/-}$ mice were provided by T. Yasui. All animal experiments were carried out with the approval of the Animal Research Committee of the Research Institute for Microbial Diseases (Osaka University). At 3 d after injection of 2 ml of 4.0% (wt/vol) thioglycollate medium (Sigma), peritoneal exudate cells were isolated from the peritoneal cavities of mice by washing with ice-cold Hank's buffered-salt solution (Invitrogen). Resting B cells were isolated from splenocyte single-cell suspensions by positive selection with anti-B220 magnetic beads (Miltenyi Biotec). T cells were isolated from splenocyte single-cell suspensions by positive selection with anti-Thy-1.2 magnetic beads (Miltenyi Biotec). Cell purity was confirmed to be above 90% by flow cytometry.

Reagents. MALP-2 was provided as described[7]. LPS from *Salmonella minnesota* strain Re-595 was from Sigma-Aldrich. Poly(I:C) was from Amersham Biosciences. R-848 was provided by the Pharmaceuticals and Biotechnology Laboratory of the Japan Energy Corporation. The CpG oligonucleotide was synthesized as described[7]. Polyclonal anti-IRAK1 has been described[7].

Measurement of cytokines and autoantibodies. Concentrations of cytokines in culture supernatants and serum were measured by ELISA. ELISA kits for mouse TNF and IL-6 were from R&D Systems. The ELISA kit for mouse IFN-α was from PBL Biomedical Laboratories. ELISA kits for mouse anti-dsDNA antibodies and antinuclear antibody were from Alpha Diagnostic International. Serum immunoglobulin concentrations were measured as described[50].

Histological analysis. Formalin-fixed tissues were stained with hematoxylin and eosin or periodic acid–Schiff reagent. For detection of renal IgG deposits, kidneys were rapidly frozen in liquid nitrogen and cryostat sections 2 μm in thickness were fixed for 15 min in 100% (vol/vol) acetone. Sections were incubated overnight at 4 °C with FITC-conjugated goat anti–mouse IgG (67228; ICN Biomedicals), FITC-conjugated donkey anti–mouse IgM (715-095-050; Jackson ImmunoResearch), FITC-conjugated sheep anti–human C3c complement (433004; Thermo Electron) or FITC-conjugated anti–mouse C1q (RmC7H8; Cedarlane Laboratories), each at a concentration of 10 μg/ml.

RNA hybridization. Peritoneal macrophages were treated for 0, 1, 4 and 8 h with 10 nM R-848, and total RNA was extracted with the TRIzol reagent (Invitrogen). The extracted RNA was separated by electrophoresis, transferred to nylon membranes and hybridized with various cDNA probes. For detection of the expression of *Tank* mRNA, a 319–base pair fragment (nucleotides 350–669) of Tank cDNA was used as a probe. The same membranes were rehybridized with an *Actb* probe.

***In vitro* kinase assay.** Peritoneal macrophages stimulated with 10 nM R-848 were lysed and immunoprecipitated with anti-IRAK1. Then, IRAK1 activity was measured by *in vitro* kinase assay as described[7].

Immunoblot analysis. Peritoneal macrophages were treated for various times with 10 nM R-848, then were lysed in a lysis buffer composed of 1.0% (vol/vol) Nonidet P-40, 150 mM NaCl, 20 mM Tris-HCl, pH 7.5, 1 mM EDTA and a protease inhibitor 'cocktail' (Roche). Lysates were separated by SDS-PAGE and analyzed by immunoblot. Polyclonal anti-TANK (2141) was from Cell Signaling. Polyclonal anti-TRAF6 (sc-7221), monoclonal anti-Ub (F-7), monoclonal anti-β-tubulin (D-10) and anti-cyclin D2 (34B1-3) were from Santa Cruz Biotechnology.

EMSA. Nuclear extracts were prepared from peritoneal macrophages (4×10^6) stimulated with 10 nM R-848 as described[7], then were incubated with or without antibodies to NF-κB p65 (C-20) or p50 (D-17; Santa Cruz) and were further incubated with a probe specific for NF-κB DNA-binding sites, before being separated by electrophoresis and visualized by autoradiography.

Immunoblot, immunoprecipitation and *in vivo* ubiquitination assays. Peritoneal macrophages (4×10^6) were stimulated for various times with 10 nM R-848. Immunoblot analysis and immunoprecipitation were done as described[7]. For detection of *in vivo* ubiquitination of TRAF6, cell lysates were boiled for 10 min at 90 °C in 1% (wt/vol) SDS for removal of noncovalently attached proteins, followed by immunoprecipitation with anti-TRAF6 in 0.1% (wt/vol) SDS lysis buffer in the presence of protease inhibitors. Ubiquitin was detected by immunoblot analysis.

B cell and T cell proliferation assays. Purified splenic B cells (5×10^4) were cultured for 48 h in 96-well plates with various concentrations of R-848, CpG DNA, anti-IgM (Jackson ImmunoResearch) or anti-CD40 (HM40-3, PharMingen). Purified splenic T cells were stimulated for 48 h with plate-bound anti-CD3 alone (1 or 5 μg/ml; 2C11; Pharmingen) or with anti-CD3 (1 μg/ml) plus anti-CD28 (1 μg/ml; 37.51; Pharmingen). Samples were pulsed with 1 μCi [^{3}H]thymidine for the final 16 h and ^{3}H uptake was measured with a β-scintillation counter (Packard).

***In vivo* immunization and ELISA.** Mice were immunized intraperitoneally with 50 μg NP-CGG (Biosearch Technologies) precipitated with Imject alum (Pierce) or with 25 μg of TNP-Ficoll (Biosearch Technologies). Antigen- and isotype-specific antibodies in serum collected from peripheral blood at various time points were measured by ELISA on plates coated with NP-BSA or TNP-BSA (Biosearch Technologies). Alkaline phosphatase–conjugated antibodies to mouse IgM (1020-04), IgG1 (1070-04) and IgG3 (1100-04) were from Southern Biotechnology.

Cell viability. Purified splenic B cells (1×10^6) were cultured for various periods in RPMI medium containing 10% (vol/vol) FCS. Cell viability was assessed with annexin V–indocarbocyanine (BioVision) and a FACSCalibur (Becton Dickinson).

Construction of TANK expression plasmids. Full-length mouse TANK cDNA was obtained by PCR from a mouse cDNA library and was cloned into the Myc-pcDNA3 vector.

Statistical analysis. Statistical significance was calculated with the two-tailed Student's *t*-test. *P* values of less than 0.05 were considered significant.

50. Sato, S. *et al.* Essential function for the kinase TAK1 in innate and adaptive immune responses. *Nat. Immunol.* **6**, 1087–1095 (2005).

nature immunology

Activation of innate immune antiviral responses by Nod2

Ahmed Sabbah[1], Te Hung Chang[1], Rosalinda Harnack[1], Victoria Frohlich[2], Kaoru Tominaga[2,3], Peter H Dube[1], Yan Xiang[1] & Santanu Bose[1]

Pattern-recognition receptors (PRRs), including Toll-like receptors (TLRs) and RIG-like helicase (RLH) receptors, are involved in innate immune antiviral responses. Here we show that nucleotide-binding oligomerization domain 2 (Nod2) can also function as a cytoplasmic viral PRR by triggering activation of interferon-regulatory factor 3 (IRF3) and production of interferon-β (IFN-β). After recognition of a viral ssRNA genome, Nod2 used the adaptor protein MAVS to activate IRF3. Nod2-deficient mice failed to produce interferon efficiently and showed enhanced susceptibility to virus-induced pathogenesis. Thus, the function of Nod2 as a viral PRR highlights the important function of Nod2 in host antiviral defense mechanisms.

Innate immune antiviral responses are the first line of defense against viral infection[1,2]. Interferon-α/β (IFN-α/β) serves an important function during innate antiviral responses by activating the kinase Jak–transcription factor STAT signaling pathway[3]. Virus-infected cells use pattern-recognition receptors (PRRs) to recognize pathogen-associated molecular patterns (PAMPs; in this case, virus-associated molecular patterns) and to trigger phosphorylation of the transcription factor interferon-regulatory factor 3 (IRF3), which then translocates to the nucleus to transactivate interferon genes[4]. So far two classes of viral PRRs have been identified: the Toll-like receptors (TLRs)[5] and the RIG-like helicase (RLH) receptors such as RIG-I and Mda5 (ref. 6).

A third class of PRR includes members of the nucleotide-binding domain (NBD)– and leucine-rich-region (LRR)–containing family of cytoplasmic proteins (known as NLRs); these proteins respond to bacterial PAMPs to activate the transcription factor NF-κB and mitogen-activated protein kinase pathways[7–9]. For example, the NLR Nod2 detects bacterial PAMPs, including muramyl dipeptide (MDP)[10]. However, so far, no NLRs have been reported to respond to virus-specific PAMPs and activate an antiviral response.

It has been shown that the NLR family member NLRX1 interacts with the mitochondrial antiviral signaling (MAVS) protein (also known as IPS-1, VISA or CARDIF) to negatively regulate the interferon pathway[11] and induces the formation of reactive oxygen species[12]. Thus, members of NLR family of proteins may modulate (either positively or negatively) the host antiviral apparatus. In addition, Nod2 facilitates production of human β-defensin 2 after stimulation with MDP, and human β-defensin 2 is also upregulated in human cells infected with respiratory syncytial virus (RSV), a paramyxovirus that has a negative-sense single-stranded RNA (ssRNA) genome[13,14].

Here, to investigate the involvement of NLRs in innate antiviral response, we examined the ability of various NLRs to activate IRF3 and interferon after infection with RSV, which causes severe lung disease in infants and children and elderly and immunocompromised people[15,16]. Among the various NLRs, Nod2 activated IRF3 and interferon in RSV-infected cells. Activation of Nod2 by ssRNA resulted in signaling dependent on MAVS. Both synthetic ssRNA and viral ssRNA genome were able to activate the MAVS-IRF3-interferon pathway. The important physiological function of Nod2 in antiviral defense was evident from the enhanced RSV pathogenesis, lung disease and viral susceptibility of Nod2-deficient mice. We found similar functions for Nod2 in responses to influenza A and parainfluenza viruses. Thus, our studies demonstrate a previously unknown function for Nod2 as a viral PRR important for the host defense against virus infection.

RESULTS

Induction of interferon production by ssRNA via Nod2

To study the involvement of NLR proteins in antiviral responses, we expressed various hemagglutinin (HA)-tagged human NLR proteins (such as Nod1, Nod2, IPAF, NAIP and Nod3) in 293 human embryonic kidney cells, which do not endogenously express most NLRs. We treated these cells with synthetic ssRNA and analyzed interferon production and IRF3 activation. We used ssRNA because several highly pathogenic viruses, including paramyxoviruses (RSV, Sendai virus, human parainfluenza viruses and measles virus), rhabdoviruses (rabies virus and vesicular stomatitis virus) and orthomyxoviruses (influenza viruses) have ssRNA genomes and because ssRNA activates PRRs, including TLR7, TLR8 and RIG-I (refs. 5,6). Nod2 but not Nod1 facilitated ssRNA-induced activation of IRF3 (**Fig. 1a**) and IFN-β (**Supplementary Fig. 1a**,**b**). Such activation was lacking in cells treated with CpG DNA (**Fig. 1a** and **Supplementary Fig. 1a**,**b**). Transfected 293 cells had high expression of HA-tagged Nod constructs (**Supplementary Fig. 1c**); in addition,

[1]Department of Microbiology and Immunology, [2]Department of Cellular and Structural Biology and [3]Sam and Ann Barshop Institute for Longevity and Aging Studies, The University of Texas Health Science Center at San Antonio, San Antonio, Texas, USA. Correspondence should be addressed to S.B. (bose@uthscsa.edu).

Received 20 April; accepted 15 July; Published online 23 August 2009; doi:10.1038/ni.1782

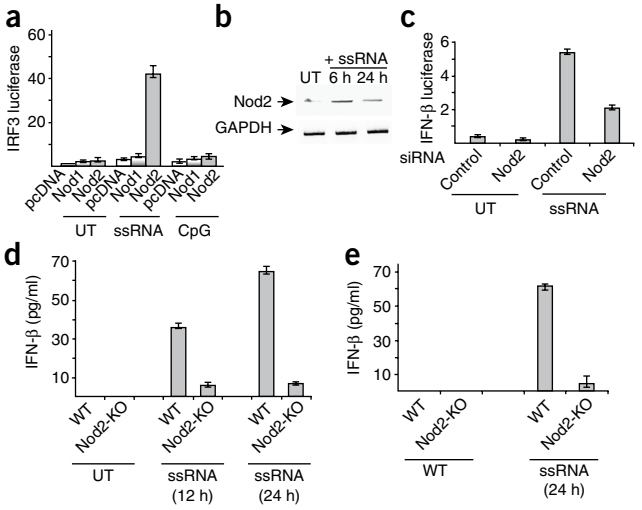

Figure 1 Activation of Nod2 by ssRNA. (**a**) Activation of an IRF3 luciferase reporter in 293 cells transfected with pcDNA, human HA-Nod1 or human HA-Nod2 and left untreated (UT) or treated for 6 h with ssRNA or CpG DNA. (**b**) RT-PCR analysis of Nod2 expression in A549 cells left untreated or stimulated with ssRNA (time, above lanes). (**c**) Activation of an IFN-β luciferase reporter in A549 cells transfected with control siRNA or Nod2-specific siRNA and left untreated or stimulated for 6 h with ssRNA. (**d**,**e**) Enzyme-linked immunosorbent assay (ELISA) of IFN-β production by wild-type (WT) and Nod2-deficient (Nod2-KO) BMMs (**d**) or MEFs (**e**) left untreated or stimulated with ssRNA (time, below graphs). Data are representative of three independent experiments (**a**,**c**–**e**; mean ± s.d.) or three experiments (**b**).

HA-Nod2 and HA-Nod1 proteins were functional, as they facilitated activation of NF-κB in 293 cells treated with MDP or γ-D-glutamyl-meso-diaminopimelic acid, respectively (**Supplementary Fig. 1d**).

To establish the physiological relevance of Nod2-mediated, ssRNA-induced activation of IRF3, we next evaluated the function of endogenous Nod2 in inducing IRF3-interferon after ssRNA treatment. For these studies we used human lung epithelial A549 cells, as these cells are permissive to most viruses that have ssRNA genomes and endogenously express various PRRs. Treatment of these cells with ssRNA resulted in higher expression of Nod2 (**Fig. 1b**); Nod1 expression remained unchanged (data not shown). Nod2-specific small interfering RNA (siRNA) diminished Nod2 expression in ssRNA-treated A549 cells (**Supplementary Fig. 2a**) and impaired ssRNA-induced activation of IRF3 and IFN-β (**Fig. 1c** and **Supplementary Fig. 2b**).

Similarly, ssRNA-induced production of IFN-β was lower in bone marrow–derived macrophages (BMMs) and mouse embryo fibroblasts (MEFs) isolated from Nod2-deficient than in those from wild-type mice (**Fig. 1d**,**e**). In contrast, wild-type and Nod2-deficient BMMs and MEFs produced similar amounts of IFN-β after treatment with poly(I:C) (double-stranded RNA that activates TLR3; **Supplementary Fig. 2c**). The ability of poly(I:C) to induce interferon (via TLR3) in both wild-type and Nod2-deficient MEFs showed that the IRF3-interferon pathway is intact in Nod2-deficient mice. Furthermore, administration of poly(I:C) *in vivo* resulted in the production of similar concentrations of IFN-β in wild-type and Nod2-deficient mice (**Supplementary Fig. 2d**). Thus, our results obtained with cell lines and primary cells demonstrate that activation of Nod2 by ssRNA results in IFN-β production.

Nod2 facilitates virus-induced interferon production

To further confirm the ability of Nod2 to launch an antiviral response, we infected 293 cells with RSV. RSV induced activation of IRF3 and IFN-β in 293 cells expressing HA-Nod2 but not in 293 cells expressing HA-Nod1 (**Fig. 2a**,**b**). Inactivation of virion particles with ultraviolet light abolished the ability of RSV to activate IRF3 in Nod2-expressing cells (**Fig. 2a**). The inability of RSV inactivated by ultraviolet light to activate IRF3 indicated that an intact viral RNA genome is essential for Nod2 activation. The direct function of viral components in Nod2 activation was further confirmed by the loss of IRF3 activation after inhibition of RSV cellular entry with an RSV-neutralizing antibody (specific for the RSV fusion protein; **Supplementary Fig. 2e**).

We established the functional importance of Nod2 in antiviral responses with the interferon-sensitive vesicular stomatitis virus (VSV). Plaque assay of VSV titers obtained from 293 cells expressing HA-Nod2 or HA-Nod1 showed that cells expressing HA-Nod2 had much lower viral titers (**Fig. 2c**). Like VSV, RSV titers were lower in Nod2-expressing cells than in Nod1-expressing cells (**Fig. 2d**). Human parainfluenza virus type 3 (ref. 17) and VSV[18] also activated IRF3 in Nod2-expressing 293 cells (**Supplementary Fig. 3a**). In contrast, vaccinia virus, a DNA virus, failed to activate IRF3 in Nod2-expressing cells (**Supplementary Fig. 3b**). These results demonstrated that like the RLH receptors RIG-I and Mda5, Nod2 can function as a cytoplasmic PRR for a viral ssRNA genome (viral ssRNA).

We next evaluated the function of endogenous Nod2 in inducing IRF3-interferon in response to RSV infection. Published studies have described IRF3 activation and IFN-β production in RSV-infected A549 cells as early as 2 h after infection[19,20]. Although uninfected A549 cells did not have detectable expression of Nod2, RSV infection resulted in higher Nod2 expression within 2 h of infection (**Fig. 3a**). RSV infection failed to induce Nod1 expression (data not shown). Nod2-specific siRNA markedly diminished Nod2 expression after RSV infection (**Supplementary Fig. 4a**) and resulted in less activation of IRF3 and IFN-β after RSV infection (**Fig. 3b** and **Supplementary Fig. 4b**). The effect was more pronounced during early time points after infection (4 h and 6 h) than later (10 h) after infection (**Fig. 3b**). This result suggests that Nod2 is critical for the early antiviral response, whereas during late time periods after infection, other PRRs (such as RIG-I) may activate the IRF3-interferon pathway.

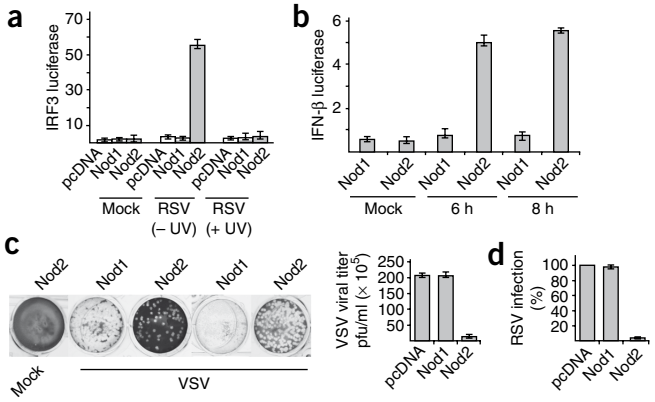

Figure 2 Activation of antiviral response by Nod2 in virus infected cells. (**a**,**b**) Activation of IRF3 (**a**) and IFN-β (**b**) luciferase reporter genes in mock-infected and RSV-infected 293 cells expressing pcDNA, HA-Nod1 or HA-Nod2. (**a**) Luciferase activity 6 h after infection in cells with (+UV) or without (–UV) treatment with ultraviolet irradiation. (**b**) Time after infection, below graph. (**c**) Plaque assay of VSV infectivity in 293 cells expressing pcDNA, HA-Nod1 or HA-Nod2, presented as crystal violet staining (left) and VSV titer (right; plaque-forming units (PFU) per ml). (**d**) RSV infectivity in 293 cells expressing pcDNA, HA-Nod1 or HA-Nod2, presented relative to viral titer in cells expressing pcDNA, set as 100%. Data are representative of three independent experiments (mean ± s.d.).

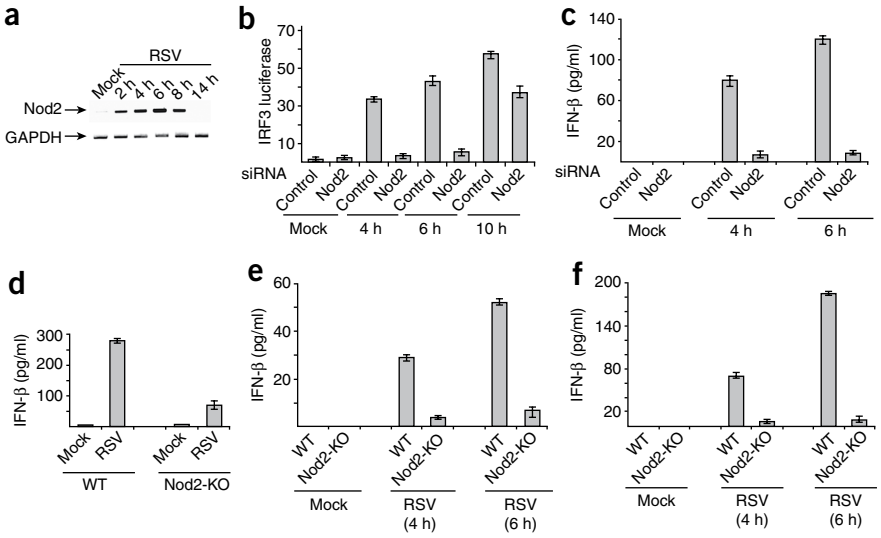

Figure 3 Nod2 is required for interferon production. (**a**) RT-PCR analysis of Nod2 expression in mock- and RSV-infected A549 cells. (**b**) Activation of an IRF3 luciferase reporter in mock- and RSV-infected A549 cells transfected with control or Nod2-specific siRNA (time after infection, below graph). (**c**) ELISA of IFN-β production by mock- and RSV-infected primary NHBE cells transfected with control or Nod2-specific siRNA. (**d**–**f**) ELISA of IFN-β production by mock- and RSV-infected alveolar macrophages (**d**), BMMs (**e**) and MEFs (**f**) isolated from wild-type or Nod2-deficient mice. Data are representative of three experiments (**a**) or three independent experiments (**b**–**f**; mean ± s.d.).

Indeed, as shown before[20], we found that RIG-I expression in A549 cells was detectable only at late time points after infection with RSV (**Supplementary Fig. 4c**). In addition, the early antiviral response was independent of RIG-I, because silencing of RIG-I had no effect in IFN-β expression during early RSV infection (**Supplementary Fig. 4d**,**e**). Like A549 cells, MEFs did not express abundant Nod2 until early time points after RSV infection, and RIG-I was undetectable until late time points after RSV infection (**Supplementary Fig. 4f**,**g**). Thus, temporal expression of Nod2 and RIG-I during early and late infection, respectively, may facilitate optimal sustained interferon production by virus-infected cells.

Next we examined the function of Nod2 in primary normal human bronchial epithelial cells (NHBE cells), as these cells constitute the main cell type infected by RSV in humans. RSV rapidly induced Nod2 expression in NHBE cells (**Supplementary Fig. 5**). Nod2 was essential for interferon production, as Nod2-specific siRNA markedly diminished IFN-β production by RSV-infected NHBE cells (**Fig. 3c**). We further established the critical function of Nod2 by demonstrating that BMMs, MEFs and alveolar macrophages derived from Nod2-deficient mice produced less IFN-β than did their wild-type counterparts after RSV infection (**Fig. 3d**–**f**). Nod2-deficient MEFs and BMMs also showed defective IFN-β production after infection with influenza A/PR/8/34 (H1N1) virus (**Supplementary Fig. 6**). Collectively these data show an important function for endogenous Nod2 in the induction of antiviral immune responses.

Nod2 interacts with viral ssRNA

We next investigated the function of viral ssRNA in Nod2 activation. Viral ssRNA genome isolated from purified RSV virion particles activated IRF3 only in Nod2-expressing cells (**Fig. 4a**). An intact ssRNA genome was required for Nod2 activation, as treatment of the viral ssRNA with RNAse abolished IRF3 activation (**Fig. 4a**). Viral ssRNA uses Nod2 for interferon production, as we found less IFN-β production after viral ssRNA treatment in MEFs and BMMs isolated from Nod2-deficient mice than in those from wild-type mice (**Fig. 4b**,**c**).

The function of viral ssRNA as an activator of Nod2 was further demonstrated by the interaction of viral ssRNA with Nod2 in a cellular milieu. We immunoprecipitated HA-Nod2 from RSV-infected 293 cells transfected with HA-Nod2 and amplified bound RNA with primers specific for either glyceraldehyde phosphate dehydrogenase (GAPDH; control) or RSV nucleocapsid protein. These experiments demonstrated association of Nod2 with viral RNA but not with control RNA (**Fig. 4d**). In a cell-free assay, we incubated HA-Nod2 bound to HA-agarose beads with RSV ssRNA genome or mRNA isolated

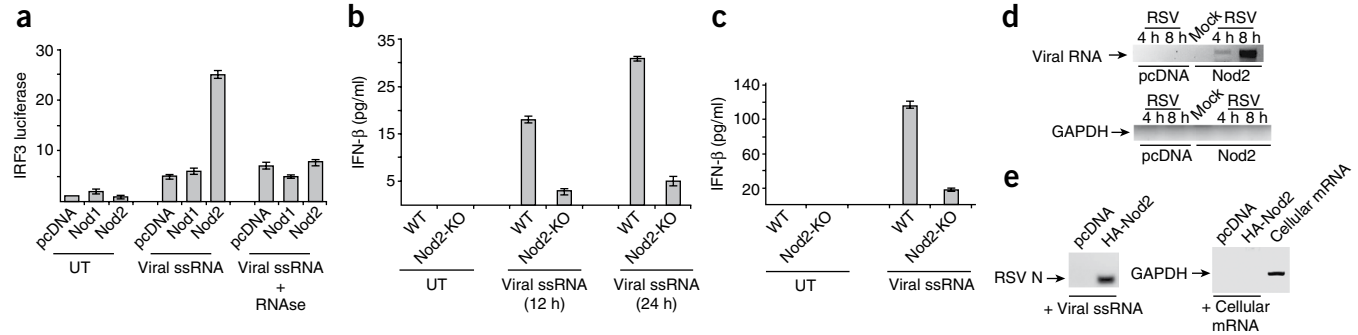

Figure 4 Activation of Nod2 by viral ssRNA. (**a**) Activation of an IRF3 luciferase reporter in 293 cells expressing pcDNA, HA-Nod1 and HA-Nod2 that were left untreated or stimulated with RSV viral ssRNA; + RNAse (below graph), viral ssRNA treated with RNAse. (**b**,**c**) ELISA of IFN-β production by wild-type or Nod2-deficient BMMs (**b**) and MEFs (**c**) left untreated or stimulated with viral ssRNA. (**d**) Association of Nod2 with RNA in 293 cells transfected with pcDNA or HA-Nod2 and then mock infected or infected with RSV; at 4 h or 8 h after infection, Nod2 was immunoprecipitated with anti-HA agarose and bound RNA was amplified with primers specific for RSV nucleocapsid protein (top) or GAPDH (bottom), followed by agarose gel electrophoresis. (**e**) Cell-free assay of HA-Nod2 bound to anti-HA agarose beads, incubated with RSV ssRNA (left) or total cellular mRNA (right); bound RNA was amplified with the primers in **d**, followed by agarose gel electrophoresis. Far right, total cellular mRNA amplified with GAPDH-specific primer (positive control). Data are representative of three independent experiments (**a**–**c**; mean ± s.d.) or two experiments (**d**,**e**).

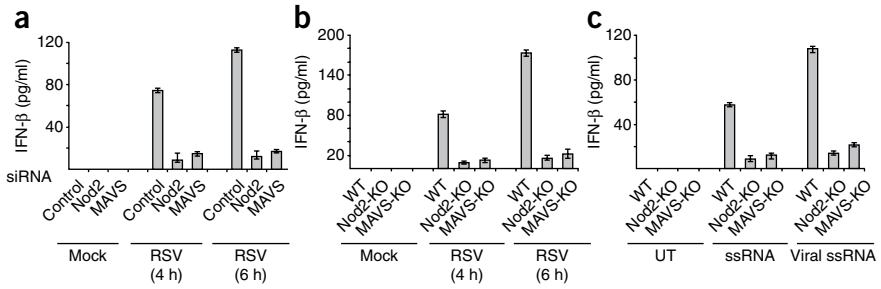

Figure 5 Function of MAVS during Nod2-mediated activation of the antiviral pathway. (**a**) ELISA of IFN-β production by mock- and RSV-infected primary NHBE cells transfected with control, Nod2-specific or MAVS-specific siRNA. (**b**) ELISA of IFN-β production by mock- and RSV-infected MEFs isolated from wild-type, Nod2-deficient or MAVS-deficient (MAVS-KO) mice. (**c**) ELISA of IFN-β production by MEFs left untreated or stimulated with synthetic ssRNA or viral (RSV) ssRNA. Data are representative of three independent experiments (mean ± s.d.).

from cells. After incubation, we amplified bound RNA with primers specific for either GAPDH or RSV nucleocapsid protein; we detected interaction of Nod2 with RSV ssRNA (**Fig. 4e**). In contrast, GAPDH mRNA (total cellular mRNA is enriched for this) did not associate with Nod2 (**Fig. 4e**). We also noted a failure of Nod1 to interact with viral ssRNA (data not shown). These results demonstrate that interaction of viral ssRNA with Nod2 results in its activation and subsequent induction of interferon production.

MAVS is required for Nod2-mediated responses

We next focused on the mechanism used by Nod2 to activate IRF3-interferon. As both RIG-I and Nod2 have caspase-recruitment domains (CARDs)[6–9], we speculated that similar to RIG-I, Nod2 may also interact with MAVS. In addition, a study has shown that the NLR family member NLRX1 interacts with mitochondria-localized MAVS through its NBD, a domain also found in Nod2 (ref. 11). The interaction of Nod2 with MAVS was essential for Nod2-mediated activation of antiviral responses, as MAVS-specific siRNA (**Supplementary Fig. 7**) and Nod2-specific siRNA (**Fig. 5a**) diminished RSV-induced production of IFN-β from infected NHBE cells to a similar extent. We obtained similar results with MEFs derived from MAVS-deficient mice infected with RSV or transfected with viral or synthetic ssRNA (**Fig. 5b**,**c**). Influenza A virus also required MAVS for interferon production, as IFN-β production by Nod2-deficient and MAVS-deficient

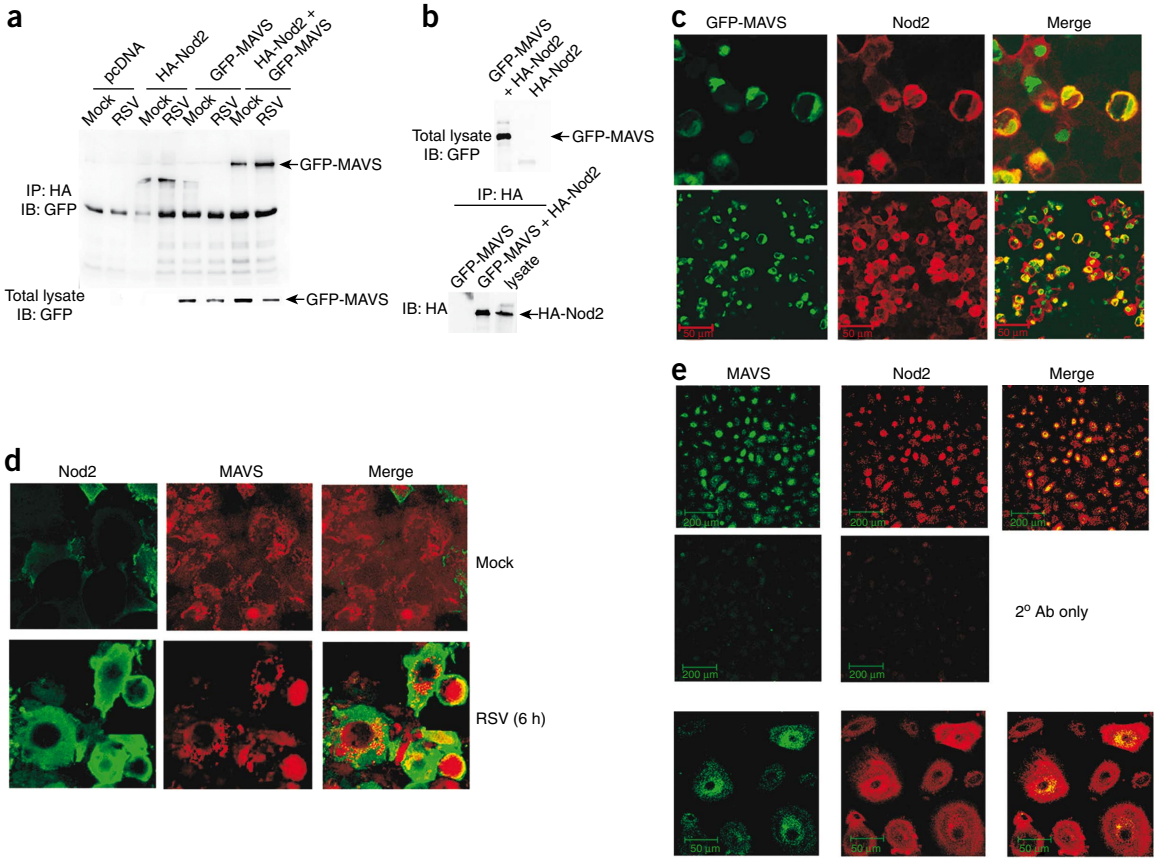

Figure 6 Interaction of MAVS with Nod2. (**a**) Immunoblot (IB) analysis of proteins immunoprecipitated (IP) with anti-HA–agarose beads from lysates of 293 cells transfected with pcDNA, HA-Nod2 and/or GFP-MAVS and mock infected or infected with RSV, probed with anti-GFP. Bottom, immunoblot analysis of 25 μg total cellular lysate with anti-GFP. (**b**) Immunoblot analysis of GFP-MAVS and HA-Nod2 in lysates (25 μg total cellular lysate protein probed with anti-GFP and anti-HA; top) and of HA-Nod2 bound to anti-HA agarose beads (bottom). (**c**) Confocal microscopy of RSV-infected (4 h) 293 cells coexpressing GFP-MAVS (green) and HA-Nod2 (red). (**d**,**e**) Confocal microscopy of mock- or RSV-infected (6 h) A549 cells (**d**) or RSV-infected (4 h) NHBE cells (**e**) stained with anti-Nod2 and anti-MAVS. Original magnification, ×40 (**c**, top row), ×20 (**c**, bottom row), ×40 (**d**), ×10 (**e**, top and middle rows) or ×40 (**e**, bottom row). Data are representative of three (**a**,**b**) or two (**c**–**e**) experiments.

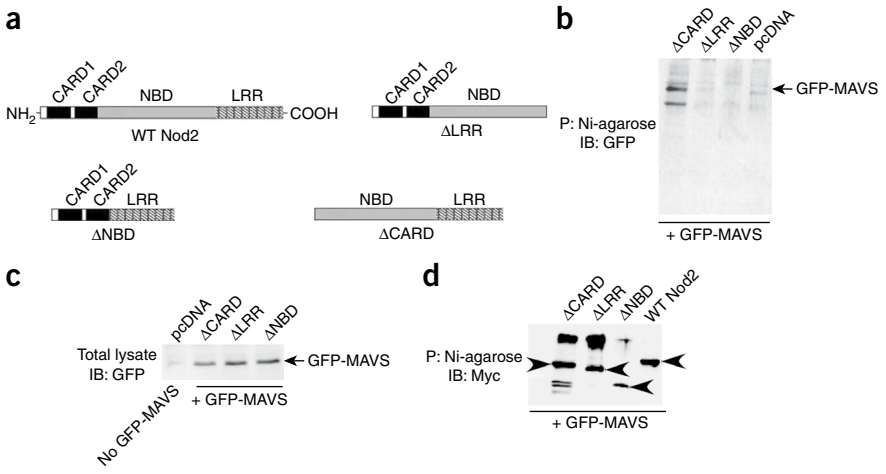

Figure 7 The NBD and LRR domains of Nod2 are essential for interaction with MAVS. (**a**) Nod2 constructs with deletion of specific domains. (**b**) Binding of Nod2 to MAVS in 293 cells expressing various His-Myc–tagged Nod2 constructs or pcDNA along with GFP-MAVS; cell lysates were incubated with nickel-agarose beads (Ni-agarose), then beads were washed and bound proteins were analyzed by immunoblot with anti-GFP. P, precipitation. (**c**) Immunoblot analysis of the expression of GFP-MAVS lysates of the cells in **b**, probed with anti-GFP. Far left, cells transfected with pcDNA only. (**d**) Immunoblot analysis of lysates of 293 cells expressing wild-type Nod2 or His-Myc–tagged Nod2 constructs along with GFP-MAVS, incubated with nickel-agarose, probed with anti-Myc to detect Nod2 constructs bound to the nickel-agarose beads. Arrowheads indicate wild-type Nod2 and deletion constructs of Nod2. Data are representative of three experiments.

MEFs was diminished to a similar extent after influenza A infection (**Supplementary Fig. 8**). These results demonstrate that MAVS is critical for virus-induced Nod2-mediated interferon production.

We next examined interaction of Nod2 with MAVS. Initially we investigated the ability of activated Nod2 to translocate to the mitochondria. Immunoblot analysis of mitochondrial extracts from RSV-infected Nod2-expressing cells showed that although approximately 6–7% of Nod2 was located in mitochondria in uninfected cells, RSV infection resulted in enrichment of Nod2 in mitochondria (40–45% of total cellular Nod2; **Supplementary Fig. 9a**,**b**). Immunofluorescence analysis also showed localization of endogenous Nod2 together with mitochondria in RSV-infected A549 cells (**Supplementary Fig. 9c**). To study the interaction of Nod2 with MAVS, we transfected 293 cells with HA-Nod2 and green fluorescent protein (GFP)-tagged MAVS. Coimmunoprecipitation analysis showed interaction of Nod2 with MAVS (**Fig. 6a**), and this interaction was enhanced after RSV infection. Cells had high expression of GFP-MAVS, as detected by immunoblot analysis of cell lysates with antibody to GFP (anti-GFP; **Fig. 6a**), and a substantial amount of HA-Nod2 was bound to the anti-HA–agarose beads used to precipitate the HA-Nod2–GFP-MAVS complex (**Fig. 6b**). In contrast to Nod2, Nod1 failed to interact with MAVS (**Supplementary Fig. 9d**). Double-labeling immunofluorescence studies with RSV-infected 293 cells expressing GFP-MAVS and HA-Nod2 confirmed the colocalization of Nod2 and MAVS (**Fig. 6c**). Similarly, RSV infection of A549 cells (**Fig. 6d**) and NHBE cells (**Fig. 6e**) enhanced the colocalization of endogenous Nod2 with endogenous MAVS. These results demonstrate that Nod2 interacts with MAVS during virus infection.

Nod2 can activate the NF-κB and mitogen-activated protein kinase pathways through the kinase RICK (also known as Rip2, CARDIAK, CCK or Ripk2)[21,22]. Bacterial products such as MDP specifically stimulate Nod2 and result in NF-κB activation via RICK. However, treatment of Nod2-expressing 293 cells with MDP did not activate IRF3 (**Supplementary Fig. 10a**). Likewise, treatment of NHBE cells and BMMs with MDP did not result in IFN-β production (**Supplementary Fig. 10b**,**c**). In addition, RICK may not be important in interferon induction by Nod2, as silencing of endogenous RICK expression did not alter Nod2-mediated production of IFN-β in RSV-infected cells (**Supplementary Fig. 11**). We also examined the efficiency of the interaction between Nod2 and MAVS relative to that of RIG-I and MAVS. Although both Nod2 and RIG-I associated with MAVS, the RIG-I–MAVS interaction was slightly more efficient than the Nod2-MAVS interaction (**Supplementary Fig. 12a**). In addition, we also noted that in RSV-infected cells, Nod2 interacted more efficiently with MAVS than with RICK (**Supplementary Fig. 12b**). However, Nod2 efficiently interacted with RICK in cells stimulated with the well-established Nod2 stimulator MDP (**Supplementary Fig. 12b**). Thus, we speculate that Nod2 uses either RICK or MAVS, depending on the stimulus (for example, MDP versus ssRNA) to activate either IRF3 or NF-κB.

In addition to IRF3, NF-κB activation is required for the expression of interferon genes. Although IRF3 alone is able to induce the transcription of interferon genes, the transactivating function of NF-κB acts synergistically with IRF3 to promote optimal interferon expression[23]. This is also true for Nod2-mediated interferon expression, as suppressing NF-κB activity in RSV-infected cells diminished interferon expression via activated Nod2 by 30–35%; as expected, expression of the NF-κB-dependent TNF gene in RSV-infected cells was diminished by 80% (**Supplementary Fig. 13**). On the basis of these results, we speculate that Nod2 activated by stimulation with viral ssRNA interacts with MAVS to induce activation of both IRF3 and NF-κB in a way similar to that of RLHs[6]. In contrast, Nod2 activated by bacterial products (such as MDP) activates NF-κB via RICK. Further detailed studies are needed to investigate the function of Nod2 in activating the NF-κB pathway during virus infection and the function of MAVS and RICK during these events.

MAVS interacts with the LRR-NBD domains of Nod2

The CARD of RIG-I promotes its association with MAVS, whereas NLRX1 uses its NBD to interact with MAVS. Thus, we next investigated the function of the NBD, CARD and LRR domains of Nod2 in MAVS association. For these studies, we generated various Nod2 deletion mutants tagged with both histidine (His) and Myc:ΔCARD (a Nod2 mutant lacking both CARDs), ΔNBD (a Nod2 mutant lacking the NBD) and ΔLRR (a Nod2 mutant lacking the LRR domain; **Fig. 7a**). We expressed these mutants in 293 cells along with GFP-MAVS. We obtained lysates of these cells and precipitated the lysates with nickel-agarose beads and, after washing the beads, analyzed the proteins bound to the beads by immunoblot with anti-GFP. Although ΔCARD was able to interact with MAVS, neither ΔNBD nor ΔLRR associated with MAVS (**Fig. 7b**). The various Nod2 mutant–expressing cells expressed similar amounts of GFP-MAVS (**Fig. 7c**). In addition, similar amounts of His-Myc–tagged Nod2 mutants were bound to the nickel-agarose beads in the experimental conditions used to study the interaction of MAVS with the Nod2 mutants (**Fig. 7d**). These results indicate that unlike RIG-I, the CARDs

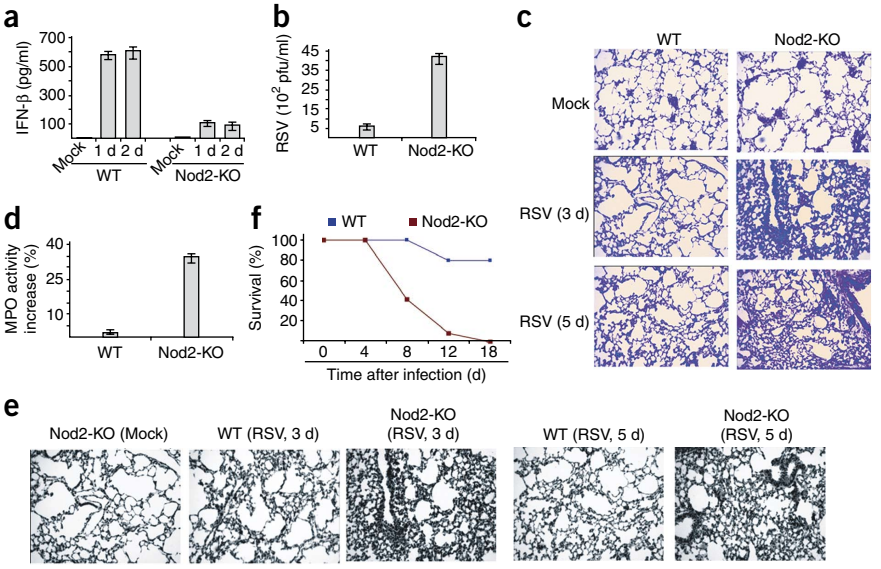

Figure 8 Nod2 is essential for host defense against viral infection. (**a**) IFN-β concentrations in BAL fluid of mock- or RSV-infected wild-type and Nod2-deficient mice ($n = 4$ mice per group). $P < 0.05$ (*t*-test for data normally distributed; Mann-Whitney rank sum test for data not normally distributed). (**b**) RSV titers in the BAL fluid of wild-type and Nod2-deficient mice at 3 d after infection. $P < 0.05$ (*t*-test for data normally distributed; Mann-Whitney rank sum test for data not normally distributed). (**c**) Hematoxylin and eosin staining of lung sections from mock- or RSV-infected wild-type and Nod2-deficient mice. Original magnification, ×10. (**d**) Neutrophil sequestration in lungs, assessed by MPO activity assay of total lung homogenates of RSV-infected wild-type and Nod2-deficient mice ($n = 5$ mice per group; 10 mice total) at 2 d after infection, presented relative to activity in mock-infected mice. $P < 0.05$. (**e**) TUNEL staining of lung sections from RSV-infected wild-type and Nod2-deficient mice. Original magnification, ×10. (**f**) Survival of wild-type and Nod2-deficient mice infected with RSV (5×10^8 PFU per mouse). $P > 0.02$, Nod2-deficient versus wild-type (Wilcoxon test). Data are representative of three (**a**,**b**,**d**) or four (**c**,**e**,**f**) experiments (mean ± s.e.m in **a**,**b**,**d**).

of Nod2 are not important for its interaction with MAVS. However, the NBD and LRR domains of Nod2 are required for the MAVS association. We further confirmed that conclusion by examining the functionality of the Nod2 mutants in activating IRF3. Infection of 293 cells transfected with either wild-type or mutant (ΔCARD, ΔNBD or ΔLRR) Nod2 constructs showed that wild-type Nod2 and ΔCARD induced IRF3 activation after infection with RSV, but neither ΔNBD nor ΔLRR did so (**Supplementary Fig. 14**).

Function of Nod2 in the host antiviral defense

Finally, we assessed the physiological function of Nod2 by infecting wild-type and Nod2-deficient mice with RSV. The mouse model of RSV infection mimics virus infection in humans, as infected mice can develop disease states resembling pneumonia[24,25]; in addition, RSV-infected mice induce a robust antiviral response in the respiratory tract characterized by production of IFN-β and expression of interferon-dependent genes such as *Mx1* during early RSV infection (within 12 h of infection)[24–30]. Moreover, RSV is sensitive to interferon in infected mice, as a dose of interferon as low as 200 units per ml inhibits RSV infection in mice by 100-fold (ref. 26). During RSV infection of the mouse respiratory tract, interferon is induced early during infection (at 12 h to 2 d after infection), but its production is lost at 3 d after infection[24–30]. This observation suggests that interferon is important in restricting the spread of RSV during early infection and that the production of interferon dictates the clinical outcome of the disease (for example, lung inflammation and apoptosis of airway cells).

We infected wild-type and Nod2-deficient mice with a sublethal dose of RSV (5×10^6 plaque-forming units per mouse, delivered by intranasal inoculation), then collected lungs and bronchoalveolar lavage (BAL) fluid at various times. We found expression of mouse Nod2 in RSV-infected lungs at 1 d after infection, and this expression was lost at 4 d after infection (**Supplementary Fig. 15a**). This result suggests an important function for Nod2 in interferon expression, as the interferon-induction kinetics correlated with the Nod2-expression kinetics[24–30]. Nod2-deficient mice had lower IFN-β production in the respiratory tract and higher viral titers than did wild-type mice (**Fig. 8a**,**b**).

It is well known that RSV causes lung disease by inducing pneumonia, a massive inflammation of the lungs[31]. A larger viral burden ultimately results in enhanced inflammation and exaggerated lung disease due to flooding of alveolar spaces with edema fluid. This occurs as a result of enhanced permeability of the epithelial barrier due to apoptosis of airway epithelial cells. RSV infection resulted in more severe lung pathology in Nod2-deficient mice, as shown by staining of lung sections with hematoxylin and eosin at 3 and 5 d after infection (**Fig. 8c**). We noted massive peribronchial lymphocytic inflammation and filling of the lumen with exudates of infiltrating neutrophils and mucus. Neutrophils constitute the main immune cells infiltrating the lung of RSV-infected mice and humans and a large number of these cells in the airway causes severe immunopathology associated with RSV clinical disease[32–34]. To examine neutrophil accumulation in the lungs, we did a myeloperoxidase (MPO) activity assay[35,36] with lung homogenates of RSV-infected wild-type and Nod2-deficient mice. Greater RSV-induced enhancement of neutrophil activity was visible in the lung tissue of Nod2-deficient mice (~35%) than in that of wild-type mice (~4%; **Fig. 8d**). The enhanced inflammation in the respiratory tract of Nod2-deficient mice was also confirmed by higher concentrations of proinflammatory cytokines and chemokines (such as tumor necrosis factor, IL-10 and RANTES) in the BAL fluid of infected Nod2-deficient than in that of wild-type mice (**Supplementary Fig. 15b–d**). A high RSV load has been associated with enhanced apoptosis of airway epithelial cells and infiltrating neutrophil granulocytes, which contributes to the development of lung lesions and injury[37]. Indeed, *in situ* apoptosis analysis of lung sections by TUNEL (terminal deoxynucleotidyl transferase–mediated dUTP nick end-labeling) showed enhanced apoptosis in the lungs of RSV-infected Nod2-deficient mice relative to that in the lungs of RSV-infected wild-type mice (**Fig. 8e**).

Notably, RSV-infected Nod2-deficient mice lost considerably more body weight and had diminished survival relative to their wild-type counterparts (**Fig. 8f** and **Supplementary Fig. 16**). We also found less IFN-β production in the BAL fluid of influenza A virus–infected Nod2-deficient mice than in that of influenza A virus–infected wild-type mice (**Supplementary Fig. 17**). These results demonstrated that Nod2 is a critical component of host antiviral defense mechanisms.

DISCUSSION

In the present study we have identified Nod2 as a viral PRR that can sense viral ssRNA to activate interferon production and antiviral defense. Like RLH receptors, Nod2 associated with MAVS to activate IRF3 and promote interferon production. The importance of Nod2 in host defense was evident from the ability of both cells of the immune response (for example, macrophages) and cells not of the immune response (for example, epithelial cells and MEFs) to use Nod2 for interferon production. The *in vivo* importance of Nod2 in antiviral responses was evident from the enhanced RSV-induced pathogenesis in infected Nod2-deficient mice.

Other PRRs, including RIG-I, may also be involved in activating an antiviral response against paramyxoviruses like RSV[20]. For some time, the *in vivo* relevance of RIG-I in antiviral function was not documented because of the embryonic death of most RIG-I-deficient mice[38]. However, one strain of RIG-I-deficient mice generated by crossing RIG-I-heterozygous mice with ICR outbred mice, followed by intercrossing of the resultant RIG-I-heterozygous mice[38], survives to adulthood. These RIG-I-deficient mice show impaired interferon production and enhanced susceptibility to two positive-sense ssRNA viruses: encephalomyocarditis virus and Japanese encephalitis virus[38]. However, no studies have been done to demonstrate the importance of RIG-I in activating the antiviral host defense apparatus against negative-sense ssRNA viruses (such as paramyxoviruses).

Uninfected mice have low Nod2 expression[39], and we have shown that its expression increased after viral infection. Our observation is similar to those of published studies demonstrating that most PRRs (such as RIG-I) have low expression but their expression is higher after pathogen invasion[40,41]. Similarly, we found that viruses mediated the induction of Nod2 in various cells. Although in our studies we noted induction of Nod2 in virus-infected MEFs, one study has reported that MDP is unable to induce Nod2 expression in wild-type MEFs; this observation may have been due to a defect in MDP transport to the cytoplasm[42]. Several other studies have shown that Nod2 expression is stimulated by various bacteria and bacterial components[40,41]. Similarly, expression of RIG-I (ref. 43) and Mda-5 (ref. 38) in uninfected, unstimulated wild-type MEFs is negligible, but treatment of cells with PAMPs results in upregulation of RIG-I expression[43]. This mechanism of restricting expression of PRRs in unstimulated cells may be critical for preventing uncontrolled inflammation.

Although Nod2 can be activated by MDP[7–10], so far no studies have demonstrated direct binding of MDP to Nod2; it is known only that lack of Nod2 expression results in loss of MDP responsiveness. Thus, MDP could directly interact with Nod2 or associate with a protein or proteins that form a complex with Nod2. In that context, the interaction of viral ssRNA with Nod2 demonstrated here could also be mediated indirectly via 'bridging' proteins. Interaction of the ssRNA genomes of viruses with RIG-I has also been noted before[44,45]. In addition to Nod2, cryopyrin (Nalp3), another NLR protein, activates the inflammasome and leads to IL-1 production after stimulation with bacterial and viral (influenza A) RNA[46–48]. Although NLRs such as cryopyrin[46–48] and NLRX1 (ref. 11) serve an important function in innate immunity by activating the inflammasome and inhibiting interferon production, respectively, no studies have determined whether other NLRs, such as Nod2, can directly contribute to antiviral responses by inducing interferon production.

Published studies have shown that transfection of Nod2 alone (in the absence of any stimulant) into wild-type MEFs results in substantial NF-κB activation[49]. However, we found that overexpression of Nod2 in 293 cells did not induce marked activation of IRF3 in the absence of external stimuli (such as RSV or synthetic or viral ssRNA). Thus, it seems that Nod2-mediated activation of IRF3 is stimulus dependent, whereas RICK activation is stimulus independent. In summary, our findings have demonstrated that in addition to RIG-I, Mda5 and TLRs, Nod2 can also function as a viral PRR and participate in inducing antiviral signaling. Distinct temporal activation of various PRRs may be needed to generate optimal antiviral responses, and various viruses may trigger the induction of different classes of PRRs.

METHODS

Methods and any associated references are available in the online version of the paper at http://www.nature.com/natureimmunology/.

Note: Supplementary information is available on the Nature Immunology website.

ACKNOWLEDGMENTS

We thank K. Li (University of Tennessee Health Science Center) for reagents; A. Garcia-Sastre (Mount Sinai School of Medicine) for influenza A virus; Z.J. Chen (University of Texas Southwestern Medical Center) for MAVS-deficient MEFs; the Core Optical Imaging Facility (University of Texas Health Science Center at San Antonio) for confocal images; and K. Moncada Gorena and C. Thomas in the Flow Cytometry Core Facility (supported by the National Institutes of Health (P30 CA54174 to the San Antonio Cancer Institute; P30 AG013319 to the Nathan Shock Center; and P01AG19316)) for flow cytometry. Supported by National Institutes of Health (AI069062 to S.B., CA129246 to S.B. and T32-DE14318 to A.S. and AI067716 to P.H.D.) and the American Lung Association (RG-49629-N to S.B. and AI067716 to P.H.D.).

AUTHOR CONTRIBUTIONS

A.S. and S.B. designed the experiments and prepared the manuscript; A.S. and T.H.C. did the experiments; R.H. provided technical assistance and did several experiments; Y.X. did the experiments with vaccinia virus; V.F. did the immunofluorescence analysis; K.T. did the studies with mouse embryo fibroblasts; and P.H.D. did the MPO assay.

Published online at http://www.nature.com/natureimmunology/.
Reprints and permissions information is available online at http://npg.nature.com/reprintsandpermissions/.

1. Kawai, T. & Akira, S. Innate immune recognition of viral infection. *Nat. Immunol.* **7**, 131–137 (2006).
2. Bose, S. & Banerjee, A.K. Innate immune response against nonsegmented negative strand RNA viruses. *J. Interferon Cytokine Res.* **23**, 401–412 (2003).
3. Stark, G.R., Kerr, I.M., Williams, B.R.G., Silverman, R.H. & Schreiber, R.D. How cells respond to interferons. *Annu. Rev. Biochem.* **67**, 227–264 (1998).
4. Uematsu, S. & Akira, S. Toll-like receptors and type I interferons. *J. Biol. Chem.* **282**, 15319–15323 (2007).
5. O'Neill, L.A. How Toll-like receptors signal: what we know and what we don't know. *Curr. Opin. Immunol.* **18**, 3–9 (2006).
6. Basler, C.F. & Garcia-Sastre, A. Sensing RNA virus infections. *Nat. Chem. Biol.* **3**, 20–21 (2007).
7. Martinon, F. & Tschopp, J. NLRs join TLRs as innate sensors of pathogens. *Trends Immunol.* **26**, 447–454 (2005).
8. Fritz, J.H., Ferrero, R.L., Philpott, D.J. & Girardin, S.E. Nod-like proteins in immunity, inflammation and disease. *Nat. Immunol.* **7**, 1250–1257 (2006).
9. Kanneganti, T.D., Lamkanfi, M. & Núñez, G. Intracellular NOD-like receptors in host defense and disease. *Immunity* **27**, 549–559 (2007).
10. Franchi, L., Warner, N., Viani, K. & Nuñez, G. Function of Nod-like receptors in microbial recognition and host defense. *Immunol. Rev.* **227**, 106–128 (2009).
11. Moore, C.B. *et al.* NLRX1 is a regulator of mitochondrial antiviral immunity. *Nature* **451**, 573–577 (2008).
12. Tattoli, I. *et al.* NLRX1 is a mitochondrial NOD-like receptor that amplifies NF-κB and JNK pathways by inducing reactive oxygen species production. *EMBO Rep.* **9**, 293–300 (2008).
13. Kota, S. *et al.* Role of human β defensin-2 during tumor necrosis factor-α/NF-κB mediated innate anti-viral response against human respiratory syncytial virus. *J. Biol. Chem.* **283**, 22417–22429 (2008).
14. Voss, E. *et al.* NOD2/CARD15 mediates induction of the antimicrobial peptide human β-defensin-2. *J. Biol. Chem.* **281**, 2005–2011 (2006).
15. Hall, C.B. Respiratory syncytial virus and parainfluenza virus. *N. Engl. J. Med.* **344**, 1917–1928 (2001).
16. Falsey, A.R., Hennessey, P.A., Formica, M.A., Cox, C. & Walsh, E.E. Respiratory syncytial virus infection in elderly and high-risk adults. *N. Engl. J. Med.* **352**, 1749–1759 (2005).
17. Bose, S., Malur, A. & Banerjee, A.K. Polarity of human parainfluenza virus type 3 infection in polarized human lung epithelial A549 cells: Role of microfilament and microtubule. *J. Virol.* **75**, 1984–1989 (2001).

18. Bose, S., Kar, N., Maitra, R., DiDonato, J.A. & Banerjee, A.K. Temporal activation of NF-κB regulates an interferon-independent innate antiviral response against cytoplasmic RNA viruses. *Proc. Natl. Acad. Sci. USA* **100**, 10890–10895 (2003).
19. Jamaluddin, M. *et al.* IFN-β mediates coordinate expression of antigen-processing genes in RSV-infected pulmonary epithelial cells. *Am. J. Physiol. Lung Cell. Mol. Physiol.* **280**, L248–L257 (2001).
20. Liu, P. *et al.* Retinoic acid-inducible gene I mediates early antiviral response and Toll-like receptor 3 expression in respiratory syncytial virus-infected airway epithelial cells. *J. Virol.* **81**, 1401–1411 (2007).
21. Inohara, N., Ogura, Y. & Nuñez, G. Nods: a family of cytosolic proteins that regulate the host response to pathogens. *Curr. Opin. Microbiol.* **5**, 76–80 (2002).
22. Franchi, L. *et al.* Intracellular NOD-like receptors in innate immunity, infection and disease. *Cell. Microbiol.* **10**, 1–8 (2008).
23. Wathelet, M.G. *et al.* Virus infection induces the assembly of coordinately activated transcription factors on the IFN-β enhancer in vivo. *Mol. Cell* **1**, 507–518 (1998).
24. Jafri, H.S. *et al.* Respiratory syncytial virus induces pneumonia, cytokine response, airway obstruction, and chronic inflammatory infiltrates associated with long-term airway hyperresponsiveness in mice. *J. Infect. Dis.* **189**, 1856–1865 (2004).
25. Bolger, G. *et al.* Primary infection of mice with high titer inoculum respiratory syncytial virus: characterization and response to antiviral therapy. *Can. J. Physiol. Pharmacol.* **83**, 198–213 (2005).
26. Guerrero-Plata, A. *et al.* Activity and regulation of α interferon in respiratory syncytial virus and human metapneumovirus experimental infections. *J. Virol.* **79**, 10190–10199 (2005).
27. Guerrero-Plata, A., Casola, A. & Garofalo, R.P. Human metapneumovirus induces a profile of lung cytokines distinct from that of respiratory syncytial virus. *J. Virol.* **79**, 14992–14997 (2005).
28. Pletneva, L.M., Haller, O., Porter, D.D., Prince, G.A. & Blanco, J.C. Induction of type I interferons and interferon-inducible Mx genes during respiratory syncytial virus infection and reinfection in cotton rats. *J. Gen. Virol.* **89**, 261–270 (2008).
29. Chávez-Bueno, S. *et al.* Respiratory syncytial virus-induced acute and chronic airway disease is independent of genetic background: an experimental murine model. *Virol. J.* **2**, 46 (2005).
30. Castro, S.M. *et al.* Antioxidant treatment ameliorates respiratory syncytial virus-induced disease and lung inflammation. *Am. J. Respir. Crit. Care Med.* **174**, 1361–1369 (2006).
31. Hippenstiel, S., Opitz, B., Schmeck, B. & Suttorp, N. Lung epithelium as a sentinel and effector system in pneumonia--molecular mechanisms of pathogen recognition and signal transduction. *Respir. Res.* **7**, 97 (2006).
32. Yasui, K. *et al.* Neutrophil-mediated inflammation in respiratory syncytial viral bronchiolitis. *Pediatr. Int.* **47**, 190–195 (2005).
33. Wang, S.Z. & Forsyth, K.D. The interaction of neutrophils with respiratory epithelial cells in viral infection. *Respirology* **5**, 1–10 (2000).
34. Wang, S.Z. *et al.* Neutrophils induce damage to respiratory epithelial cells infected with respiratory syncytial virus. *Eur. Respir. J.* **12**, 612–618 (1998).
35. Bubeck, S.S., Cantwell, A.M. & Dube, P.H. Delayed inflammatory response to primary pneumonic plague occurs in both outbred and inbred mice. *Infect. Immun.* **75**, 697–705 (2007).
36. Wilmott, R.W., Kitzmiller, J.A., Fiedler, M.A. & Stark, J.M. Generation of a transgenic mouse with lung-specific overexpression of the human interleukin-1 receptor antagonist protein. *Am. J. Respir. Cell Mol. Biol.* **18**, 429–434 (1998).
37. Welliver, T.P. *et al.* Severe human lower respiratory tract illness caused by respiratory syncytial virus and influenza virus is characterized by the absence of pulmonary cytotoxic lymphocyte responses. *J. Infect. Dis.* **195**, 1126–1136 (2007).
38. Kato, H. *et al.* Differential roles of MDA5 and RIG-I helicases in the recognition of RNA viruses. *Nature* **441**, 101–105 (2006).
39. Opitz, B. *et al.* Nucleotide-binding oligomerization domain proteins are innate immune receptors for internalized *Streptococcus pneumoniae*. *J. Biol. Chem.* **279**, 36426–36432 (2004).
40. Matikainen, S. *et al.* Tumor necrosis factor alpha enhances influenza A virus-induced expression of antiviral cytokines by activating RIG-I gene expression. *J. Virol.* **80**, 3515–3522 (2006).
41. Le Goffic, R., Pothlichet, J., Vitour, D., Fujita, T., Meurs, E., Chignard, M. & Si-Tahar, M. Influenza A virus activates TLR3-dependent inflammatory and RIG-I-dependent antiviral responses in human lung epithelial cells. *J. Immunol.* **178**, 3368–3372 (2007).
42. Abbott, D.W. *et al.* Coordinated regulation of Toll-like receptor and NOD2 signaling by K63-linked polyubiquitin chains. *Mol. Cell. Biol.* **27**, 6012–6025 (2007).
43. Wang, J. *et al.* Retinoic acid-inducible gene-I mediates late phase induction of TNF-α by lipopolysaccharide. *J. Immunol.* **180**, 8011–8019 (2008).
44. Hornung, V. *et al.* 5′-Triphosphate RNA is the ligand for RIG-I. *Science* **314**, 994–997 (2006).
45. Pichlmair, A. *et al.* RIG-I-mediated antiviral responses to single-stranded RNA bearing 5′-phosphates. *Science* **314**, 997–1001 (2006).
46. Kanneganti, T.D. *et al.* Bacterial RNA and small antiviral compounds activate caspase-1 through cryopyrin/Nalp3. *Nature* **440**, 233–236 (2006).
47. Kanneganti, T.D. *et al.* Critical role for Cryopyrin/Nalp3 in activation of caspase-1 in response to viral infection and double-stranded RNA. *J. Biol. Chem.* **281**, 36560–36568 (2006).
48. Ichinohe, T., Lee, H.K., Ogura, Y., Flavell, R. & Iwasaki, A. Inflammasome recognition of influenza virus is essential for adaptive immune responses. *J. Exp. Med.* **206**, 79–87 (2009).
49. Kobayashi, K. *et al.* RICK/Rip2/CARDIAK mediates signalling for receptors of the innate and adaptive immune systems. *Nature* **416**, 194–199 (2002).

ONLINE METHODS

Viruses and cell culture. RSV (A2 strain) and VSV were propagated in HeLa and BHK cells, respectively[13,18]. Influenza A virus (A/PR/8/34 (H1N1)) was grown in the allantoic cavities of 10-day-old embryonated eggs. All viruses were purified by centrifugation (twice) on discontinuous sucrose gradients. A549 and 293 cells were maintained in DMEM supplemented with 10% (vol/vol) FBS, penicillin, streptomycin and glutamine. Primary NHBE cells (from Lonza) were maintained in bronchial epithelial growth medium according to the supplier's instruction.

Luciferase assay. First, 293 cells were transfected (Lipofectamine 2000; Invitrogen) with 1 μg of various plasmids (HA-Nod2, HA-Nod1, pcDNA6.1, IRF3-luciferase or IFN-β–luciferase) and 100 ng pRL-null–renilla luciferase. The cells were then infected or treated with RSV, ssRNA or CpG DNA. A549 cells were transfected (Lipofectamine 2000; Invitrogen) with 80 nM Nod2-specific siRNA or control siRNA. At 24 h after siRNA transfection, cells were cotransfected with pRL-null–renilla luciferase (100 ng), IRF3-luciferase (1 μg) or IFN-β–luciferase (1 μg). After 24 h, cells were infected with RSV (multiplicity of infection (MOI), 0.5) or were treated with ssRNA40-LyoVec (1 μg/ml; Invivogen) for various times. Luciferase activity was measured with the Dual-Luciferase Reporter Assay system according to the manufacturer's protocol (Promega). Transfection efficiency was normalized by comparison to expression of renilla luciferase. Luciferase units are presented as relative luciferase activity, which represents the 'fold induction' of luciferase activity after subtraction of the background (cells transfected with pRL-renilla-luciferase plasmid only).

RT-PCR. Primers for detecting the various genes by RT-PCR are in **Supplementary Table 1**.

Generation of siRNA. All siRNA was from Qiagen (sequences, **Supplementary Table 1**). AllStars Negative Control siRNA (proprietary sequence; 1027281; from Qiagen) was used as a negative control. A549 or 293 cells were transfected with siRNA using Lipofectamine 2000 (Invitrogen) and NHBE cells were transfected with siRNA using PrimeFect Primary Cell siRNA Transfection reagent according to the manufacturer's protocol (Lonza).

Viral infection. A549 or 293 cells were infected with purified RSV (MOI, 0.5) in serum-free antibiotic free Opti-MEM (Gibco). After adsorption for 1.5 h at 37 °C, cells were washed twice with serum containing DMEM and infection was continued for various times in the presence of serum-containing DMEM. MEFs were infected with purified RSV or influenza A (A/PR/8/34 virus) at an MOI of 1 in serum-free, antibiotic-free Opti-MEM.

Coimmunoprecipitation. After 293 cells were transfected with various tagged constructs, they were infected with RSV. Cell pellets were lysed (in TBS containing 1% (vol/vol) Triton X-100) and sonicated. All lysates were incubated for 12 h at 4 °C with monoclonal anti-HA agarose beads (HA-7; Sigma-Aldrich). Proteins bound to washed anti-HA–agarose were eluted at a pH of 2.8. Eluted proteins were analyzed by immunoblot with anti-GFP (sc-9996; Santa Cruz) or monoclonal anti-HA (HA-7; Sigma).

Immunofluorescence analysis. Cells plated on four-well glass chamber slides were transfected with various tagged constructs. Cells were then infected for 4 h or 6 h with RSV (MOI, 1). After infection, cells were fixed with 3.7% (wt/vol) formaldehyde and were made permeable and blocked in permeabilization buffer containing 0.2% (vol/vol) Triton X-100 and 3% (wt/vol) BSA and then were incubated for 1 h at 37 °C with monoclonal anti-HA (Sigma), monoclonal anti-Nod2 (2D9; Cayman Chemical) or anti-MAVS (3993; Cell Signaling Technology). The washed cells were then incubated with secondary antibody (Vector Laboratories). Finally, the washed cells were mounted and then imaged with an LSM510 META laser-scanning confocal microscopy (Zeiss).

Interaction of Nod2 with viral ssRNA. After 293 cells were transfected with HA-Nod2, they were infected with RSV. Lysates were immunoprecipitated for 4 h at 4 °C with anti-HA–agarose. After beads were washed with TBS, Tri reagent (TRIzol; Sigma-Aldrich) was added for isolation of bound RNA. Primers specific for RSV nucleocapsid protein or GAPDH were used for RT-PCR. For the cell-free interaction assay, lysates of 293 cells expressing HA-Nod2 were incubated with HA–agarose beads. HA-Nod2 bound to the beads was incubated for 45 min at 4 °C with RSV ssRNA or total cellular mRNA (isolated with an RNeasy Mini kit; Qiagen). Beads were washed and RNA isolated from the washed beads was amplified with primers described above.

Virus infection of mice. Animal studies were approved by the Institutional Animal Care and Use Committee of The University of Texas Health Science Center at San Antonio. Pathogen-free C57BL/6 mice and Nod2-deficient mice (C57BL/6J background) 6–8 weeks old were obtained from The Jackson Laboratory. These Nod2-deficient mice were further back-crossed to the C57BL/6 background for a total of eight generations. Genome-wide single-nucleotide polymorphism analysis of these mice (Harlan Laboratories) showed that wild-type and Nod2-deficient mice are genetically identical, except for the Nod2 deletion (data not shown). Mice were anesthetized with inhaled methoxyfluorane and were inoculated intranasally with RSV (5×10^6 PFU per mouse) in 100 μl low-serum Opti-MEM (Invitrogen). Uninfected control mice were 'sham inoculated' with 100 μl Opti-MEM. For another set of studies, mice were infected intranasally with RSV (5×10^8 PFU per mouse) and the survival of infected mice was monitored for 18 d.

TUNEL and MPO assay. Formalin-fixed lungs were stained with an *in situ* TUNEL assay kit Dead End Colorimetric TUNEL system (Promega). Lung neutrophil content was assessed by measurement of MPO activity[35,36].

Generation of Nod2 mutants. Nod2 cDNA was cloned into the pcDNA6-Myc-His vector (Invitrogen) and deletion mutants of Nod2 were constructed by PCR.

Treatment with synthetic and viral ssRNA. Cells were treated with synthetic ssRNA (1 μg/ml) already conjugated with the transfection reagent (ssRNA40-LyoVec; Invivogen). For isolation of viral ssRNA, purified RSV virion particles were centrifuged for 4 h at 28,000 r.p.m. with an SW32Ti rotor. The ssRNA genome was isolated from the viral pellet with the RNeasy Mini kit. Cells were transfected with viral ssRNA using Lipofectamine 2000 (Invitrogen).

Isolation of MEFs and macrophages. Alveolar macrophages were collected by centrifugation of BAL fluid at 1,300*g* for 10 min at 4 °C. After being washed, cell pellets were seeded in 24-well plates. MEFs were prepared as described[50]. BMMs were obtained from femurs and tibias of wild-type and Nod2-deficient mice and were cultured for 6–8 d.

ELISA. Human or mouse IFN-β-specific ELISA kits (PBL InterferonSource) were used for ELISA.

50. Tominaga, K. *et al.* MRG15 regulates embryonic development and cell proliferation. *Mol. Cell. Biol.* **25**, 2924–2937 (2005).

JOURNAL OF VIROLOGY, Sept. 2008, p. 8465–8475 Vol. 82, No. 17
0022-538X/08/$08.00+0 doi:10.1128/JVI.00918-08

Interferon Regulatory Factor IRF-7 Induces the Antiviral Alpha Interferon Response and Protects against Lethal West Nile Virus Infection▽

Stephane Daffis,[1] Melanie A. Samuel,[2] Mehul S. Suthar,[4] Brian C. Keller,[4] Michael Gale, Jr.,[4] and Michael S. Diamond[1,2,3]*

Departments of Medicine,[1] Molecular Microbiology,[2] and Pathology & Immunology,[3] Washington University School of Medicine, St. Louis, Missouri 63110, and Department of Immunology, University of Washington School of Medicine, Seattle, Washington 98195-7650[4]

Received 2 May 2008/Accepted 4 June 2008

Type I interferon (IFN-α/β) comprises a family of immunomodulatory cytokines that are critical for controlling viral infections. In cell culture, many RNA viruses trigger IFN responses through the binding of RNA recognition molecules (RIG-I, MDA5, and TLR-3) and induction of interferon regulatory factor IRF-3-dependent gene transcription. Recent studies with West Nile virus (WNV) have shown that type I IFN is essential for restricting infection and that a deficiency of IRF-3 results in enhanced lethality. However, IRF-3 was not required for optimal systemic IFN production in vivo or in vitro in macrophages. To begin to define the transcriptional factors that regulate type I IFN after WNV infection, we evaluated IFN induction and virus control in IRF-7$^{-/-}$ mice. Compared to congenic wild-type mice, IRF-7$^{-/-}$ mice showed increased lethality after WNV infection and developed early and elevated WNV burdens in both peripheral and central nervous system tissues. As a correlate, a deficiency of IRF-7 blunted the systemic type I IFN response in mice. Consistent with this, IFN-α gene expression and protein production were reduced and viral titers were increased in IRF-7$^{-/-}$ primary macrophages, fibroblasts, dendritic cells, and cortical neurons. In contrast, in these cells the IFN-β response remained largely intact. Our data suggest that the early protective IFN-α response against WNV occurs through an IRF-7-dependent transcriptional signal.

The production of type I interferon (IFN-α/β) after viral infection usually is triggered by the recognition of pathogen-associated molecular patterns (PAMP) on viral proteins or nucleic acids by specific host sensors known as pattern recognition receptors (PRR) (reviewed in reference 20 and 34). PRR for RNA viruses recognize single- or double-stranded RNA motifs on the cell surface, in endosomes (TLR3, TLR7, and TLR8), or in the cytoplasm (MDA5 and RIG-I) and activate the downstream transcriptional factors IRF-3 and IRF-7 to induce IFN gene transcription and protein production (reviewed in references 5 and 17).

IFN production and signaling generally are thought to occur through a two-step amplification model (27, 39, 40) in which IFN-β initially is produced in an IRF-3-dependent manner from virus-infected cells to trigger the expression of interferon-stimulated genes (ISGs), including IRF-7. The activation of IRF-7 then promotes additional IFN-α and IFN-β production via a positive feedback loop. More recently, a model has been proposed in which IRF-3 and IRF-7 both activate the initial phase of IFN-α and IFN-β gene expression in specific cell types (17–19).

Innate immune responses are required for the control of West Nile virus (WNV) infection (reviewed in reference 35 and 49). IFN-α and IFN-β gene induction is essential to the host response against WNV, as mice lacking the IFN-α/β receptor (IFN-αβR$^{-/-}$) are vulnerable to WNV infection, with expanded tissue tropism, uncontrolled viral replication, rapid dissemination to the central nervous system (CNS), and uniform death (36). Studies in cell culture suggest that WNV triggers IFN production through processes involving RIG-I, MDA5 (13), and protein kinase R (PKR) (15). Pathogenic WNV strains disrupt IFN-α/β signaling by modulating JAK-STAT pathway signals, thereby attenuating specific ISG expression and the innate antiviral response, resulting in the enhanced spread of infection (10, 16, 21, 24). The WNV control of JAK-STAT signaling might be expected to impact the overall level of IRF-7 expression that is induced by the IFN response within infected cells.

WNV is a potent trigger of IRF-3 activation (4, 14, 41, 45), and its antiviral response limits the spread of infection. Accordingly, IRF-3$^{-/-}$ mice, similarly to IFN-αβR$^{-/-}$ mice, show greater WNV burden in the periphery, expanded tissue tropism, and early entry into the CNS, leading to uniform lethality after subcutaneous infection with low doses of virus (6). Somewhat surprisingly, and in contrast to that observed with encephalomyocarditis virus (EMCV) infection (40), an absence of IRF-3 in vivo did not impair the systemic IFN-α or IFN-β responses after WNV infection (4, 6). Ex vivo experiments in primary macrophages showed IRF-3-restricted WNV infection through an IFN-independent mechanism by regulating the basal expression of key host defense molecules, including ISG54, ISG56, RIG-I, and MDA5 (6). In contrast, IRF-3 directly regulated IFN-α/β gene expression and protein produc-

* Corresponding author. Mailing address: Departments of Medicine, Molecular Microbiology and Pathology & Immunology, Washington University School of Medicine, 660 South Euclid Avenue, Box 8051, St. Louis, MO 63110. Phone: (314) 362-2842. Fax: (314) 362-9230. E-mail: diamond@borcim.wustl.edu.

▽ Published ahead of print on 18 June 2008.

TABLE 1. Viral burden in IRF-3$^{-/-}$ and IRF-7$^{-/-}$ animals[a]

Viremia or infection site	Change in viral burden					
	IRF-3$^{-/-}$			IRF-7$^{-/-}$		
	D2	D4	D6	D2	D4	D6
Viremia	↑ 11	↑ 5	↑ 10	↑ 57	↑ 11	↑ 21
Lymph node	↑ 2	↑ 5	ND[b]	↑ 22	↑ 16	ND
Spleen	↑ 8	↑ 10	↑ 32	↑ 400	↑ 80	↑ 56
Kidney	No change	No change	↑ 4	No change	↑ 250	↑ 100
Brain	No change	↑ 25	↑ 20	No change	↑ 320	↑ 500
Spinal Cord	No change	No change	↑ 20	No change	↑ 16	↑ 5,000

[a] Data are expressed as the *n*-fold increase (↑) or decrease (↓) in viral burden compared to that of wild-type tissues, as determined in this paper or in reference 6. D2, D4, D6, day 2, day 4, and day 6, respectively.
[b] ND, not determined.

tion in cortical neuron cultures. Thus, IRF-3 exerts its antiviral activity against WNV through IFN-dependent and IFN-independent pathways in a cell type-specific manner (4, 6).

IRF-7, which is downstream of the Myd88-dependent TLR7 and TLR8 responses, has been suggested as a master transcriptional regulator of type I IFN-dependent immune responses (19). Initial studies with Sendai virus in HeLa cells suggested that IRF-3 and IRF-7 coordinately induce IFN-β gene transcription after infection (50). Subsequent experiments in murine embryonic fibroblasts (MEF) showed that IRF-7 activates IFN-α genes through a positive feedback loop after IFN-β gene induction (23, 27, 39). However, the specific role of IRF-7 in regulating IFN-α/β gene expression in distinct tissue and cell types and its effect on viral replication remain controversial. Given that IRF-3 modulated WNV replication but was not required for systemic IFN production, we hypothesized that IRF-7 has a dominant regulatory role in specific cell types. Herein, we show that IRF-7$^{-/-}$ mice are vulnerable to WNV infection with uncontrolled viral replication and rapid mortality. Moreover, IRF-7 controls WNV replication in peripheral and CNS tissues in vivo and in primary cells ex vivo, in part by its ability to directly regulate IFN-α gene responses.

MATERIALS AND METHODS

Mouse experiments and quantitation of viral burden. C57BL/6 wild-type inbred mice were commercially obtained (Jackson Laboratories, Bar Harbor, ME). The congenic, backcrossed IRF-7$^{-/-}$ mice were the generous gift of T. Taniguchi (Tokyo, Japan) (19). All mice were genotyped and bred in the animal facilities of the Washington University School of Medicine, and experiments were performed in accordance with Washington University animal studies guidelines. Eight- to 12-week-old mice were used for all in vivo studies. For peripheral infection, 10^2 PFU of WNV was diluted in Hanks balanced salt solution (HBSS) supplemented with 1% heat-inactivated fetal bovine serum (FBS) and inoculated by footpad injection in a volume of 50 μl. Intracranial (i.c.) inoculation was performed by injecting 10^1 PFU of WNV diluted in 10 μl of HBSS with 1% FBS.

Viruses. The WNV strain (3000.0259) was isolated in New York in 2000 and passaged once in C6/36 cells to generate a stock virus that was used in all experiments.

Quantification of tissue viral burden and viremia. To monitor viral spread in vivo, mice were infected with 10^2 PFU of WNV by footpad inoculation and sacrificed at days 1, 2, 4, 6, 8, and 10 after inoculation. For the subcutaneous infection experiments, the wild-type control data were from a previous publication on WNV and IRF-3$^{-/-}$ mice (6). Indeed, control experiments with wild-type mice were performed concurrently with IRF-3$^{-/-}$ and IRF-7$^{-/-}$ mice (although samples were processed at different times) to facilitate direct comparisons (Tables 1 and 2). In other experiments, mice were infected with 10^1 PFU of WNV by an i.c. route and sacrificed at days 2 and 4 after infection. After extensive cardiac perfusion with phosphate-buffered saline, organs were harvested, weighed, and homogenized, and virus was titrated by standard plaque assay as previously described (9). Viral burden also was measured by analyzing RNA levels using fluorogenic quantitative reverse transcription-PCR (qRT-PCR) as previously described (38).

Quantification of IFN activity. (i) L929 bioassay. The relative levels of biologically active IFN in serum were determined using an EMCV L929 cytopathic effect bioassay as described previously (6). The specificity of the assay for type I IFN was confirmed using a previously described neutralizing anti-IFN-α/β receptor monoclonal antibody (MAb; MAR1-5A3) (44).

(ii) IFN-α and IFN-β mRNA qRT-PCR assay. Total RNA was isolated from primary cells using the RNeasy kit according to the manufacturer's instructions (Qiagen). During the isolation, to remove any contaminating DNA, samples were treated with RNase-free DNase (Qiagen). IFN-α and IFN-β mRNA were amplified and quantified from total RNA by qRT-PCR using previously published primer sets (36). To analyze the relative change (*n*-fold) in the induction of IFN-α and IFN-β mRNA, 18S rRNA expression levels also were determined for normalization using the threshold cycle method as described previously (25).

(iii) IFN-α and IFN-β protein ELISA. To measure levels of secreted IFN-α and IFN-β protein in cell supernatants, a commercial capture enzyme-linked immunosorbent assay (ELISA) with a standard curve was used according to the manufacturer's instructions (PBL Biomedical Laboratories, NJ).

Macrophage and dendritic cell infection. Macrophages and myeloid dendritic cells (mDC) were generated as described previously (6). Briefly, cells were isolated from the bone marrow of wild-type or IRF-7$^{-/-}$ mice and cultured for 7 days either in the presence of 40 ng/ml macrophage colony-stimulating factor (PeproTech Inc., Rocky Hill, NJ) to generate macrophages or with 20 ng/ml granulocyte-macrophage colony-stimulating factor and 20 ng/ml interleukin-4 (PeproTech Inc., Rocky Hill, NJ) to generate mDC. Multistep virus growth curves were performed after infection at a multiplicity of infection (MOI) of 0.01 for macrophages and 0.001 for mDC. Supernatants were titrated by plaque assay on BHK21-15 cells (9). To test for the induction of IFN-α and IFN-β after WNV infection, 5×10^5 macrophages or 2×10^5 mDC were infected at an MOI of 0.1. IFN-α and IFN-β mRNA were quantified by qRT-PCR, and protein was measured from supernatants as described above.

MEF infection. MEF were generated from day-14 wild-type or IRF-7$^{-/-}$ embryos and maintained in Dulbecco's modified Eagle's medium (DMEM) supplemented with 10% FBS according to established protocols. Multistep virus growth curves and IFN-α and IFN-β gene induction and protein secretion assays were performed as described above after infection at MOIs of 0.001 and 0.1, respectively.

Primary neuron infection. Primary cortical neurons were prepared from day-15 wild-type and IRF-7$^{-/-}$ mouse embryos as described previously (22, 37). Neurons were seeded in 24-well poly-D-lysine/laminin-coated plates in DMEM containing 5% heat-inactivated FBS and 5% horse serum for 24 h. Cortical neurons then were cultured for 4 days with Neurobasal medium containing B27 and L-glutamine (Invitrogen). Multistep virus growth curves and IFN-α and IFN-β gene induction and protein secretion assays were performed as described above after infection at MOIs of 0.001 and 0.1, respectively.

Immunoblotting. MEF or macrophages (10^6 cells) were lysed in radioimmunoprecipitation assay buffer (10 mM Tris, 150 mM NaCl, 0.02% sodium azide, 1% sodium deoxycholate, 1% Triton X-100, 0.1% sodium dodecyl sulfate [SDS], pH 7.4) with protease inhibitors (Sigma) and 1 mM okadaic acid (Sigma). Samples (30 μg) were resolved on 10% SDS-polyacrylamide gels. Following transfer, membranes were blocked with 5% nonfat dried milk overnight at 4°C. Membranes were probed with the following panel of monoclonal or polyclonal

TABLE 2. IFN production in IRF-$3^{-/-}$ and IRF-$7^{-/-}$ cells[a]

Cell type	Change in IFN production					
	IRF-$3^{-/-}$			IRF-$7^{-/-}$		
	24 h	48 h	72 h	24 h	48 h	72 h
Macrophages						
Virus production	↑16	↑63	↑8	No change	↑16	↑12
IFN-α mRNA induction	↑5	No change	ND[b]	↓7	↓9	ND
IFN-β mRNA induction	↑14	↑6	ND	↑2	↑7	ND
Bone marrow-DC						
Virus production	↑6	↑13	↑10	↑3	↑2	↑4
IFN-α production	No change	No change	No change	No change	↓16	↓20
IFN-β production	No change	No change	No change	No change	↓2	↓2
MEF[c]						
Virus production	No change	↑16	↑95	No change	↑7	↑11
IFN-α production	No change	No change	ND	No change	↓9	ND
IFN-β production	No change	No change	ND	No change	No change	ND
Cortical neurons						
Virus production	No change	↑5	ND	↑7	↑12	ND
IFN-α mRNA induction	↓100	↓5	ND	↓140	↓140	ND
IFN-β mRNA induction	↓115	↓3	ND	↓3	No change	ND

[a] Data are expressed as the *n*-fold increase (↑) or decrease (↓) in virus production or IFN gene expression compared to that of wild-type cells, as determined in this paper or in reference 6.
[b] ND, not determined.
[c] The data for IRF-$3^{-/-}$ MEF are from an unpublished source.

antibodies: anti-WNV (Centers for Disease Control and Prevention), anti-tubulin (Santa Cruz Biotechnology), anti-PKR (Santa Cruz Biotechnology), and anti-mouse ISG56 and anti-mouse ISG54 (gifts from G. Sen, Cleveland, OH). The RIG-I antibody was described previously (12). Blots were incubated with peroxidase-conjugated secondary antibodies (Jackson Immunoresearch) and visualized using ECL-plus immunoblotting reagents (Amersham Biosciences).

Statistical analysis. For in vitro experiments, an unpaired two-tailed *t* test was used to determine statistically significant differences. For viral burden analysis, differences in log titers were analyzed by the Mann-Whitney test. Kaplan-Meier survival curves were analyzed by the log rank test. All data were analyzed using Prism software (GraphPadPrism4, San Diego, CA).

RESULTS

IRF-7 is required for control of lethal WNV infection. Mice lacking IFN-α/β receptors are vulnerable to WNV infection due to rapid and overwhelming viral replication and altered tissue tropism (36). IRF-$3^{-/-}$ mice also showed uniform mortality but, surprisingly, had a largely intact systemic IFN response (6). To better understand the regulation of type I IFN and the modulation of WNV infection in vivo, we infected IRF-$7^{-/-}$ C57BL/6 mice with a highly pathogenic strain. After footpad inoculation with 10^2 PFU of a New York strain of WNV, IRF-$7^{-/-}$ mice showed an increased rate and severity of clinical signs and symptoms of illness, including hunchback posture, weight loss, fur ruffling, and reduced activity. Whereas wild-type mice show 65% survival and a mean time of death of 10.7 ± 2 days after inoculation with 10^2 PFU of WNV, IRF-$7^{-/-}$ mice were more vulnerable, with a 0% survival rate and a mean time of death of 7.4 ± 0.5 days ($P < 0.0001$) (Fig. 1A). In comparison, in studies performed in parallel, congenic IRF-$3^{-/-}$ mice had a mean time of death of 9.3 ± 1 days after WNV infection at this dose (6). Thus, WNV infection causes a more severe phenotype in IRF-$7^{-/-}$ mice than IRF-$3^{-/-}$ mice, and signaling through IRF-7 is absolutely essential for protection.

IRF-$7^{-/-}$ mice show expanded tissue tropism and enhanced WNV replication. As IRF-7 has been identified as a transcriptional regulator of the type I IFN response (19), we hypothesized that the observed increased lethality would correlate with higher viral burdens in tissue. To evaluate this, IRF-$7^{-/-}$ and wild-type mice were infected with 10^2 PFU of WNV, and the viral burden was measured by fluorogenic qRT-PCR or viral plaque assay at days 1, 2, 4, and 6 postinfection in serum, peripheral organs (draining lymph nodes, spleen, and kidney), and the CNS (brain and spinal cord).

(i) Viral RNA in serum and lymph node. Within 2 days of WNV infection, 50-fold higher ($P < 0.005$) levels of viral RNA were detected in serum of IRF-$7^{-/-}$ mice. Increased RNA levels (9- to 15-fold; $P < 0.005$) persisted in IRF-$7^{-/-}$ mice through day 6 (Fig. 1B), after which the mice succumbed to infection. In the draining popliteal lymph node, increased WNV replication also was observed at day 1 after infection and remained elevated at days 2 and 4 (15- to 22-fold; $P < 0.05$) (Fig. 1C). Based on virological analysis, IRF-7 has a key role in restricting WNV replication soon after infection.

(ii) Viral RNA in spleen and kidney. Consistent with prior studies (6, 38), WNV was not detected in the spleen by plaque assay at day 2 after infection in wild-type mice ($n = 10$). In contrast, 80% (8 of 10) of IRF-$7^{-/-}$ mice had a measurable infection at day 2 (mean titer of $10^{4.8}$ PFU/g; $P < 0.005$) (Fig. 1D). By day 4, which corresponds to the peak of splenic infection in wild-type animals, higher WNV titers were observed in IRF-$7^{-/-}$ mice (mean titer of $10^{5.4}$ PFU/g for IRF-$7^{-/-}$ mice and $10^{3.6}$ PFU/g for wild-type mice; $P < 0.005$). Elevated levels of infectious WNV (mean titer of $10^{3.9}$ PFU/g; $P < 0.0001$) still were detected at day 6 in all (8 of 8) IRF-$7^{-/-}$ mice, whereas WNV was cleared from the spleen in the majority (3 of 10 remained positive)

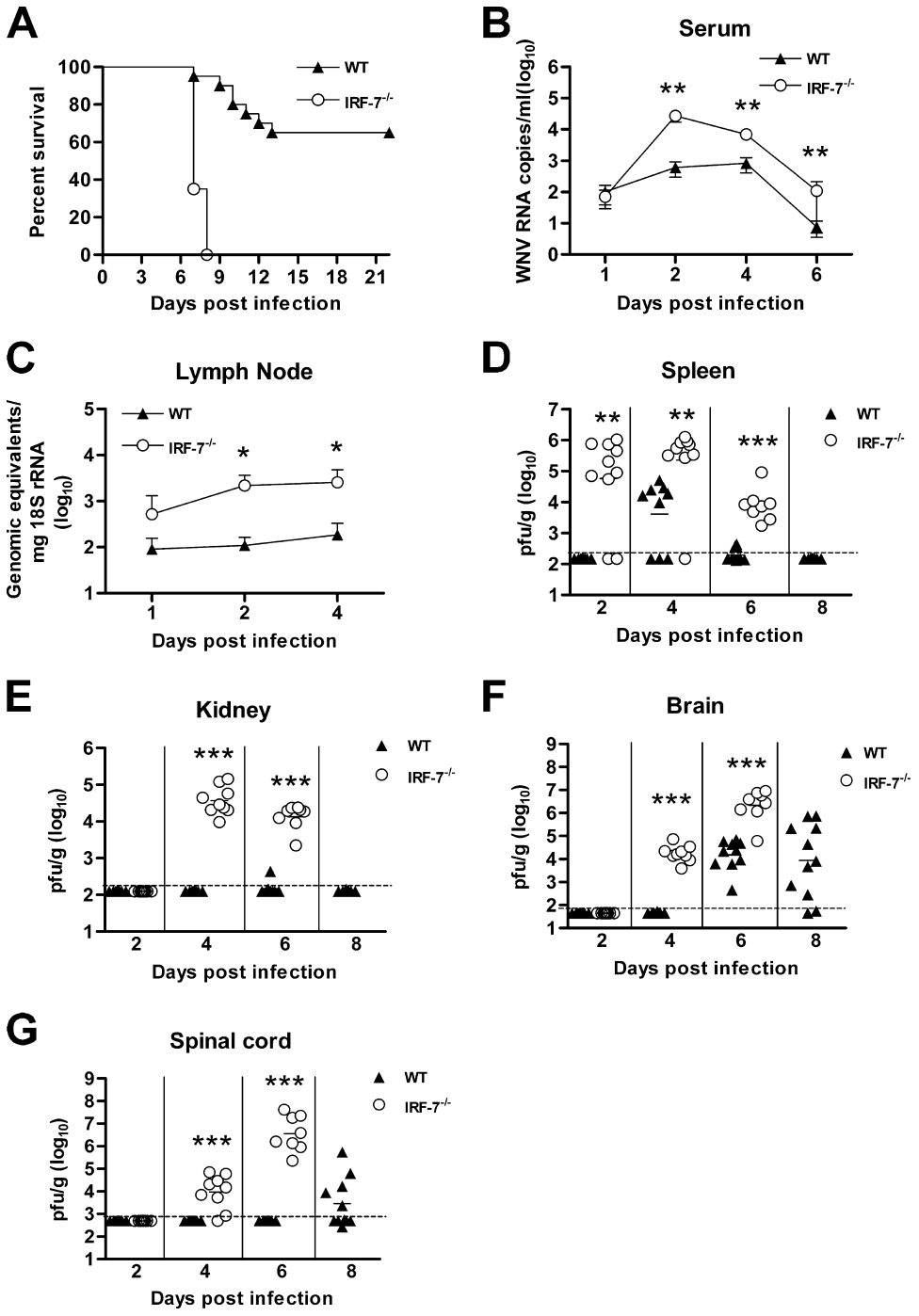

FIG. 1. Survival and viral burden analysis for wild-type (WT) and IRF-7$^{-/-}$ C57BL/6 mice. (A) Eight- to 12-week-old mice were inoculated with 10^2 PFU of WNV by footpad injection and were monitored for mortality for 21 days. Survival differences were statistically significant (wild-type mice, $n = 20$; IRF-7$^{-/-}$ mice, $n = 20$; $P < 0.0001$). (B to G) Viral burden in peripheral and CNS tissues after WNV infection. WNV RNA in serum (B) and draining lymph node (C) and infectious virus in the spleen (D), kidney (E), brain (F), and spinal cord (G) were determined from samples harvested on days 1, 2, 4, 6, and 8 using qRT-PCR (B and C) or viral plaque assay (D to G). Data are shown as viral RNA equivalents or PFU per gram of tissue for 10 to 12 mice per time point. For all viral data, the solid line represents the median PFU per gram at the indicated time point, and the dotted line represents the limit of the sensitivity of the assay. Asterisks indicate values that are statistically significant (*, $P < 0.05$; **, $P < 0.005$; ***, $P < 0.0001$) compared to results for wild-type mice. As discussed in Materials and Methods, the control wild-type viral burden and survival data in this figure have been reported in a prior publication (6).

of the wild-type animals. The kidney in wild-type C57BL/6 mice is relatively resistant to WNV infection, as the virus is not usually detected in this organ. Nonetheless, similarly to that observed with IFN-α/βR$^{-/-}$ mice (36), significant WNV replication was detected in the kidneys of IRF-7$^{-/-}$ mice (at day 4, $10^{4.6}$ PFU/g; day 6, $10^{4.1}$ PFU/g) (Fig. 1E). Thus, IRF-7-dependent signaling pathways modulate WNV infection in peripheral tissues and restrict tissue tropism.

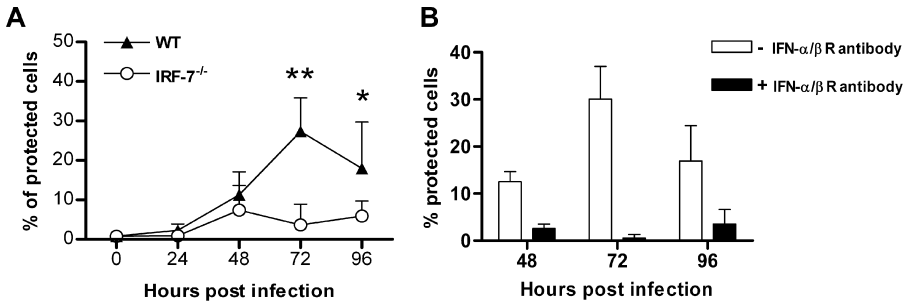

FIG. 2. Relative type I IFN levels in sera of wild-type (WT) and IRF-7$^{-/-}$ mice infected with WNV. (A) Mice were inoculated with 10^2 PFU of WNV by footpad injection and sacrificed at the indicated times. Relative type I IFN activity was determined from sera collected on days 1 to 4 after WNV infection by an EMCV bioassay in L929 cells. Data reflect the averages from serum samples harvested from 5 to 10 mice per time point and are shown as the percentages of cells protected from lysis by EMCV (see Materials and Methods). Asterisks indicate differences that are statistically significant (*, $P < 0.05$; **, $P < 0.005$). (B) Specificity of bioassay for type I IFN. L929 cells either were untreated or pretreated with a neutralizing MAb (10 μg/ml) against the IFN-α/β receptor. Sera from WNV-infected mice obtained at the indicated times were added to cells. After subsequent infection with EMCV, the cytopathic effect was measured 7 h later.

(iii) Viral RNA in the CNS. WNV spread to the CNS more rapidly and replicated to higher levels in IRF-7$^{-/-}$ mice. Infectious WNV was present in the brains of all IRF-7$^{-/-}$ mice (9 of 9) at day 4 after infection ($10^{4.3}$ PFU/g), whereas in wild-type mice WNV was not detected until day 6. IRF-7$^{-/-}$ mice also averaged significantly higher (~200-fold) viral titers than wild-type mice in the brain on day 6 after infection ($10^{6.4}$ PFU/g for IRF-7$^{-/-}$ mice and $10^{4.1}$ PFU/g for wild-type mice; $P < 0.0001$), corresponding with the increased mortality rate (Fig. 1F). A similar pattern of early infection in the spinal cord was observed, with 78% (7 of 9) and 100% (8 of 8) of IRF-7$^{-/-}$ mice having detectable viral loads at day 4 ($10^{4.0}$ PFU/g) and at day 6 ($10^{6.5}$ PFU/g), respectively. In contrast, none of the wild-type mice had measurable WNV in the spinal cord at these time points. These data show that an absence of IRF-7 signaling resulted in early spread to and sustained WNV replication in the CNS.

IFN-α/β levels in circulation are blunted in IRF-7$^{-/-}$ mice. We hypothesized that the enhanced replication and spread of WNV in IRF-7$^{-/-}$ mice was due to the blunted production of type I IFN. To evaluate this, IRF-7$^{-/-}$ and wild-type mice were infected with WNV, and the relative levels of biologically active type I IFN in serum was monitored using a validated EMCV-L929 cell protection bioassay (1). Type I IFN protective activity in the serum of infected wild-type mice peaked at 72 h and then slightly decreased at 96 h (Fig. 2A). The specificity of the assay for measuring type I IFN activity was confirmed with a neutralizing MAb against the IFN-α/β receptor (Fig. 2B). In IRF-7$^{-/-}$ mice, the relative levels of IFN at 48 h were slightly but not significantly reduced (1.5-fold reduction; $P > 0.2$). However, by 72 and 96 h after infection, serum IFN activity was reduced in IRF-7$^{-/-}$ mice (up to 8-fold; $P < 0.05$) despite the higher viral loads.

IRF-7 restricts WNV infection, IFN induction, and ISG regulation in MEF. To begin to investigate the cell-specific roles of IRF-7, we assayed WNV infection and IFN production in wild-type and IRF-7$^{-/-}$ MEF, a primary cell that has been used extensively in virus infection-host immune response assays (13, 27, 39). Whereas virologic analysis showed no significant difference in WNV burden at 24 h after infection, modestly enhanced viral replication was observed in IRF-7$^{-/-}$ MEF at 48 (a sixfold increase; $P < 0.001$) and 72 h postinfection (a fourfold increase; $P < 0.001$) (Fig. 3A). Thus, IRF-7 signaling partially controls WNV infection in MEF.

As we previously showed that increased replication could result from altered antiviral protein expression, we examined both the basal and induced expression of host defense molecules by immunoblotting. In wild-type MEF, IRF-7 was not basally expressed. The infection of the cells with WNV rapidly induced IRF-7 protein production, as high levels were detected within 24 h (Fig. 3B). IRF-7 expression in wild-type MEF was transient and was no longer detected 48 h postinfection. These results are consistent with a WNV-imposed block of JAK-STAT signaling that occurs during infection and attenuates the expression of ISGs, possibly including IRF-7 (10, 16, 21, 24, 29), and also may reflect the rapid degradation of IRF-7 that occurs after its activation (19). Whereas the expression of PKR in resting and WNV-infected IRF-7$^{-/-}$ MEF did not differ from that of wild-type cells, the induction of RIG-I, ISG54, and ISG56 after WNV infection was blunted in IRF-7$^{-/-}$ MEF during the first 24 h.

To assess whether this phenotype also correlated with a defect in the IFN response, IFN-α/β gene transcription (Fig. 3C and D) and protein secretion (Fig. 3E and F) were measured. In wild-type MEF, IFN-α/β mRNA levels rapidly increased at 24 h (80- and 1,000-fold, respectively), and by 48 h, levels of secreted IFN-α (~780 pg/ml) and IFN-β (~3,300 pg/ml) were easily measured. In contrast, in IRF-7$^{-/-}$ MEF increases in IFN-α mRNA and protein were virtually abolished at all time points, whereas IFN-β mRNA and protein levels were largely sustained after WNV infection. Thus, IRF-7 modestly restricts WNV infection in MEF and is required for the induction of IFN-α but is almost completely dispensable for the stimulation of IFN-β.

IRF-7 restricts WNV infection and IFN induction in macrophages. To explore further the cellular basis for the virologic and immunologic phenotypes in IRF-7$^{-/-}$ mice, we next investigated the effect of IRF-7 on WNV infection in macrophages, a cell type that is permissive for WNV infection in vivo (33, 35). Although no difference was observed at 24 h, enhanced replication was detected in IRF-7$^{-/-}$ macrophages beginning at 48 h and gradually increased at 72 h, resulting in a

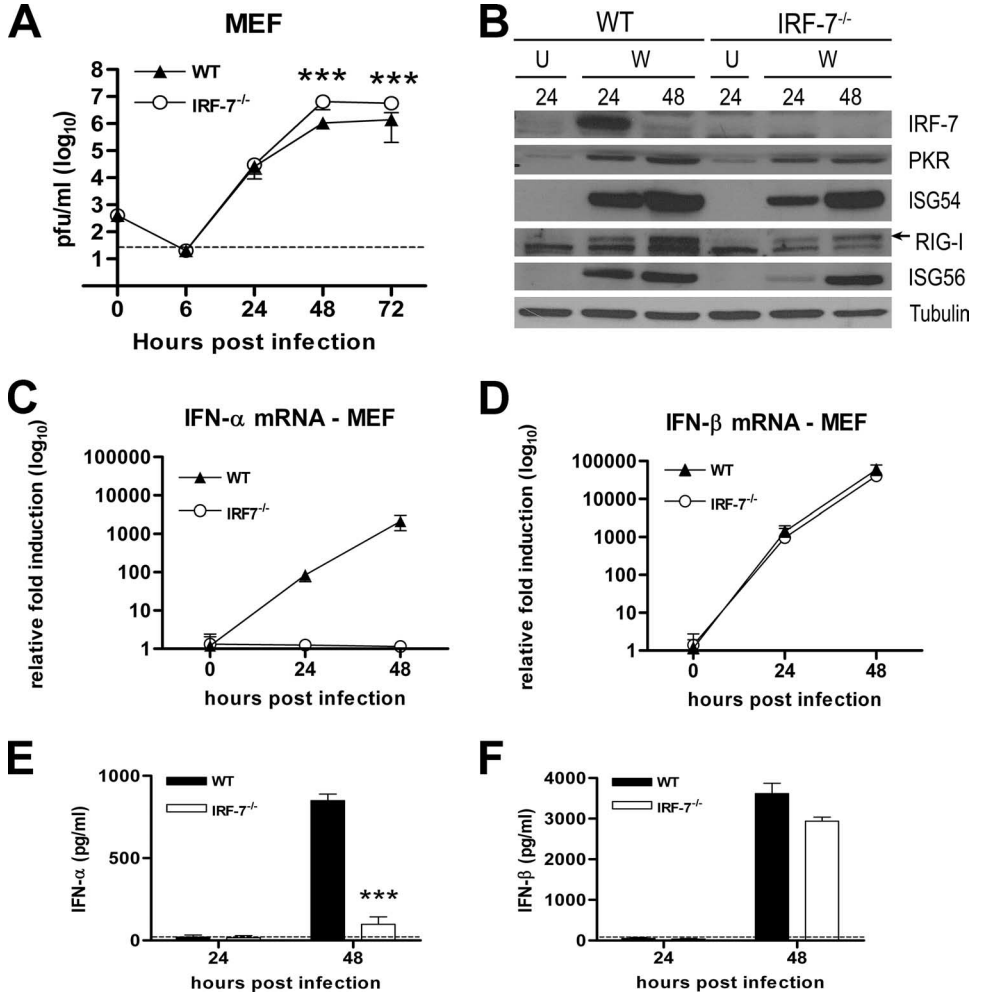

FIG. 3. IRF-7 limits WNV replication and controls IFN-α induction and early host defense activation in primary MEF. (A) MEF generated from wild-type (WT) or IRF-7$^{-/-}$ mice were infected at an MOI of 0.001, and virus production was evaluated at the indicated times postinfection by plaque assay. Values are averages from quadruplicate samples generated from at least three independent experiments. The dotted line represents the limit of the sensitivity of the assay. (B) Whole-cell lysates were generated at the indicated times from wild-type or IRF-7$^{-/-}$ MEF that were uninfected (U) or infected with WNV (W). Protein levels of IRF-7, PKR, ISG54, RIG-I, ISG56, and tubulin were examined by immunoblot analysis. (C and D) Total RNA from uninfected and WNV-infected MEF was harvested and analyzed for IFN-α (C) and IFN-β (D) mRNA expression by qRT-PCR. Data are normalized to values for 18S rRNA and are expressed as the relative (*n*-fold) increase above the level of RNA from uninfected controls. Average values are averages from duplicate samples from at least three independent experiments. (E and F) Accumulation of IFN-α (E) and IFN-β (F) protein in supernatants of WNV-infected MEF as determined by ELISA. The data are the averages from at least three independent experiments performed in quadruplicate (***, $P < 0.0001$).

~20-fold increase ($P \leq 0.005$) (Fig. 4A). In comparison, IRF-3$^{-/-}$ macrophages display significantly increased WNV replication at 24 h after infection (6) (Table 2). Thus, although IRF-7-dependent signals limit WNV replication in macrophages, they do so at a later stage of infection relative to that of IRF-3.

IRF-3 restricts WNV replication in macrophages by regulating the basal expression of host defense molecules (6). To test whether IRF-7 inhibited WNV infection through a similar mechanism, we performed immunoblot analysis. IRF-7 rapidly accumulated in wild-type macrophages following WNV infection, with levels peaking at 24 h and again falling by 48 h after infection (Fig. 4B). In contrast to MEF, resting macrophages basally expressed IRF-7, which could contribute to the relatively low permissiveness of these cells to WNV. Immunoblot analysis before or after infection showed similar expression levels of ISG54 among wild-type and IRF-7$^{-/-}$ macrophages, with modestly reduced levels of RIG-I in the latter (Fig. 4B). Basal PKR production was somewhat reduced in IRF-7$^{-/-}$ macrophages, whereas infection-induced levels were comparable to those of wild-type cells. As a deficiency of IRF-7 did not extensively alter the expression profile of host defense genes, we hypothesized that it might restrict viral replication in macrophages by directly modulating the IFN response. To evaluate this, we measured IFN-α and IFN-β mRNA levels after WNV infection (Fig. 4C and D). Whereas IFN-α mRNA levels in wild-type macrophages gradually increased throughout the time course, IFN-α gene induction in IRF-7$^{-/-}$ macrophages was blunted (five- to sixfold reduction at 24 and 48 h; $P < 0.0001$). In comparison, the induction of IFN-β mRNA re-

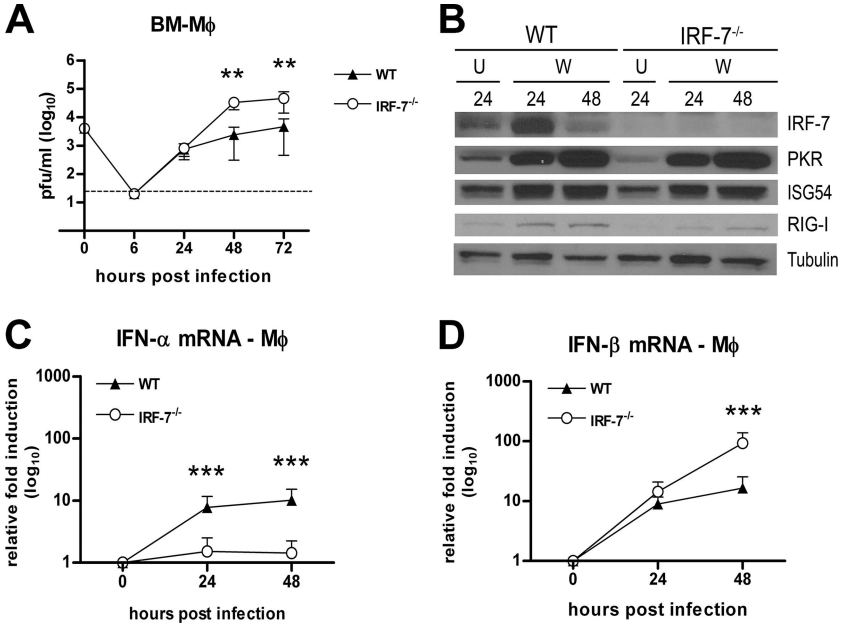

FIG. 4. IRF-7 modulates WNV infection and regulates IFN-α induction in primary macrophages. (A) Bone marrow-derived macrophages (BM-Mϕ) generated from wild-type or IRF-7$^{-/-}$ mice were infected at an MOI of 0.01, and virus production was evaluated at the indicated times postinfection by plaque assay. Values are averages from quadruplicate samples generated from at least three independent experiments (**, $P <$ 0.005). The dotted line represents the limit of the sensitivity of the assay. (B) Whole-cell lysates were generated at the indicated times from wild-type (WT) or IRF-7$^{-/-}$ macrophages that were uninfected (U) or infected with WNV (W). Protein levels of IRF-7, PKR, ISG54, RIG-I, and tubulin were examined by immunoblot analysis. (C and D) The induction of IFN-α (C) and IFN-β (D) mRNA in WNV-infected macrophages was analyzed by qRT-PCR as described in the legend to Fig. 3.

mained largely intact in IRF-7$^{-/-}$ macrophages: at 24 h, a similar ~10-fold induction of IFN-β mRNA levels was observed, and by 48 h, fivefold higher IFN-β mRNA levels were apparent in IRF-7$^{-/-}$ macrophages ($P < 0.0001$), possibly because of the higher viral burden that may trigger increased IFN-β expression. Overall, these experiments suggest that IRF-7 restricts WNV replication in macrophages only after the first 24 h through an IFN-α-dependent, but IFN-β-independent, mechanism.

IRF-7-dependent regulation of the IFN response in mDC. mDC may be early targets for flavivirus infection in vivo (7, 28, 35, 48) and are important for inducing innate and adaptive antiviral immune responses. To further evaluate the role of IRF-7 in regulating host defense responses, we infected wild-type and IRF-7$^{-/-}$ bone marrow-derived CD11c^{+} mDC with WNV and assayed viral replication and IFN production (Fig. 5). Multistep viral growth curve analysis showed a small (two- to threefold; $P < 0.05$) yet statistically significantly higher viral burden in IRF-7$^{-/-}$ mDC than in wild-type cells (Fig. 5A). An analysis of IFN gene induction revealed a pattern consistent with that of other cell types (Fig. 5B and C): whereas both IFN-α and IFN-β mRNA levels rapidly increased (~7,000- and ~1,500-fold, respectively) in wild-type mDC, IRF-7$^{-/-}$ mDC showed blunted IFN-α gene induction (~25-fold less; $P <$ 0.0001) yet relatively intact IFN-β mRNA levels (~2-fold less; $P < 0.05$). Consistently with this, infected IRF-7$^{-/-}$ mDC failed to secrete detectable IFN-α but produced only slightly reduced amounts of IFN-β (1.5- to 2-fold reduction; $P <$ 0.001) (Fig. 5D and E). These data suggest that in mDC, IRF-7 contributes slightly to IFN-β production but is essential for the expression and production of IFN-α.

IRF-7 controls WNV replication and induces IFN in primary cortical neurons. Neurons produce type I IFN after infection by WNV and by other RNA viruses (8, 32). To evaluate whether IRF-7 limits WNV replication and/or regulates antiviral responses in a key CNS target cell, we cultured wild-type and IRF-7$^{-/-}$ cortical neurons (98 to 99% purity) and performed multistep growth curve and IFN induction analyses (Fig. 6). IRF-7$^{-/-}$ cortical neurons produced higher levels of WNV at 24 h that increased by 48 h after infection (~7-fold [$P < 0.05$] and ~12-fold, [$P < 0.005$], respectively) (Fig. 6A). Associated with this, markedly decreased levels of IFN-α mRNA (~150-fold decrease at 24 and 48 h postinfection) were observed in WNV-infected IRF-7$^{-/-}$ cortical neurons (Fig. 6B). In contrast, levels of IFN-β mRNA were normal or higher in WNV-infected IRF-7$^{-/-}$ cortical neurons than in wild-type cells (Fig. 6C). Overall, these experiments show that IRF-7 limits WNV replication in cortical neuron cultures and regulates the antiviral IFN-α response.

IRF-7 controls WNV replication in the CNS. In vivo experiments were performed to support our results with primary cortical neuron cultures. Although CNS viral titers after peripheral WNV infection in IRF-7$^{-/-}$ mice were elevated, it was unclear whether this effect was due directly to an increased permissiveness of IRF-7$^{-/-}$ neurons or indirectly through greater CNS dissemination associated with the elevated and sustained viremia. To address this, wild-type and IRF-7$^{-/-}$ mice were infected with 10^1 PFU of WNV via an i.c. route, and

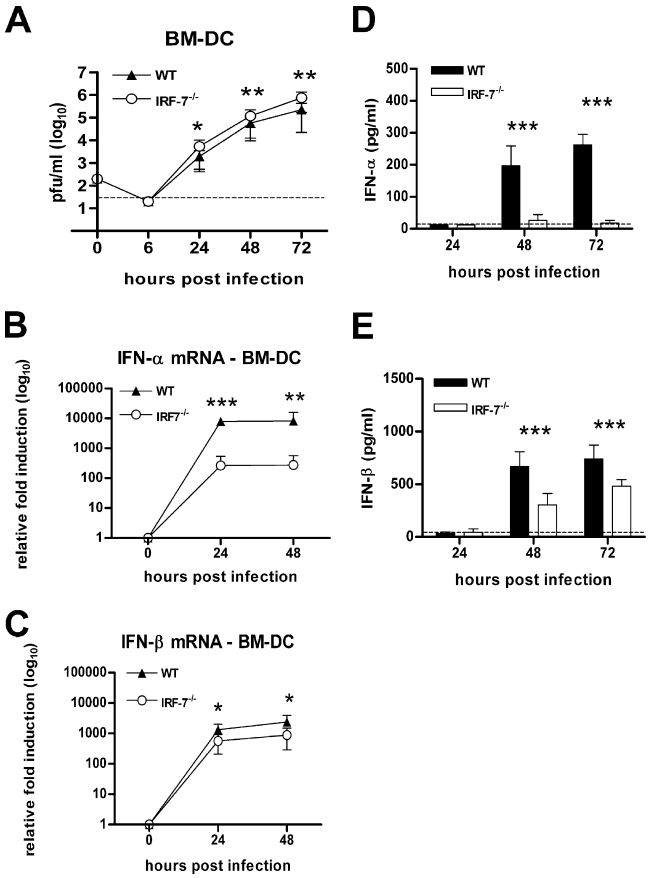

FIG. 5. IRF-7 restricts WNV infection and regulates IFN responses in mDC. (A) Bone marrow-derived mDC (BM-DC) generated from wild-type (WT) or IRF-7$^{-/-}$ mice were infected at an MOI of 0.001, and virus production was evaluated at the indicated times postinfection by plaque assay. Values are averages from quadruplicate samples generated from at least three independent experiments. (B and C) The induction of IFN-α (B) and IFN-β (C) mRNA in WNV-infected mDC was analyzed by qRT-PCR as described in the legend to Fig. 3. *, $P < 0.05$; **, $P < 0.005$; ***, $P < 0.0001$. (D and E) The accumulation of IFN-α (D) and IFN-β (E) protein in supernatants of WNV-infected mDC was determined by ELISA. The data are the averages from at least three independent experiments performed in quadruplicate. The dotted lines represent the limit of sensitivity of the individual assays.

the viral burdens in the brain and spinal cord were measured on days 2 and 4 (Fig. 7A). Whereas no significant differences were observed at day 2, IRF-7$^{-/-}$ mice showed ~50-fold higher average viral burdens at day 4 after infection in the brain ($10^{7.3}$ PFU/g and $10^{5.6}$ PFU/g for IRF-7$^{-/-}$ and wild-type mice, respectively; $P < 0.005$) and spinal cord ($10^{6.2}$ PFU/g and $10^{4.0}$ PFU/g for IRF-7$^{-/-}$ and wild-type mice, respectively; $P < 0.0001$). These results suggest that IRF-7 directly limits WNV infection in the brain and spinal cord. To ascertain whether increased CNS titers in IRF-7$^{-/-}$ mice correlated with a difference in the IFN response, we analyzed IFN-α and IFN-β gene expression in the cerebral cortex at day 4 after i.c. infection (Fig. 7B and C). Levels of IFN-β mRNA in the cerebral cortex of IRF-7$^{-/-}$ and wild-type mice were similar. In contrast, IFN-α mRNA levels were ~60-fold lower in IRF-7$^{-/-}$ mice at day 4 ($P < 0.005$). These experiments establish that in the brain, IFN-α but not IFN-β gene induction requires signaling through IRF-7.

DISCUSSION

Protection against viral infections in mice requires an intact type I IFN signaling pathway to limit replication. Different cell types secrete various amounts of IFN and, thus, play distinct roles in protecting against viral infection (11, 47). Nonetheless, the cell-specific mechanism(s) for IFN induction remains incompletely characterized. Here, we demonstrate that IRF-7 is an essential transcriptional regulator of the early IFN-α response after WNV infection. Mice lacking IRF-7 showed a rapid, uniformly lethal infection, with higher viral burden, expanded tissue tropism, and earlier entry in the CNS. Correspondingly, the systemic type I IFN production in the blood was blunted in IRF-7$^{-/-}$ mice despite an increased viral burden. A deficiency of IRF-7 preferentially depressed the induction and accumulation of IFN-α, with the relative sparing of the IFN-β response in primary MEF, macrophages, mDC, and cortical neurons. Our data are most consistent with a model in which IRF-7 protects against WNV largely through its ability to induce IFN-α-dependent antiviral responses.

Recent studies using cell cultures have made progress in elucidating how antiviral pathways become activated. IFN gene

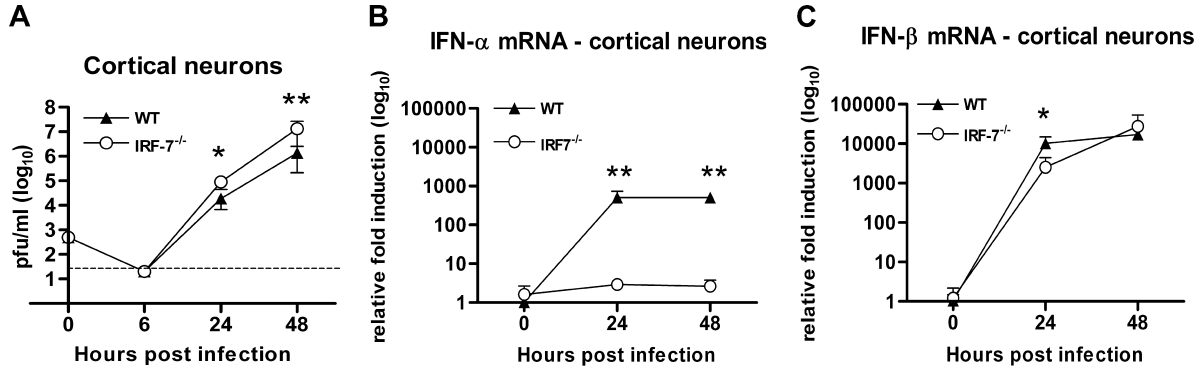

FIG. 6. IRF-7 restricts WNV infection and modulates IFN induction in primary cortical neurons. (A) Primary cortical neurons generated from wild-type (WT) or IRF-7$^{-/-}$ mice were infected at an MOI of 0.001, and virus production was evaluated at the indicated times by plaque assay. Values are averages from triplicate samples generated from three independent experiments. Asterisks indicate values that are statistically significant (*, $P < 0.05$; **, $P < 0.005$). The dotted line represents the limit of the sensitivity of the assay. (B and C) The induction of IFN-α (B) and IFN-β mRNA (C) in WNV-infected cortical neurons was analyzed by qRT-PCR as described in the legend to Fig. 3.

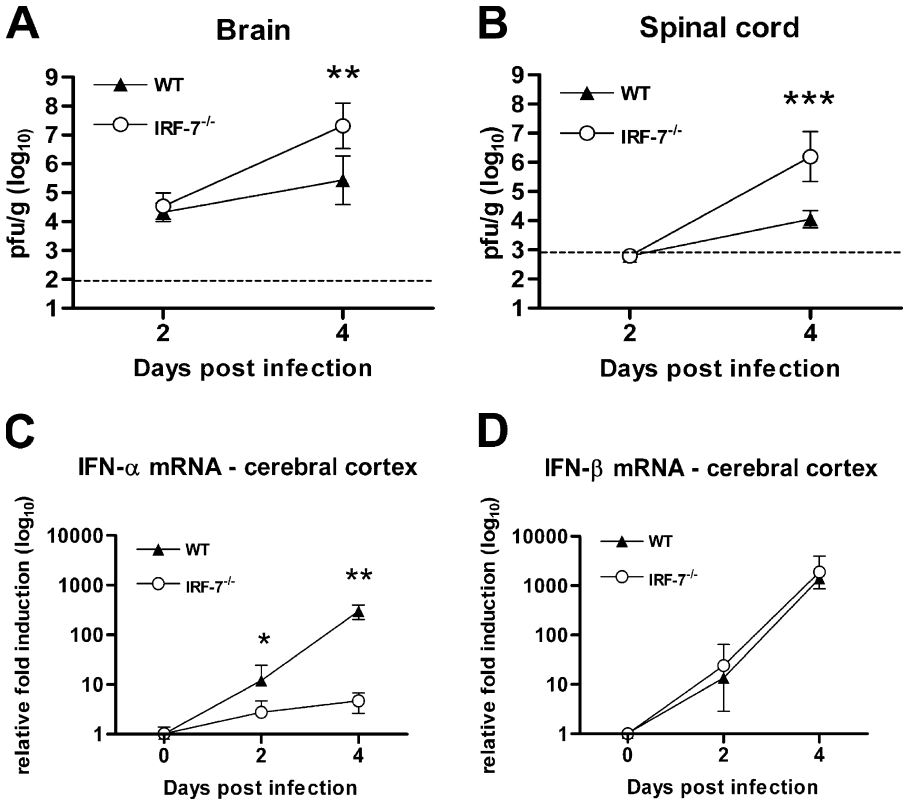

FIG. 7. IRF-7 controls viral replication and IFN-α induction in the CNS after i.c. WNV infection. (A and B) Wild-type (WT) or IRF-$7^{-/-}$ mice were inoculated with 10^1 PFU of WNV. Brains (A) and spinal cords (B) were harvested at the indicated time points, and viral titers were determined as described in the legend to Fig. 1. (C and D) The induction of IFN-α (C) and IFN-β (B) mRNA in WNV-infected cerebral cortices was analyzed by qRT-PCR as described in the legend to Fig. 3. *, $P < 0.05$; **, $P < 0.005$.

induction is downstream of PRR, which detect viral nucleic acids and PAMPs. For positive-strand RNA viruses, RIG-I, MDA, and TLR3 recognize double-stranded RNA in the cytoplasm and endosome and induce IFN-β expression via the nuclear localization of the transcription factors IRF-3 and, possibly, IRF-7 (13, 18, 26). Although IRF-3 and IRF-7 appear to have overlapping transcriptional activities, studies suggest they may differentially activate IFN-α, IFN-β, and specific ISGs (30, 40, 43). These activities may be influenced by unique expression patterns; whereas IRF-3 often is constitutively expressed in many cells, the basal expression of IRF-7 may be restricted (31). Our experiments demonstrate that macrophages also constitutively express IRF-7. The basal expression of IRF-7 and other host defense molecules by macrophages may account for the relatively efficient control of WNV infection compared to that of other cell types.

Our experiments with mice and primary cells demonstrate that IRF-7 is essential for the regulation of the early induction of IFN-α. These findings are consistent with those of a prior study in which depressed systemic type I IFN levels and blunted IFN-α gene induction were observed in IRF-$7^{-/-}$ mice and primary MEF, mDC, and plasmacytoid DC after herpes simplex virus and EMCV infections (19). Beyond cell type-specific antiviral pathways, different viruses may themselves stimulate unique innate immune response patterns. In contrast to our results with WNV, IFN-β gene induction was markedly reduced in IRF-$7^{-/-}$ MEF after infection with herpes simplex virus, vesicular stomatitis virus, or EMCV and was lost in IRF-$3^{-/-}$ and IRF-$7^{-/-}$ MEF (19). In the context of these pathogens, IRF-3 and IRF-7 both may regulate IFN-β gene expression. While it is generally believed that IRF-3 regulates the early phase of IFN-β induction after RNA virus infection (40), in vivo WNV may not follow this paradigm. A direct comparison of the virologic and IFN phenotypes after WNV infection in different tissues and cell types (Tables 1 and 2) shows that in several cell types (macrophages, mDC, and MEF), only a deficiency of IRF-7 resulted in decreased IFN gene expression. This was unexpected, as IRF-7 signaling is thought to be downstream of IRF-3 activation and, thus, IRF-$3^{-/-}$ cells should have blunted levels of both IFN-α and IFN-β. Thus, in several cell types, (i) IRF-3 or IRF-7 by itself can induce IFN-β at wild-type levels or (ii) additional undefined signaling pathways stimulate IFN-β expression after WNV infection. Future studies with IRF-$3^{-/-}$ and IRF-$7^{-/-}$ mice and additional primary cells are planned to determine whether these two transcriptional activators solely determine type I IFN activation after WNV infection or whether other IRF proteins (e.g., IRF-1, IRF-5, or IRF-8) contribute (2, 3, 42, 46).

In addition to diverse IFN induction pathways, distinct cell types have different capacities to respond to IFN-α or IFN-β. For example, central and peripheral neuron subtypes showed inherent differences in the ability of IFN-α or IFN-β pretreatment to limit WNV infection (38). Consistently with this, there was no absolute correlation between the degree of IFN-α pro-

duction and changes in viral replication. The increase in late-phase WNV replication in IRF-7$^{-/-}$ macrophages correlated with reduced levels of IFN-α, whereas smaller virological differences were observed in IRF-7$^{-/-}$ mDC and MEF despite a complete loss of IFN-α production. The exact contribution of individual IFN (e.g., IFN-α versus IFN-β) in regulating viral infection in vivo remains an unanswered question. The ability of WNV to evade IFN in part through the viral suppression of JAK-STAT signaling has been defined as a virulence determinant; attenuated ISG expression releases WNV from antiviral processes imposed by IFN (16, 21). Since IRF-7 is an ISG in many cell types, it is possible that the WNV regulation of IFN signaling confers altered levels of IRF-7 induction or abundance. It is interesting that the reduced levels of IRF-7 that occurred at 48 h after WNV infection in macrophages and fibroblasts (Fig. 3B and 4B) temporally associate with the WNV-imposed suppression of JAK-STAT signaling (21). Thus, altered levels of IRF-7 may further support WNV infection and spread among cells and tissues.

While this and other studies highlight the importance of IRF-7 in peripheral innate immune responses, little is known about its function in the brain. Our studies suggest an independent role for IRF-7 in regulating viral infection and IFN production in the CNS. Viral burden in the brain and spinal cord after i.c. infection was greater in IRF-7$^{-/-}$ mice at time points that precede the development of an adaptive immune response. Moreover, IFN-α induction in the cerebral cortex and primary cortical neurons was IRF-7 dependent, suggesting that IRF-7 plays a dominant role in the CNS and restricts WNV through IFN-dependent mechanisms. In contrast, IFN-β gene induction after WNV infection in cortical neurons apparently was not regulated by IRF-7. These results complement previous studies with WNV-infected IRF-3$^{-/-}$ neurons that showed blunted IFN-α and IFN-β gene responses (Table 2). Thus, the regulation of IFN-α and IFN-β in neurons appears to follow the more canonical, or two-step, model in which IRF-3 acts as a primary transcriptional activator and IRF-7 amplifies the response.

In summary, IRF-7 is essential for restricting WNV infection and inducing IFN-α-dependent antiviral responses. A deficiency of IRF-7 did not dramatically alter the primary IFN-β response but rather more specifically abrogated IFN-α induction. This study, combined with previous work, suggests that cell- and tissue-specific roles of IRF-3 and IRF-7 regulate antiviral programs against WNV and, likely, other viruses. An enhanced understanding of the molecular mechanisms of the earliest protective antiviral immune response may provide novel strategies for therapeutic intervention against viral pathogens.

ACKNOWLEDGMENTS

We thank A. Blasius and M. Colonna for experimental advice and T. Taniguchi for the IRF-7$^{-/-}$ mice. We appreciate the critical reading of the manuscript by M. Colonna.

This work was supported by a New Scholar Award in Global Infectious Disease from the Ellison Medical Foundation (M.S.D.), a predoctoral fellowship from the Howard Hughes Medical Institute (M.A.S.), and by NIH AI057568 (M.G.).

The authors report no conflicts of interest.

REFERENCES

1. **Austin, B. A., C. James, R. H. Silverman, and D. J. Carr.** 2005. Critical role for the oligoadenylate synthetase/RNase L pathway in response to IFN-beta during acute ocular herpes simplex virus type 1 infection. J. Immunol. **175:** 1100–1106.
2. **Barnes, B. J., A. E. Field, and P. M. Pitha-Rowe.** 2003. Virus-induced heterodimer formation between IRF-5 and IRF-7 modulates assembly of the IFNA enhanceosome in vivo and transcriptional activity of IFNA genes. J. Biol. Chem. **278:**16630–16641.
3. **Barnes, B. J., J. Richards, M. Mancl, S. Hanash, L. Beretta, and P. M. Pitha.** 2004. Global and distinct targets of IRF-5 and IRF-7 during innate response to viral infection. J. Biol. Chem. **279:**45194–45207.
4. **Bourne, N., F. Scholle, M. C. Silva, S. L. Rossi, N. Dewsbury, B. Judy, J. B. De Aguiar, M. A. Leon, D. M. Estes, R. Fayzulin, and P. W. Mason.** 2007. Early production of type I interferon during West Nile virus infection: role for lymphoid tissues in IRF3-independent interferon production. J. Virol. **81:**9100–9108.
5. **Colonna, M.** 2007. TLR pathways and IFN-regulatory factors: to each its own. Eur. J. Immunol. **37:**306–309.
6. **Daffis, S., M. A. Samuel, B. C. Keller, M. Gale, Jr., and M. S. Diamond.** 2007. Cell-specific IRF-3 responses protect against West Nile virus infection by interferon-dependent and independent mechanisms. PLoS. Pathog. **3:**e106.
7. **Davis, C. W., H. Y. Nguyen, S. L. Hanna, M. D. Sanchez, R. W. Doms, and T. C. Pierson.** 2006. West Nile virus discriminates between DC-SIGN and DC-SIGNR for cellular attachment and infection. J. Virol. **80:**1290–1301.
8. **Delhaye, S., S. Paul, G. Blakqori, M. Minet, F. Weber, P. Staeheli, and T. Michiels.** 2006. Neurons produce type I interferon during viral encephalitis. Proc. Natl. Acad. Sci. USA **103:**7835–7840.
9. **Diamond, M. S., B. Shrestha, A. Marri, D. Mahan, and M. Engle.** 2003. B cells and antibody play critical roles in the immediate defense of disseminated infection by West Nile encephalitis virus. J. Virol. **77:**2578–2586.
10. **Evans, J. D., and C. Seeger.** 2007. Differential effects of mutations in NS4B on WNV replication and inhibition of interferon signaling. J. Virol. **81:** 11809–11816.
11. **Fitzgerald-Bocarsly, P., and D. Feng.** 2007. The role of type I interferon production by dendritic cells in host defense. Biochimie **89:**843–855.
12. **Fredericksen, B. L., and M. Gale, Jr.** 2006. West Nile virus evades activation of interferon regulatory factor 3 through RIG-I-dependent and -independent pathways without antagonizing host defense signaling. J. Virol. **80:** 2913–2923.
13. **Fredericksen, B. L., B. C. Keller, J. Fornek, M. G. Katze, and M. Gale, Jr.** 2008. Establishment and maintenance of the innate antiviral response to West Nile virus involves both RIG-I and MDA5 signaling through IPS-1. J. Virol. **82:**609–616.
14. **Fredericksen, B. L., M. Smith, M. G. Katze, P. Y. Shi, and M. Gale.** 2004. The host response to West Nile virus infection limits spread through the activation of the interferon regulatory factor 3 pathway. J. Virol. **78:**7737–7747.
15. **Gilfoy, F. D., and P. W. Mason.** 2007. West Nile virus-induced IFN production is mediated by the double-stranded RNA-dependent protein kinase, PKR. J. Virol. **81:**11148–11158.
16. **Guo, J. T., J. Hayashi, and C. Seeger.** 2005. West Nile virus inhibits the signal transduction pathway of alpha interferon. J. Virol. **79:**1343–1350.
17. **Hiscott, J.** 2007. Triggering the innate antiviral response through IRF-3 activation. J. Biol. Chem. **282:**15325–15329.
18. **Honda, K., and T. Taniguchi.** 2006. IRFs: master regulators of signalling by Toll-like receptors and cytosolic pattern-recognition receptors. Nat. Rev. Immunol. **6:**644–658.
19. **Honda, K., H. Yanai, H. Negishi, M. Asagiri, M. Sato, T. Mizutani, N. Shimada, Y. Ohba, A. Takaoka, N. Yoshida, and T. Taniguchi.** 2005. IRF-7 is the master regulator of type-I interferon-dependent immune responses. Nature **434:**772–777.
20. **Kawai, T., and S. Akira.** 2006. Innate immune recognition of viral infection. Nat. Immunol. **7:**131–137.
21. **Keller, B. C., B. L. Fredericksen, M. A. Samuel, R. E. Mock, P. W. Mason, M. S. Diamond, and M. Gale, Jr.** 2006. Resistance to alpha/beta interferon is a determinant of West Nile virus replication fitness and virulence. J. Virol. **80:**9424–9434.
22. **Klein, R. S., E. Lin, B. Zhang, A. D. Luster, J. Tollett, M. A. Samuel, M. Engle, and M. S. Diamond.** 2005. Neuronal CXCL10 directs CD8$^+$ T-cell recruitment and control of West Nile virus encephalitis. J. Virol. **79:**11457–11466.
23. **Levy, D. E., I. Marie, E. Smith, and A. Prakash.** 2002. Enhancement and diversification of IFN induction by IRF-7-mediated positive feedback. J. Interferon Cytokine Res. **22:**87–93.
24. **Liu, W. J., X. J. Wang, V. V. Mokhonov, P. Y. Shi, R. Randall, and A. A. Khromykh.** 2005. Inhibition of interferon signaling by the New York 99 strain and kunjin subtype of West Nile virus involves blockage of STAT1 and STAT2 activation by nonstructural proteins. J. Virol. **79:**1934–1942.
25. **Livak, K. J., and T. D. Schmittgen.** 2001. Analysis of relative gene expression

data using real-time quantitative PCR and the $2^{-\Delta\Delta}CT$ method. Methods **25:**402–408.
26. **Loo, Y. M., J. Fornek, N. Crochet, G. Bajwa, O. Perwitasari, L. Martinez-Sobrido, S. Akira, M. A. Gill, A. Garcia-Sastre, M. G. Katze, and M. Gale, Jr.** 2008. Distinct RIG-I and MDA5 signaling by RNA viruses in innate immunity. J. Virol. **82:**335–345.
27. **Marié, I., J. E. Durbin, and D. E. Levy.** 1998. Differential viral induction of distinct interferon-alpha genes by positive feedback through interferon regulatory factor-7. EMBO J. **17:**6660–6669.
28. **Martina, B. E., P. Koraka, P. van den Doel, G. F. Rimmelzwaan, B. L. Haagmans, and A. D. Osterhaus.** 2008. DC-SIGN enhances infection of cells with glycosylated West Nile virusin vitro and virus replication in human dendritic cells induces production of IFN-alpha and TNF-alpha. Virus Res. **135:**64–71.
29. **Muñoz-Jordán, J. L., M. Laurent-Rolle, J. Ashour, L. Martinez-Sobrido, M. Ashok, W. I. Lipkin, and A. Garcia-Sastre.** 2005. Inhibition of alpha/beta interferon signaling by the NS4B protein of flaviviruses. J. Virol. **79:**8004–8013.
30. **Nakaya, T., M. Sato, N. Hata, M. Asagiri, H. Suemori, S. Noguchi, N. Tanaka, and T. Taniguchi.** 2001. Gene induction pathways mediated by distinct IRFs during viral infection. Biochem. Biophys. Res. Commun. **283:**1150–1156.
31. **Prakash, A., E. Smith, C. K. Lee, and D. E. Levy.** 2005. Tissue-specific positive feedback requirements for production of type I interferon following virus infection. J. Biol. Chem. **280:**18651–18657.
32. **Préhaud, C., F. Megret, M. Lafage, and M. Lafon.** 2005. Virus infection switches TLR-3-positive human neurons to become strong producers of beta interferon. J. Virol. **79:**12893–12904.
33. **Rios, M., M. J. Zhang, A. Grinev, K. Srinivasan, S. Daniel, O. Wood, I. K. Hewlett, and A. I. Dayton.** 2006. Monocytes-macrophages are a potential target in human infection with West Nile virus through blood transfusion. Transfusion **46:**659–667.
34. **Saito, T., and M. Gale, Jr.** 2007. Principles of intracellular viral recognition. Curr. Opin. Immunol. **19:**17–23.
35. **Samuel, M. A., and M. S. Diamond.** 2006. Pathogenesis of West Nile virus infection: a balance between virulence, innate and adaptive immunity, and viral evasion. J. Virol. **80:**9349–9360.
36. **Samuel, M. A., and M. S. Diamond.** 2005. Type I IFN protects against lethal West Nile virus infection by restricting cellular tropism and enhancing neuronal survival. J. Virol. **79:**13350–13361.
37. **Samuel, M. A., J. D. Morrey, and M. S. Diamond.** 2007. Caspase-3 dependent cell death of neurons contributes to the pathogenesis of West Nile virus encephalitis. J. Virol. **81:**2614–2623.
38. **Samuel, M. A., K. Whitby, B. C. Keller, A. Marri, W. Barchet, B. R. G. Williams, R. H. Silverman, M. Gale, and M. S. Diamond.** 2006. PKR and RNAse L contribute to protection against lethal West Nile virus infection by controlling early viral spread in the periphery and replication in neurons. J. Virol. **80:**7009–7019.
39. **Sato, M., N. Hata, M. Asagiri, T. Nakaya, T. Taniguchi, and N. Tanaka.** 1998. Positive feedback regulation of type I IFN genes by the IFN-inducible transcription factor IRF-7. FEBS Lett. **441:**106–110.
40. **Sato, M., H. Suemori, N. Hata, M. Asagiri, K. Ogasawara, K. Nakao, T. Nakaya, M. Katsuki, S. Noguchi, N. Tanaka, and T. Taniguchi.** 2000. Distinct and essential roles of transcription factors IRF-3 and IRF-7 in response to viruses for IFN-alpha/beta gene induction. Immunity **13:**539–548.
41. **Scherbik, S. V., B. M. Stockman, and M. A. Brinton.** 2007. Differential expression of interferon (IFN) regulatory factors and IFN-stimulated genes at early times after West Nile virus infection of mouse embryo fibroblasts. J. Virol. **81:**12005–12018.
42. **Schmitz, F., A. Heit, S. Guggemoos, A. Krug, J. Mages, M. Schiemann, H. Adler, I. Drexler, T. Haas, R. Lang, and H. Wagner.** 2007. Interferon-regulatory-factor 1 controls Toll-like receptor 9-mediated IFN-beta production in myeloid dendritic cells. Eur. J. Immunol. **37:**315–327.
43. **Servant, M. J., B. Tenoever, and R. Lin.** 2002. Overlapping and distinct mechanisms regulating IRF-3 and IRF-7 function. J. Interferon Cytokine Res. **22:**49–58.
44. **Sheehan, K. C., K. S. Lai, G. P. Dunn, A. T. Bruce, M. S. Diamond, J. D. Heutel, C. Dungo-Arthur, J. A. Carrero, J. M. White, P. J. Hertzog, and R. D. Schreiber.** 2006. Blocking monoclonal antibodies specific for mouse IFN-alpha/beta receptor subunit 1 (IFNAR-1) from mice immunized by in vivo hydrodynamic transfection. J. Interferon Cytokine Res. **26:**804–819.
45. **Silva, M. C., A. Guerrero-Plata, F. D. Gilfoy, R. P. Garofalo, and P. W. Mason.** 2007. Differential activation of human monocyte-derived and plasmacytoid dendritic cells by West Nile virus generated in different host cells. J. Virol. **81:**13640–13648.
46. **Tailor, P., T. Tamura, H. J. Kong, T. Kubota, M. Kubota, P. Borghi, L. Gabriele, and K. Ozato.** 2007. The feedback phase of type I interferon induction in dendritic cells requires interferon regulatory factor 8. Immunity **27:**228–239.
47. **Tailor, P., T. Tamura, and K. Ozato.** 2006. IRF family proteins and type I interferon induction in dendritic cells. Cell Res. **16:**134–140.
48. **Tassaneetrithep, B., T. Burgess, A. Granelli-Piperno, C. Trumpfheller, J. Finke, W. Sun, M. Eller, K. Pattanapanyasat, S. Sarasombath, D. Birx, R. M. Steinman, S. Schlesinger, and M. Marovich.** 2003. DC-SIGN (CD209) mediates dengue virus infection of human dendritic cells. J. Exp. Med. **197:**823–829.
49. **Wang, T., and E. Fikrig.** 2004. Immunity to West Nile virus. Curr. Opin. Immunol. **16:**519–523.
50. **Wathelet, M. G., C. H. Lin, B. S. Parekh, L. V. Ronco, P. M. Howley, and T. Maniatis.** 1998. Virus infection induces the assembly of coordinately activated transcription factors on the IFN-beta enhancer in vivo. Mol. Cell **1:**507–518.

Induction of IFN-β and the Innate Antiviral Response in Myeloid Cells Occurs through an IPS-1-Dependent Signal That Does Not Require IRF-3 and IRF-7

Stephane Daffis[1], Mehul S. Suthar[2], Kristy J. Szretter[1], Michael Gale, Jr.[2], Michael S. Diamond[1,3,4]*

1 Department of Medicine, Washington University School of Medicine, St. Louis, Missouri, United States of America, **2** Department of Immunology, University of Washington School of Medicine, Seattle, Washington, United States of America, **3** Department of Molecular Microbiology, Washington University School of Medicine, St. Louis, Missouri, United States of America, **4** Department of Pathology & Immunology, Washington University School of Medicine, St. Louis, Missouri, United States of America

Abstract

Interferon regulatory factors (IRF)-3 and IRF-7 are master transcriptional factors that regulate type I IFN gene (IFN-α/β) induction and innate immune defenses after virus infection. Prior studies in mice with single deletions of the IRF-3 or IRF-7 genes showed increased vulnerability to West Nile virus (WNV) infection. Whereas mice and cells lacking IRF-7 showed reduced IFN-α levels after WNV infection, those lacking IRF-3 or IRF-7 had relatively normal IFN-b production. Here, we generated IRF-$3^{-/-}\times$ IRF-$7^{-/-}$ double knockout (DKO) mice, analyzed WNV pathogenesis, IFN responses, and signaling of innate defenses. Compared to wild type mice, the DKO mice exhibited a blunted but not abrogated systemic IFN response and sustained uncontrolled WNV replication leading to rapid mortality. Ex vivo analysis showed complete ablation of the IFN-α response in DKO fibroblasts, macrophages, dendritic cells, and cortical neurons and a substantial decrease of the IFN-β response in DKO fibroblasts and cortical neurons. In contrast, the IFN-β response was minimally diminished in DKO macrophages and dendritic cells. However, pharmacological inhibition of NF-κB and ATF-2/c-Jun, the two other known components of the IFN-β enhanceosome, strongly reduced IFN-β gene transcription in the DKO dendritic cells. Finally, a genetic deficiency of IPS-1, an adaptor involved in RIG-I- and MDA5-mediated antiviral signaling, completely abolished the IFN-β response after WNV infection. Overall, our experiments suggest that, unlike fibroblasts and cortical neurons, IFN-β gene regulation after WNV infection in myeloid cells is IPS-1-dependent but does not require full occupancy of the IFN-β enhanceosome by canonical constituent transcriptional factors.

Citation: Daffis S, Suthar MS, Szretter KJ, Gale M, Jr., Diamond MS (2009) Induction of IFN-β and the Innate Antiviral Response in Myeloid Cells Occurs through an IPS-1-Dependent Signal That Does Not Require IRF-3 and IRF-7. PLoS Pathog 5(10): e1000607. doi:10.1371/journal.ppat.1000607

Editor: Ganes Sen, Cleveland Clinic, United States of America

Received March 11, 2009; **Accepted** September 8, 2009; **Published** October 2, 2009

Funding: This study was supported by NIH grants AI057568, U54 AI081680, U19 AI083019, and AI074973. The funders had no role in study design, data collection and analysis, decision to publish, or preparation of the manuscript.

Competing Interests: The authors have declared that no competing interests exist.

* E-mail: diamond@borcim.wustl.edu

Introduction

The rapid production of type I interferon (IFN-α/β) and the IFN-induced antiviral response serve as primary host defense mechanisms against infection by many viruses (reviewed in [1–3]). IFN-α/β gene transcription is induced after host pattern recognition receptors (PRR) bind pathogen-associated molecular patterns (PAMP), such as viral nucleic acids (reviewed in [4–6]). A current paradigm for type I IFN production after RNA virus infection describes a two-step or positive feedback model that is modulated by the master transcription factors interferon regulatory factors (IRF)-3 and -7 [7–9]. In the initial phase, viral sensing by PRR induces nuclear localization of IRF-3, which stimulates gene transcription and production of IFN-β and IFN-α4 by infected cells. In the second phase, these IFNs bind to a common IFN-α/β receptor in a paracrine and autocrine manner and signal through the JAK-STAT pathway resulting in the induced expression of hundreds of interferon stimulated genes (ISG) (e.g., PKR, RNAse L, viperin, ISG15, and ISG20), which limit viral replication through multiple mechanisms [10–13]. Whereas IRF-3 is constitutively expressed throughout many tissues and functions downstream of specific PRR (e.g., TLR3, MDA5, and RIG-I) to inhibit RNA viruses, IRF-7 is both an ISG and a transcriptional activator downstream of distinct PRR (e.g., TLR7 and TLR8); IRF-7 participates in an IFN amplification loop by inducing IFN-β and many subtypes of IFN-α [14].

Recognition of West Nile virus (WNV), a neurotropic virus of the *Flaviviridae* family of RNA viruses, by the intrinsic cellular immune response is believed to occur through concerted signals by several PRR (TLR3, TLR7, TLR8, RIG-I, and MDA5) that recognize single or double-stranded RNA and signal through their constituent adaptor molecules (TRIF, MyD88, and IPS-1). Tissue culture experiments with murine embryonic fibroblasts (MEF) suggested that RIG-I is an initial and primary PRR for WNV as genetically deficient cells had an abrogated ISG response at early time points after infection [15]. The late ISG response appears more dependent on MDA5, suggesting a dual requirement of both RIG-I and MDA5 for activation of an effective cellular antiviral response against WNV, at least in MEF [16]. In contrast, a deficiency of TLR3 in MEF, macrophages, and dendritic cells did not alter IFN-α/β production or viral burden, indicating a more limited role of this sensor in recognizing WNV in these cell types

Author Summary

West Nile virus (WNV) is a mosquito-transmitted virus that infects birds, horses, and humans and has become an emerging infectious disease threat in the Western Hemisphere. In humans, WNV can invade into the brain and spinal cord and destroy neurons, causing severe neurological disease, particularly in the immunocompromised and elderly. A better understanding of how the immune system controls WNV infection is critical for developing new treatments and vaccines. In this study, using a mouse model of WNV infection, we evaluate the combined role of two key transcription factors, interferon-regulatory factor-3 (IRF-3) and IRF-7, that orchestrate antiviral and interferon (IFN) responses after infection. Mice that lack both IRF-3 and IRF-7 were highly vulnerable to lethal infection and cells lacking IRF-3 and IRF-7 had a markedly attenuated IFN-α response. Surprisingly, macrophages and dendritic cells lacking IRF-3 and IRF-7 showed a relatively normal IFN-β response. Furthermore, a genetic deficiency of IPS-1, a protein that signals downstream of the RIG-I- and MDA5 cytoplasmic viral RNA sensors, completely abolished IFN-β production. Our experiments suggest that in specific cell types infected with WNV, IFN-β can be induced through an IPS-1-dependent transcriptional signal that does not require the master transcriptional regulators IRF-3 and IRF-7.

[17]. To date, no experiments have been published on the direct role of TLR7 and TLR8 in the priming of IFN responses after WNV infection in cells. A recent study demonstrated no decrease in systemic production of type I IFN in TLR7$^{-/-}$ mice infected with WNV [18]. However, investigations with other RNA viruses suggest that the TLR7/MyD88/IRF-7 axis regulates type I IFN responses in specific subsets of dendritic cells [19,20].

Studies with genetically deficient mice have established an important role of IRF-3 in protection against lethal WNV infection by controlling viral burden in peripheral and central nervous system (CNS) tissues without affecting the systemic type I IFN response [21]. Experiments performed with primary cells established that IRF-3 restricts WNV replication in cortical neurons and MEF through type I IFN-dependent mechanisms whereas in myeloid cells IRF-3 limits WNV infection independently of IFN by regulating basal or WNV-induced expression of host defense molecules [21]. More recent studies demonstrated a pivotal role of IRF-7 in vivo in controlling WNV infection [22]. IRF-7$^{-/-}$ mice developed markedly elevated WNV burdens in multiple tissues and had a blunted systemic type I IFN response. Studies with primary cells showed that IRF-7 controls WNV infection largely through an IFN-α-dependent mechanism. Surprisingly, the IFN-β response remained intact suggesting possible redundant effects of IRF-3 and IRF-7 in regulating IFN-β gene expression. These results agree with an independent study in which IRF-7$^{-/-}$ MEF infected with herpes simplex (HSV), vesicular stomatitis (VSV), or encephalomyocarditis (EMCV) virus showed residual IFN-β responses that were abolished in IRF-3$^{-/-}$× IRF-7$^{-/-}$ MEF [14].

To understand the combined roles of IRF-3 and IRF-7 in innate immune programs following WNV infection in vivo, we generated IRF-3$^{-/-}$× IRF-7$^{-/-}$ double knockout (DKO) mice. An absence of both IRF-3 and IRF-7 led to uncontrolled WNV replication in tissues and more rapid death than either of the single gene deletions. Although severe, the DKO phenotype did not recapitulate that observed in congenic IFN-αβR$^{-/-}$ mice. Despite a complete absence of both IRF-3 and IRF-7, IFN-β induction remained largely intact in some cell types. Remarkably, in experiments with myeloid dendritic cells (mDC) ex vivo, the IFN-β response after WNV infection was abolished by the absence of IPS-1 but was largely unaffected by a combined deficiency or the transcription factors IRF-3 and IRF-7 or individual deficiencies of IRF-1, IRF-5, or IRF-8. However, pharmacological inhibition of signaling by both NF-κB and ATF-2/c-Jun, the two other factors, beside IRF-3 and IRF-7, that form the IFN-β gene transcriptional complex enhanceosome [23–25], strongly reduced the IFN-β response in DKO but not wild type mDC after WNV infection. These studies define cell type-specific molecular mechanisms and roles for IRFs in antiviral defense, and reveal a differential requirement for components of the enhanceosome in inducing the IFN-β gene in response to RNA viruses.

Results

Increased lethality of DKO mice after infection with WNV

Because of the possible functional redundancy of IRF-3 and IRF-7, and to fully evaluate their net contribution to the regulation of the IFN-β transcriptional response after WNV infection, we generated IRF-3$^{-/-}$× IRF-7$^{-/-}$ (DKO) mice. These animals were infected subcutaneously with 10^2 PFU of a highly pathogenic New York strain of WNV. Whereas wild type C57BL/6 mice exhibited a ~60% survival rate, congenic DKO mice displayed a severe phenotype with 100% mortality and a mean time to death of 6.0 days (**Fig 1A**). In comparison, IRF-3$^{-/-}$ or IRF-7$^{-/-}$ single knockout mice infected with the same dose of WNV also had a 100% mortality rate but with mean time to deaths of 9.3 and 7.4 days, respectively [21,22].

As IRF-3 and IRF-7 are key regulators of the type I IFN response to viral infection, we also compared the DKO phenotype with congenic IFN-αβR$^{-/-}$ mice. Similar to what we previously observed [13,26], IFN-αβR$^{-/-}$ mice were vulnerable to WNV infection with 100% mortality by 4 days and a mean time to death of 3.5 days (**Fig 1A**, $P<0.001$ of average survival time compared to DKO mice). Thus, although a combined deficiency of IRF-3 and IRF-7 has a more severe phenotype after WNV infection than their respective single deficiencies, the survival pattern did not fully recapitulate that observed in IFN-αβR$^{-/-}$ mice, suggesting type I IFN induction and/or regulation after WNV infection may require additional transcriptional regulators.

DKO mice show uncontrolled WNV replication in tissues

To more completely evaluate the impact of the IRF-3 and IRF-7 deficiency on WNV pathogenesis in vivo, wild type and DKO mice were infected subcutaneously with 10^2 PFU of WNV and viral burden was measured by fluorogenic quantitative RT-PCR or viral plaque assay at days 1, 2, 3, 4, 5, 6 and 8 in blood, peripheral organs (draining lymph nodes, spleen and kidney) and the CNS tissues (brain and spinal cord) (**Fig 1B–G**).

Elevated viremia was observed in DKO mice when compared to wild type mice (**Fig 1B**). By one day after infection, ~$10^{1.5}$-fold higher levels of viral RNA ($P<0.0001$) were detected in the DKO mice. Markedly enhanced ($10^{4.6}$ to $10^{6.2}$-fold increase, $P<0.0001$) WNV RNA levels were observed in serum of DKO mice on days 2 through 5, after which most animals succumbed to infection.

In the draining lymph nodes, similarly high levels ($10^{2.8}$ to $10^{5.0}$-fold increase, $P<0.0001$) of WNV RNA were observed in the DKO mice throughout infection (**Fig 1C**). In the spleen, infectious WNV was not detected in wild type mice until day 3. In contrast, all DKO mice (10 of 10) had markedly elevated viral titers by day 2 (mean titer of $10^{7.7}$ PFU/g) (**Fig 1D**). Although WNV infection gradually increased in the spleens of wild type mice at days 3 through 5, significantly higher ($10^{4.5}$ to $10^{4.9}$-fold) viral burdens

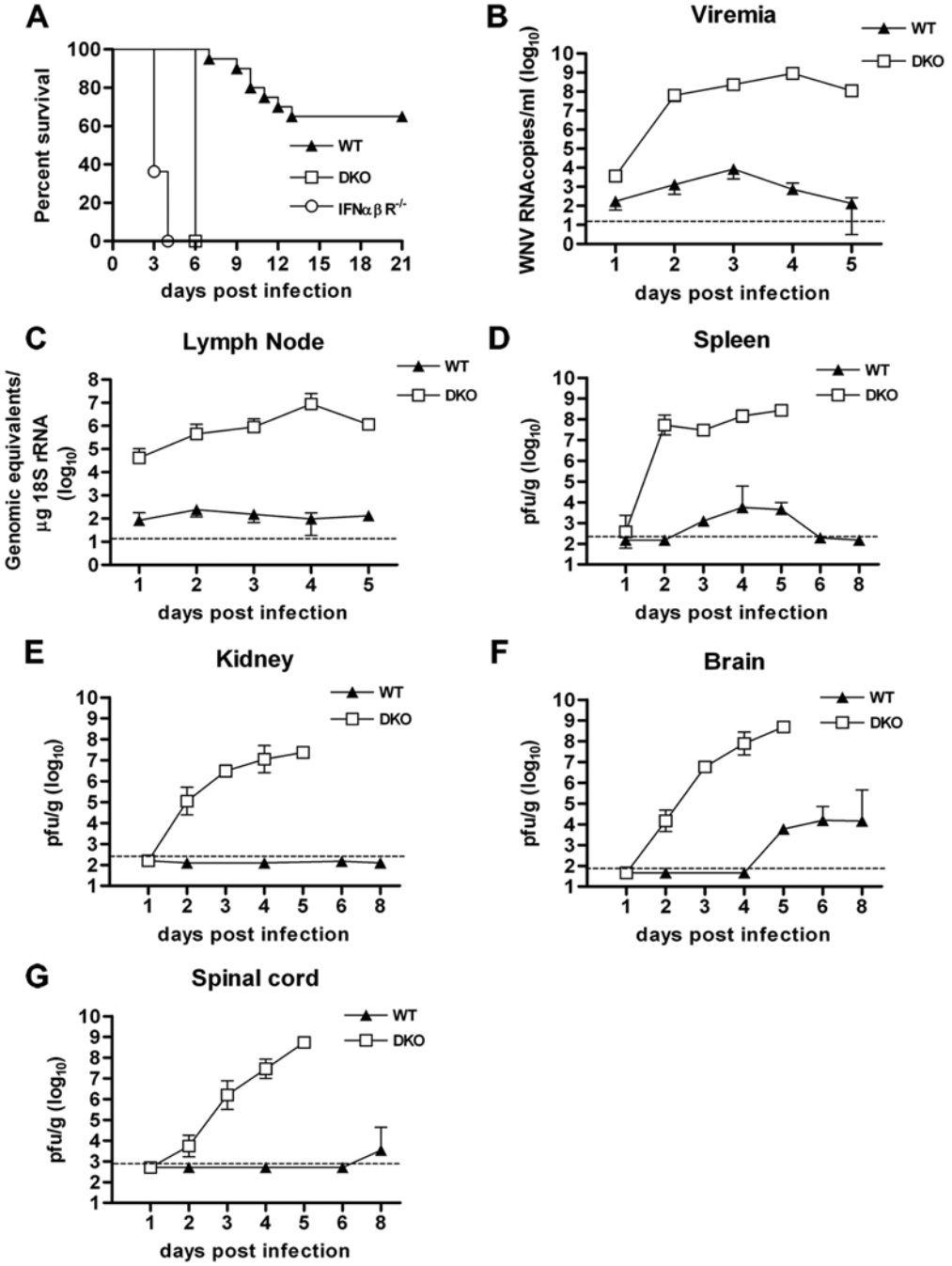

Figure 1. Survival and viral burden analysis in mice. A. Eight to 12 week-old C57BL/6 mice were inoculated with 10^2 PFU of WNV by footpad injection and followed for mortality for 21 days. Survival differences were statistically significant between immunodeficient and wild type mice (n = 11, IFN-αβR$^{-/-}$; n = 20, DKO; and n = 20, wild type mice, P<0.0001). Average survival time between IFN-αβR$^{-/-}$ (3.5 days) and DKO (6 days) mice was also statistically different (P<0.001). **B–G**. Viral burden in peripheral and CNS tissues after WNV infection. WNV RNA in (**B**) serum and (**C**) draining lymph node, and infectious virus in (**D**) spleen, (**E**) kidney, (**F**) brain and (**G**) spinal cord were determined from samples harvested on the indicated days using qRT-PCR (**B** and **C**) or viral plaque assay (**D–G**). Data is shown as viral RNA equivalents or PFU per gram of tissue for 10 to 12 mice per time point. For all viral load data, the solid line represents the median PFU per gram at the indicated time point, and the dotted line represents the limit of sensitivity of the assay.
doi:10.1371/journal.ppat.1000607.g001

were observed in DKO mice. Altered tissue tropism was also observed in DKO mice with significant infection of the kidneys (e.g. 10^5 PFU/g, by day 2 and $10^{7.5}$ PFU/g, by day 5, **Fig 1E**), whereas wild type mice showed no productive infection of the kidneys. Thus, a combined deficiency of IRF-3 and IRF-7 results in sustained and elevated WNV infection in peripheral compartments including spread to and propagation within normally non-permissive organs.

Analysis of viral burden in the brain and spinal cord showed a rapid entry of WNV into the CNS of DKO mice. WNV was detected in all brains from DKO mice at day 2 compared to wild type mice, where WNV was not observed until day 5 (**Fig 1F**).

Notably, at day 5, DKO mice had $\sim 10^{5.2}$ -fold higher viral titers in the brain compared to wild type mice. A similar pattern was observed in the spinal cord of DKO mice with all animals showing markedly elevated viral loads after day 2 (**Fig 1G**). In contrast, in wild type mice, infectious WNV was not detected in the majority of animals until day 8 after infection. Thus, a combined absence of IRF-3 and IRF-7 results in early neuroinvasion and uncontrolled WNV replication.

The systemic type I IFN response in DKO mice is blunted but not abolished

Previous studies have reported that an absence of IRF-3 in vivo does not profoundly reduce the levels of type I IFN in serum after WNV [21,27] or other viral infections [14]. In contrast, IRF-$7^{-/-}$ mice infected with WNV had a reduced but not abrogated systemic IFN response [22]. We therefore used the DKO mice to define whether signaling through IRF-3 could explain the residual systemic type I IFN response after WNV infection in IRF-$7^{-/-}$ mice. Using a highly sensitive L929 cell bioassay, we compared the serum IFN levels in DKO and wild type mice after WNV infection. As observed previously [21,22], in wild type mice type I IFN was detected in serum by day 1 with peak levels measured at days 3 and 4 after infection (**Fig 2**). In contrast, in the DKO mice, serum IFN levels at day 1 were below the detection level (0.01 IU/ml) of the assay. Despite the higher viremia, serum IFN levels in the DKO mice were reduced at days 2, 3 and 4 when compared to wild type animals ($\sim$5 to 14-fold lower, $P<0.005$), but were not abolished. This antiviral activity in the serum of infected DKO mice was confirmed as type I IFN-dependent by depletion experiments with a neutralizing mAb against the IFN-α/βR (data not shown). Thus, a combined deficiency of IRF-3 and IRF-7 in vivo delays and diminishes the accumulation of type I IFN in serum. However, over time, type I IFN accumulates in the serum of DKO mice after WNV infection. Thus, additional regulatory factors must contribute to the systemic IFN response. Notably, these results agree with a recent study in which independently-generated DKO mice infected with mouse cytomegalovirus (MCMV) showed a residual systemic IFN response that was entirely specific for IFN-β [28].

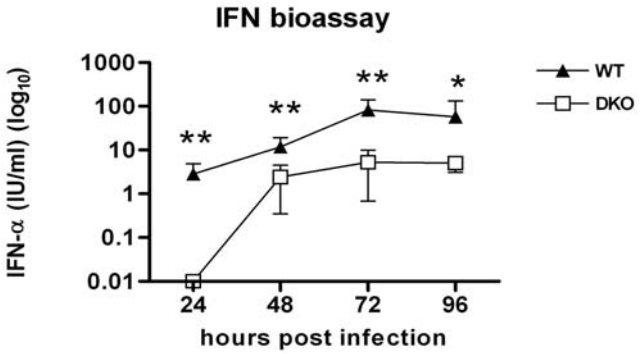

Figure 2. Levels of type I IFN levels in serum of wild type and DKO mice infected with WNV. Mice were inoculated with 10^2 PFU of WNV by footpad injection and sacrificed at the indicated times. Type I IFN levels were determined from serum collected on days 1 to 4 after WNV infection by an EMCV bioassay in L929 cells. Data reflect averages of serum samples from 5 to 10 mice per time point and the data are expressed as international units (IU) of IFN-α per ml. The specificity of the assay was confirmed with an anti-IFN-$\alpha\beta$R neutralizing antibody (data not shown). Asterisks indicate values that are statistically significant (**, $P<0.005$, *, $P<0.05$).
doi:10.1371/journal.ppat.1000607.g002

IRF-3 and IRF-7 are required for the type I IFN and ISG response in MEF after WNV infection

To better understand the net effect of IRF-3 and IRF-7 on WNV infection and induction of a protective IFN response, we infected primary cells from DKO and wild type mice. Because MEF have been studied extensively in virus infection-host immune response assays [16,29,30], we initially evaluated the effect of an IRF-3 $\times$ IRF-7 deficiency in these cells. Previous experiments had shown a blunted IFN-α response and a normal IFN-β response in IRF-$7^{-/-}$ MEF infected with WNV [22]. In contrast, IRF-$3^{-/-}$ MEF had a diminished IFN-α and -β response early after infection but developed normal levels at later time points (S. Daffis and M. Diamond, unpublished data). In DKO MEF, IFN-α mRNA and protein secretion were completely abolished after WNV infection (**Fig 3A and 3B**). Similarly, levels of IFN-β mRNA were strongly reduced at 24 h ($\sim$70-fold decrease, $P<0.0001$) and 48 h after infection ($\sim$130-fold decrease, $P<0.0001$) but not entirely abolished (**Fig 3C**). Measurement of secreted IFN-β in the cell supernatants corroborated these findings as a $\sim$4 and 20-fold reduction ($P<0.0001$) was observed in DKO MEF at 24 and 48 hours, respectively (**Fig 3D**). Thus, normal induction of IFN-α and IFN-β in MEF after WNV infection primarily requires transcriptional activation by IRF-3 and IRF-7.

We next assessed the expression pattern of selected ISG including ISG49, ISG54 and RIG-I by Western blot analysis. In wild type MEF, these proteins become rapidly induced at 24 h after infection and were sustained at 48 h. In contrast, induction was absent in DKO MEF at 24 h after infection and levels were comparably reduced at 48 h (**Fig 3E**). To assess how this phenotype affected WNV replication, multi-step viral growth analysis was performed (**Fig 3F**). Although no difference in viral titers was observed at 24 hours, enhanced WNV replication was seen at 48 h (13-fold, $P = 0.004$) and 72 h (58-fold, $P<0.0001$) in DKO MEF. Moreover, the levels of WNV at 48 and 72 h in the DKO MEF were greater than those previously observed with the single IRF-$3^{-/-}$ or IRF-$7^{-/-}$ MEF (S. Daffis and M. Diamond, unpublished results and [22]). As IRF-3 and IRF-7 appear to primarily regulate the IFN and ISG responses in MEF, we predicted that the WNV replication phenotype in the DKO MEF should not differ substantially from congenic IFN-$\alpha\beta$R$^{-/-}$ MEF. Indeed, when directly compared, only small differences in viral growth were observed between DKO and IFN-$\alpha\beta$R$^{-/-}$ MEF (2.7 fold, $P<0.03$ at 48 h and 2.3 fold, $P<0.002$ at 72 h) (**Fig 3F**).

IRF-3 and IRF-7 regulate the type I IFN and ISG response in cortical neurons after WNV infection

To evaluate the combined roles of IRF-3 and IRF-7 in control of viral replication and the IFN response in neuronal cells, we assessed WNV infection of primary cortical neurons isolated from DKO mice. Analysis of viral growth kinetics confirmed that IRF-3 and IRF-7 restrict WNV replication as a $\sim$5 to 6-fold increase ($P<0.0001$) in viral titer was observed at 24 h and 48 h compared to wild type cells (**Fig 4A**). Somewhat surprisingly, the DKO neurons did not show increased replication relative to cells lacking either IRF-3 or IRF-7 (data not shown and [21,22]). The relatively modest replication phenotype in the absence of IRF-3 and IRF-7 is consistent with only a small IFN-dependent antiviral effect in these cells: IFN-α or -β pre-treatment inhibits WNV infection in cortical neurons a maximum of 5 to 8-fold [13]. Analysis of the IFN response of WNV-infected DKO neurons showed a complete ablation of the IFN-α gene induction confirming results with the IRF-$7^{-/-}$ cortical neurons [22] (**Fig 4B**). In contrast, and unlike that observed with MEF or other primary myeloid cells (see

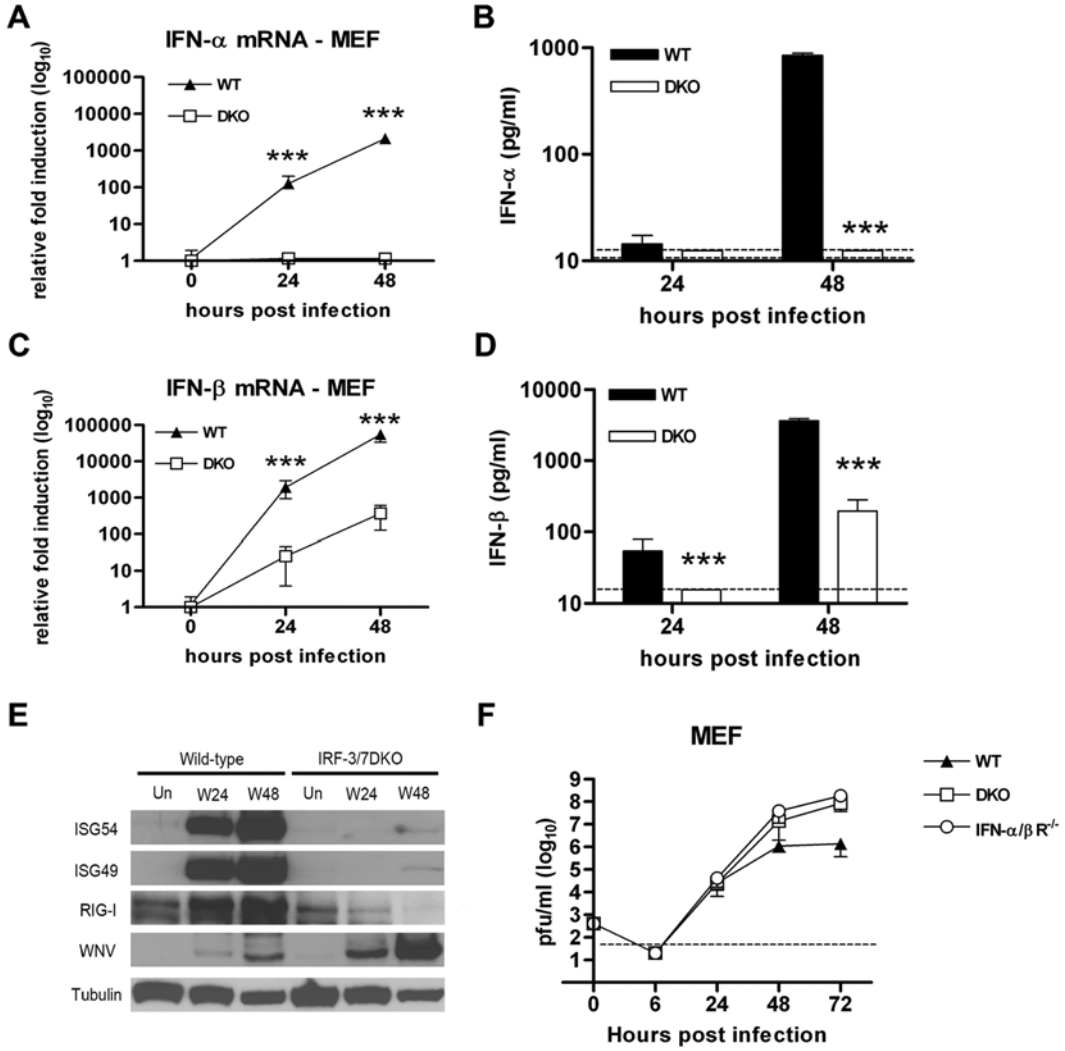

Figure 3. IRF-3 and IRF-7 control the IFN-α/β gene induction and ISG expression in MEF. A–D. MEF generated from wild type or DKO mice were infected at an MOI of 0.1 and analyzed for IFN-α/β gene induction. Total RNA from uninfected and WNV-infected MEF was harvested at the indicated times after infection and levels of (**A**) IFN-α and (**C**) IFN-β mRNA were measured by qRT-PCR. Data are normalized to 18S rRNA and are expressed as the relative fold increase over normalized RNA from uninfected controls. Accumulation of (**B**) IFN-α and (**D**) IFN-β protein in supernatants was evaluated by ELISA. **E**. Whole cell lysates were generated at the indicated times from wild type or DKO MEF that were uninfected (Un) or infected with WNV (W). Protein levels of ISG49, ISG54, RIG-I, WNV and tubulin were examined by immunoblot analysis. **F**. MEF generated from wild type, IFN-αβR$^{-/-}$ and DKO mice were infected at an MOI of 0.001 and virus production was evaluated by plaque assay. The data is the average of at least three independent experiments performed in quadruplicate, (***, $P<0.0001$).
doi:10.1371/journal.ppat.1000607.g003

below), induction of IFN-β mRNA in DKO cortical neurons was also entirely abolished (**Fig 4C**). Consistent with this, analysis of ISG in DKO neurons showed a complete loss of induction of ISG54, RIG-I and MDA5 following WNV infection (**Fig 4D**). Thus, in cortical neurons coordinate signals through the transcriptional regulators IRF-3 and IRF-7 are required for IFN-α and IFN-β gene induction after WNV infection.

IFN-β response in Mϕ after WNV infection is partially IRF-3 and IRF-7-dependent

As previous studies suggested cell type-specific differences in type I IFN induction [21], we evaluated the effect of the combined IRF-3 and IRF-7 deficiency in macrophages (Mϕ), a cell type that is permissive to WNV in vivo [26]. Prior experiments established that Mϕ lacking either IRF-3 or IRF-7 were more susceptible to WNV infection [21,22]. Analogously, DKO Mϕ supported increased WNV replication (~35, 250 and 310-fold, $P<0.0001$ at 24, 48 and 72 h after infection, respectively) compared to wild type or even IRF-3$^{-/-}$ or IRF-7$^{-/-}$ singly deficient cells (**Fig 5A** and [21,22]). In contrast to that observed with MEF (see **Fig 3**), the DKO Mϕ produced ~14-fold less ($P<0.05$) WNV at 72 h compared to IFN-αβR$^{-/-}$ Mϕ infected in parallel. Thus, an absence of both IRF-3 and IRF-7 in Mϕ did not recapitulate the replication phenotype of IFN-αβR$^{-/-}$ cells. As such a discrepancy could be related to differences in the type I IFN and/or ISG response, we analyzed these in DKO Mϕ after WNV infection. As expected, levels of IFN-α mRNA were completely abolished (**Fig 5B**), consistent with results from IRF-7$^{-/-}$ Mϕ [22]. Whereas IFN-β mRNA levels were reduced at 24 h after infection in DKO Mϕ, they accumulated to normal levels by 48 h (**Fig 5C**). Western blot analysis of ISG expression confirmed this pattern, as the early induction of several ISG was altered at 24 h but not 48 h

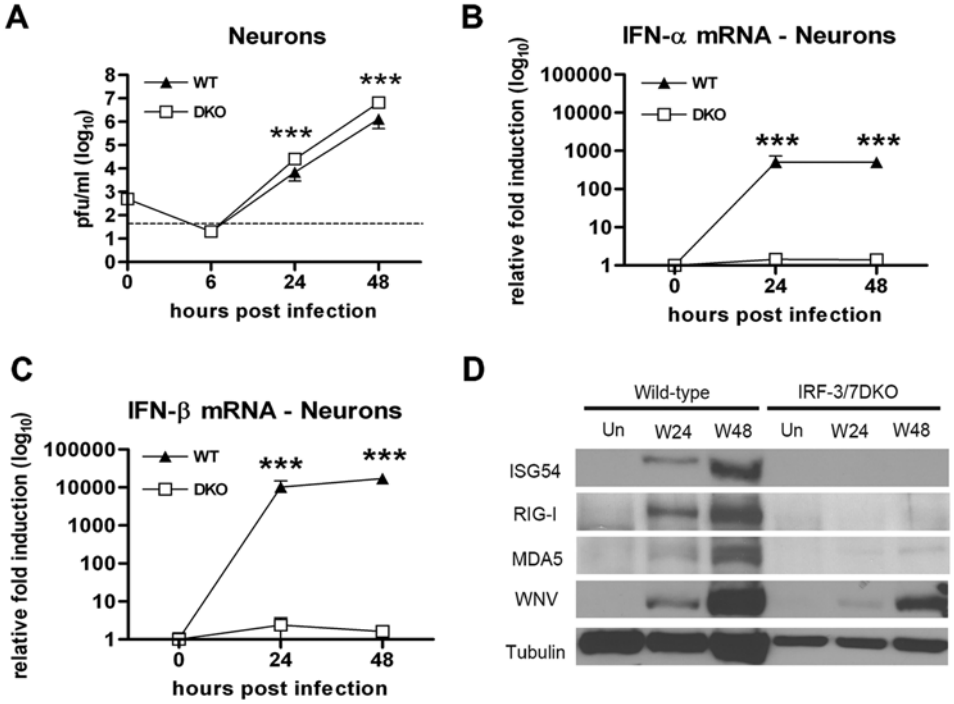

Figure 4. IRF-3 and IRF-7 restrict WNV infection by regulating the IFN-α/β response and ISG expression in primary cortical neurons. **A**. Primary cortical neurons generated from wild type or DKO mice were infected at an MOI of 0.001 and virus production was evaluated at the indicated times by plaque assay. Values are an average of triplicate samples generated from three independent experiments. Asterisks indicate values that are statistically significant (***, $P<0.0001$). **B** and **C**. Levels of (**B**) IFN-α and (**C**) IFN-β mRNA in WNV-infected cortical neurons were measured by qRT-PCR as described in the legend of Figure 3. **D**. Whole cell lysates were generated at the indicated times from wild type or DKO MEF that were uninfected (Un) or infected with WNV (W). Protein levels of ISG54, RIG-I, and MDA5 were examined by immunoblot analysis. The data is the average of at least three independent experiments performed in quadruplicate (***, $P<0.0001$).
doi:10.1371/journal.ppat.1000607.g004

following WNV infection (**Fig 5D**). Thus, after WNV infection of Mϕ, IRF-3 and IRF-7 coordinately regulate the early but are dispensable for the later IFN-β and ISG responses.

IRF-3 and IRF-7 are also dispensable for the IFN-β response in mDC after WNV infection

Because mDC are likely early targets for WNV infection in animals [31–33] and help orchestrate innate and adaptive antiviral immune responses [34], we evaluated IFN and ISG responses in bone marrow-derived mDC. Prior studies showed that mDC lacking either IRF-3 or IRF-7 support enhanced WNV replication, IRF-$3^{-/-}$ mDC developed normal IFN-α/β responses after WNV infection, and IRF-$7^{-/-}$ mDC had reduced IFN-α but relatively intact IFN-β responses after WNV infection (S. Daffis and M. Diamond, unpublished results and [22]). Multi-step growth curve analysis of DKO mDC infected with WNV showed a higher viral burden compared to wild type cells (16 to 95-fold, $P<0.0001$) and IRF-$3^{-/-}$ or IRF-$7^{-/-}$ mDC (**Fig 6A**, S. Daffis and M. Diamond, unpublished results, and [22]). The viral titers in DKO mDC were similar to those obtained in IFN-αβR$^{-/-}$ mDC, suggesting a defect in type I IFN signaling in the DKO cells. Surprisingly, whereas levels of IFN-α mRNA and protein were abolished (**Fig 6B and 6C**), induction of IFN-β gene and protein production was not significantly affected ($P>0.2$) after WNV infection of DKO mDC (**Fig 6D and 6E**). Thus, in mDC, IRF-3 and IRF-7 regulate the IFN-α response but are largely dispensable for inducing IFN-β after WNV infection. Western blot analysis of ISG corroborated these findings as similar levels of ISG were observed in wild type and DKO mDC at 24 and 48 h after WNV infection (**Fig 6F**). These data suggest that the expression of ISG is primarily IFN-β-dependent or that the IFN-α and -β have redundant effects in these cells. Nonetheless, as higher viral replication was sustained in DKO mDC despite a relatively normal IFN-β response and ISG expression profile, it remains possible that IRF-3 directly regulates expression of a key subset of ISG that accounts for anti-WNV activity in this cell type.

To determine whether the IFN-β induction response in DKO mDC was specific for WNV, we performed experiments with agonists for the TLR3 and TLR4 pathways and with unrelated viruses (Chikungunya virus (CHIK), an emerging human alphavirus, and EMCV, a model rodent picornavirus). As expected, wild type mDC that were treated extracellularly with TLR3 (poly I:C) or TLR4 (LPS) agonists rapidly induced IFN-β mRNA (**Fig 7A**). In DKO cells, and in contrast to that observed with WNV, the IFN-β response downstream of TLR treatment was effectively abolished. Thus, activation of the IFN-β response in mDC after TLR3 and TLR4 stimulation requires both IRF-3 and IRF-7. To define whether the IRF-3/IRF-7-independent IFN-β response was specific to WNV, we infected mDC with additional RNA viruses (**Fig 7B**). In wild type mDC, EMCV infection induced a robust IFN-β response similar to WNV, and high levels of IFN-β mRNA were detected by 24 hours post infection (~100-fold increase). Infection with CHIK at a higher MOI also resulted in a similar IFN-β gene induction at 24 hours post infection. In DKO cells, the IFN-β response after infection with WNV, EMCV, and CHIK was equivalent to that observed in wild type cells. Thus, in mDC, IRF-3 and IRF-7 are dispensable for activation of IFN-β gene transcription, not only in response to WNV but also to other positive strand RNA viruses that are genetically unrelated.

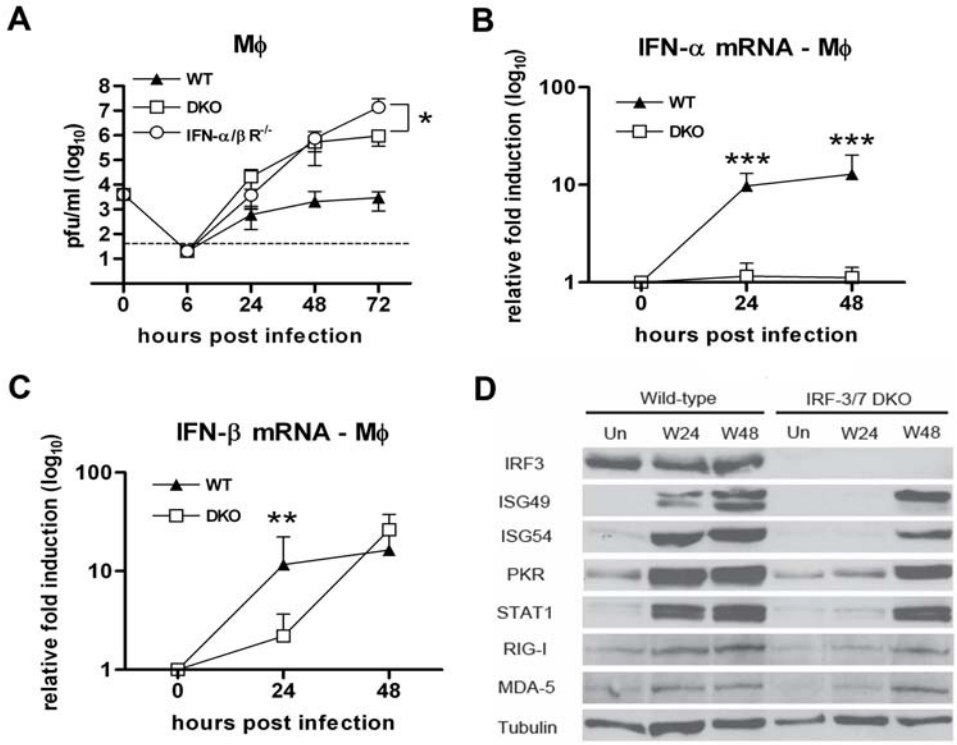

Figure 5. IRF-3 and IRF-7 partially modulate the IFN-β response and ISG expression in primary Mϕ. A. Mϕ generated from wild type, IFN-αβR$^{-/-}$ and DKO mice were infected at an MOI of 0.01 and virus production was evaluated at the indicated times post infection by plaque assay. Values are an average of quadruplicate samples generated from at least three independent experiments. **B**. Whole cell lysates were generated at the indicated times from wild type and DKO Mϕ that were uninfected (Un) or infected with WNV (W). Protein levels of ISG49, ISG54, PKR, STAT1, RIG-I, MDA5 and tubulin were examined by immunoblot analysis. **C** and **D**. The induction of (**C**) IFN-α and (**D**) IFN-β mRNA in WNV-infected Mϕ was analyzed by qRT-PCR as described in Figure 3. Asterisks indicate values that are statistically significant (***, P<0.0001, **, P<0.005, *, P<0.05).
doi:10.1371/journal.ppat.1000607.g005

The IFN-β response in mDC after WNV infection does not rely on type I IFN signaling and IRF-1 or IRF-8

To begin to investigate the mechanism(s) that regulate IFN-β gene induction in mDC, we infected IRF-1$^{-/-}$ and IRF-8$^{-/-}$ mDC with WNV. These transcription factors have been implicated in type I IFN gene transcription in DC after TLR stimulation or viral infection [35,36]. Notably, no difference in IFN-α and IFN-β mRNA levels was observed in IRF-1$^{-/-}$ mDC (**Fig 8A and 8B**). Subsequently, we assessed whether the regulator of IFN-β transcription was IFN-inducible, as has been suggested for IRF-8 in the context of infection by MCMV [36] or paramyxovirus [37]. IFN-αβR$^{-/-}$ mDC were infected with WNV and the levels of IFN-α and IFN-β mRNA were measured. Whereas the IFN-α response was diminished in these cells, likely because of the abolition of the type I IFN positive feedback loop (**Fig 8C**), the IFN-β gene response in IFN-αβR$^{-/-}$ mDC was greater (5 to 10-fold, P<0.05) compared to wild type cells (**Fig 8D**). These results suggest that, unlike the regulation of the IFN-α response, activation of the IFN-β gene after WNV infection in mDC is independent of the type I IFN positive feedback loop. Consistent with this, no difference in IFN-α and IFN-β induction was observed after WNV infection of IRF-8$^{-/-}$ mDC (**Fig 8A and 8B**).

Recent studies have suggested that IRF-5 can activate transcription of IFN and other inflammatory cytokine genes after viral infection or TLR stimulation [38–41]. As IRF-5 also has been implicated in IFN production and protection in vivo after infection by negative strand RNA viruses (Newcastle Disease virus (NDV) and VSV) and DNA viruses (HSV) [38,42], we evaluated whether the transcriptional signal after WNV infection of mDC cells was dependent on IRF-5. IRF-5$^{-/-}$ mDC showed only a modest yet reproducible reduction (2.5-fold, P<0.05) in IFN-β gene transcription within 24 hours of WNV infection (**Fig 8D**). By 48 hours, however, these deficits were no longer apparent as equivalent or even greater levels of IFN-β mRNA were detected in IRF-5$^{-/-}$ cells. Taken together, our experiments suggest that IRF-1 and IRF-8 are dispensable for induction of IFN-β gene transcription in mDC, whereas an IRF-5 has a small and transient regulatory effect in these cells after WNV infection.

A combined inhibition of NF-κB and ATF-2/c-Jun in DKO mDC reduces the IFN-β response after WNV infection

The transcriptional activation of the IFN-β gene requires full occupancy of an enhancer complex known as the ''enhanceosome'' [23–25]. In vitro, the active IFN-β enhanceosome is formed after association of the transcription factors IRF-3, IRF-7, ATF-2/c-Jun, and NF-κB. Although synergy in transcription of the IFN-β gene occurs after coordinate binding of these regulatory factors in several cell types [25], the mechanistic basis for full occupancy of the enhanceosome remains incompletely understood. Since a combined deficiency of IRF-3 and IRF-7 only modestly reduced the IFN-β gene induction in mDC after WNV infection, we hypothesized that the residual IFN-β activity could occur through a NF-κB-dependent and/or ATF-2/c-Jun-dependent signal that is mediated directly through PRR signaling. To test this possibility, we used the highly specific and validated pharmacological inhibitors of NF-κB (BAY 11-7082) [43,44] and p38 MAP kinase (SB 202190), which is essential for phosphorylating and activating

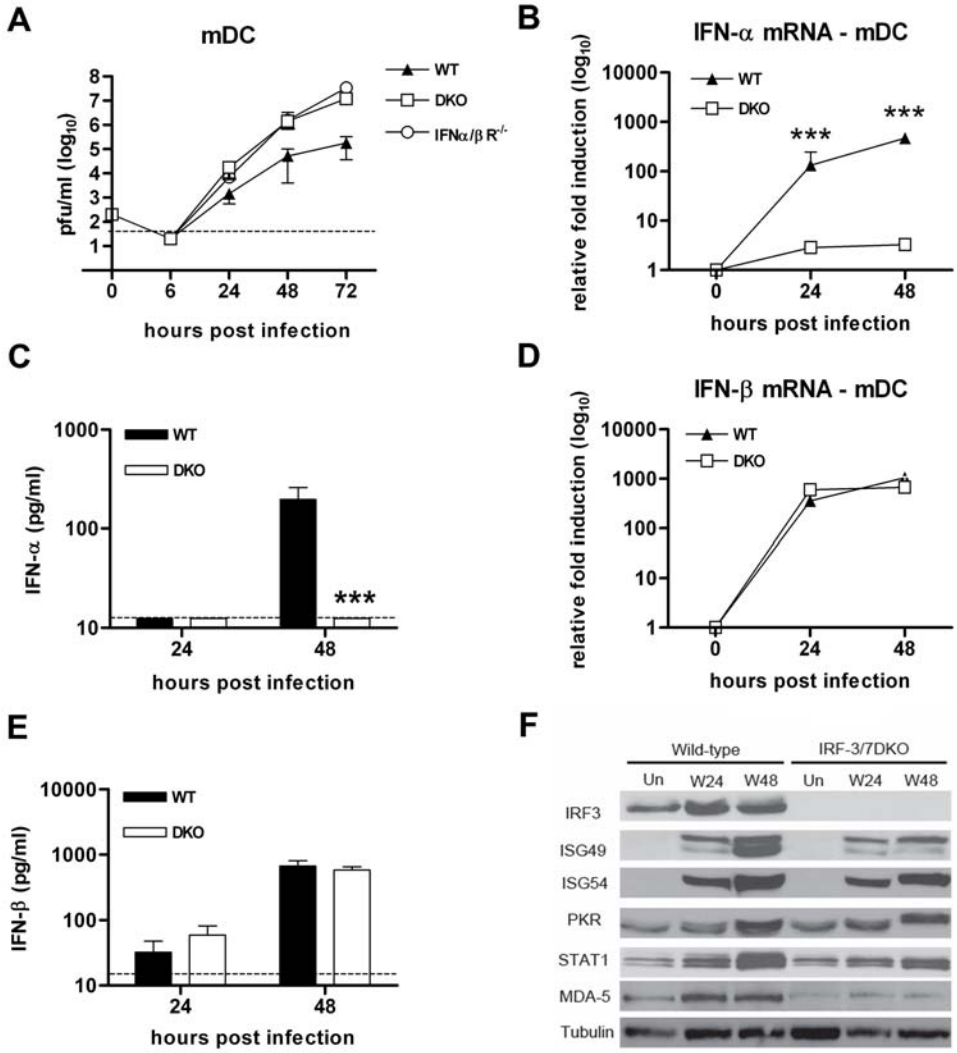

Figure 6. The WNV-induced IFN-β response and ISG expression is primarily IRF-3 and IRF-7-independent in mDC. A. mDC generated from wild type, IFN-αβR$^{-/-}$ and DKO mice were infected at an MOI of 0.001 and virus production was evaluated at the indicated times post infection by plaque assay. Values are an average of quadruplicate samples generated from at least three independent experiments (***, $P<0.0001$). **B–E**. Levels of (**B**) IFN-α and (**D**) IFN-β mRNA as well as (**C**) IFN-α and (**E**) IFN-β protein in WNV-infected mDC were measured by qRT-PCR or ELISA as described in the legend of Figure 3. **F**. Whole cell lysates were generated at the indicated times from wild type and DKO mDC that were uninfected (Un) or infected with WNV (W). Protein levels of ISG49, ISG54, PKR, STAT1, RIG-I, MDA5 and tubulin were examined by immunoblot analysis.
doi:10.1371/journal.ppat.1000607.g006

the ATF-2/c-Jun complex [45]. Treatment of DKO mDC with increasing concentrations of BAY 11-7082, the NF-κB inhibitor, yielded only a small reduction of WNV-induced IFN-β response (maximum of 3.9 fold decrease, $P = 0.006$) (**Fig 9A**). In contrast, the LPS-induced TNF-α response, which is dominantly regulated by NF-κB [46,47], was dose-dependently inhibited in wild type and DKO mDC treated with BAY 11-7082 (**Fig 9C**). Analogously, treatment of DKO mDC with SB 202190 had a limited effect on the WNV-induced IFN-β response (3.5 fold decrease, $P = 0.02$) (**Fig 9A**). Thus, in mDC lacking IRF-3 and IRF-7, inhibition of NF-κB or ATF-2/c-Jun alone only modestly reduced the IFN-β gene transcription after WNV infection. However, a combined inhibition of both NF-κB and ATF-2/c-Jun in DKO mDC strongly diminished the IFN-β response (29-fold decrease, $P<0.0001$). In contrast, a more subtle decrease (2.5-fold decrease, $P = 0.006$) of IFN-β transcription after WNV infection was observed in wild type mDC that retained expression of IRF-3 and IRF-7. Parallel experiments using an ATP metabolism assay confirmed that the difference in effect by the inhibitors was not due to differential cytotoxicity between wild type and DKO cells (**Fig 9A**). These experiments suggest that, in mDC, efficient activation of the IFN-β gene does not require the full enhanceosome occupancy, as a combined functional absence of IRF-3, IRF-7, NF-κB and ATF-2/c-Jun is necessary to strongly inhibit the IFN-β gene activation after WNV infection.

Since the activation of the IFN-β response in MEF was markedly reduced in the absence of both IRF-3 and IRF-7, we hypothesized that, in contrast to that observed in DC, the regulation of the IFN-β gene in MEF would depend more strongly on the full occupancy of the enhanceosome with canonical constituents. To assess this, wild type MEF were treated with BAY 11-7082 and/or SB 202190, infected with WNV, and levels of IFN-β mRNA were measured. In contrast to that observed with wild type mDC, inhibition of NF-κB in wild type MEF slightly decreased the IFN-β response (~2-fold decrease, $P = 0.01$) (**Fig 9B**). Similarly, inhibition of ATF-2/c-Jun in wild type MEF

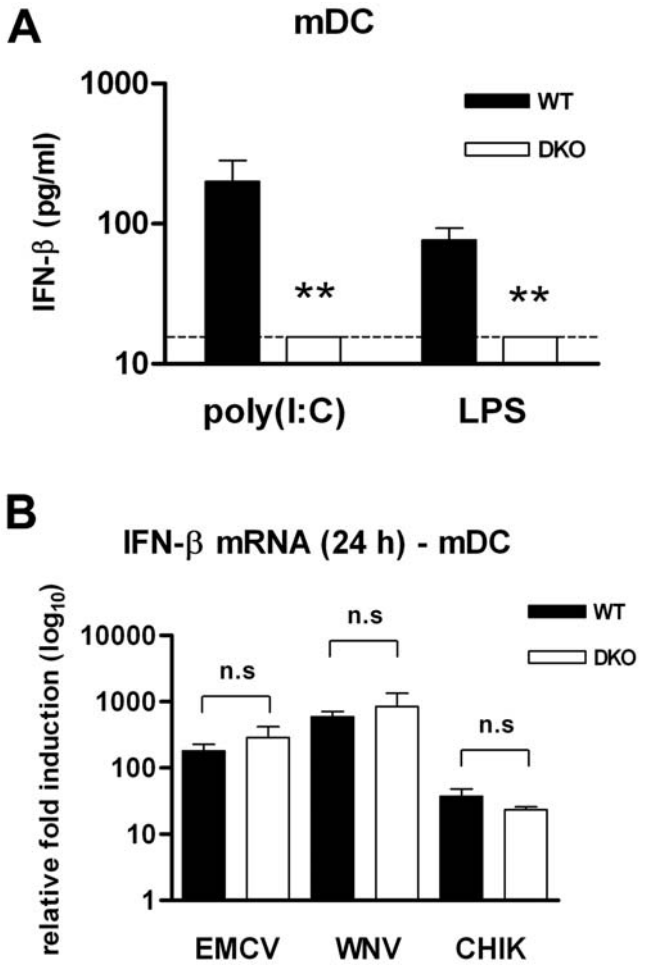

Figure 7. The IFN-β response in mDC after TLR stimulation and viral infection. mDC generated from wild type and DKO mice were (**A**) stimulated with 50 μg/ml of poly(I:C) or 2 μg/ml LPS for 24 h or (**B**) infected with EMCV (MOI 0.1), WNV (MOI 0.1) and CHIK (MOI 1) for 24 h. Levels of IFN-β were measured either by ELISA or qRT-PCR. Values are an average of triplicate samples generated from three independent experiments. Asterisks indicate values that are statistically significant (***, $P<0.0001$, ** $P<0.0005$) from wild type cells; n.s. indicates differences that were not statistically significant.
doi:10.1371/journal.ppat.1000607.g007

also reduced the IFN-β response (~5-fold decrease, $P = 0.007$). More strikingly, inhibition of both NF-κB and ATF-2/c-Jun in wild type MEF strongly attenuated the IFN-β gene transcription (~20-fold decrease, $P<0.0001$). Thus, disruption of function of single components of the enhanceosome is sufficient to reduce the IFN-β transcriptional response in MEF. Consistent with this, inhibition of NF-κB and/or ATF-2/c-Jun in DKO MEF essentially abolished the residual IFN-β response (**Fig 9B**). Taken together, these data suggest that optimal regulation of the IFN-β gene transcription in mDC, in contrast to MEF, does not require complete occupancy four canonical components of the enhanceosome.

A deficiency of IPS-1 abolishes the IFN-β response in MEF and mDC

Immune detection of WNV by mDC likely occurs through the cytosolic PRR, RIG-I and MDA5 and requisite signaling through the IPS-1 adaptor protein; this leads to activation of downstream IRF family proteins and IFN gene transcription [16]. To better understand the signaling pathway between PRR and IFN gene induction after exposure to WNV, we infected IPS-$1^{-/-}$ MEF and mDC. Whereas levels of IFN-α and -β mRNA increase over time in wild type mDC and MEF, induction of both was virtually abolished in IPS-$1^{-/-}$ cells (**Fig 10A–D**). Consistent with this, we did not detect any secreted IFN-α and β from IPS-$1^{-/-}$ DC or MEF supernatants (data not shown). Thus, the induction of type I IFN genes in mDC or MEF after WNV infection is entirely dependent on IPS-1 signaling. Since IRF-5 may play a partial role in IFN-β gene regulation in mDC (**Fig 8D**) and since MyD88 has been suggested to mediate the TLR- and IRF-5-dependent cell type-specific induction of type I IFN after NDV infection [38], we also assessed the role of MyD88 in triggering the IFN-β response in mDC. As shown (**Fig 10E and F**), the IFN-α and β transcription induced by WNV infection in mDC was essentially independent of MyD88. Thus, an optimal IFN-β transcriptional signal in mDC after WNV infection is generated through a pathway that requires IPS-1, a subset of the four (IRF-3, IRF-7, NF-κB and ATF-2/c-Jun) components of the canonical enhanceosome and possibly, IRF-5, after a MyD88-independent activation signal.

TRAF3 and TBK1 regulate the early IPS-1-dependent type I IFN response whereas TRAF6 modulates a later phase

Although our experiments suggested that IFN-β induction after WNV infection required IPS-1 yet was mediated by a cell type-specific complex of transcriptional regulators, the signaling adaptors that connected these pathways remained uncertain. As IPS-1-dependent regulation of the type I IFN genes in response to VSV and Sendai virus requires activation of TRAF3 [48], we infected TRAF3$^{-/-}$ MEF with WNV and measured the levels of IFN-β mRNA and secreted cytokine. TRAF3$^{-/-}$ MEF showed a significant reduction of IFN-β mRNA levels at 24 hours and 48 hours post infection (7.8-fold, $P<0.0001$ and 2.4-fold, $P<0.05$, respectively), which was confirmed by measuring IFN-β in the cell supernatant (3.7- and 1.4-fold decrease, respectively, $P<0.0001$) (**Fig 11B and 11D**). These data suggest that initial IPS-1-dependent trigger of the IFN-β response after WNV infection is mediated at least partially by TRAF3. Consistent with this, the levels of IFN-α mRNA and protein, which reflect the type I IFN positive feedback, also were decreased in TRAF3$^{-/-}$ MEF (mRNA: 32-fold and 36- fold decreases, $P<0.0001$; protein: 1.3-fold, $P<0.0001$) (**Fig 11A and 11C**). As TBK1 is a kinase that reportedly mediates the signal to induce IFN production downstream of the IPS-1/TRAF3 axis [49], we assayed IFN-α/β induction after WNV infection in TBK1$^{-/-}$ MEF. Similar to that observed in TRAF3$^{-/-}$ MEF, the levels of mRNA and more importantly, secreted IFN-β were decreased in TBK1$^{-/-}$ MEF (3.7- and 1.5-fold decrease, respectively, $P<0.0001$) (**Fig 11D**). However, levels of IFN-α mRNA and secreted cytokine in TBK1$^{-/-}$ MEF were not different compared to wild type MEF ($P\geq0.2$) (**Fig 11A and 11C**). Thus, TBK1 appears to mediate the early IFN-β response downstream of TRAF3 after WNV infection but appears dispensable for the later activation of IFN amplification loop. Collectively, these data suggest that, in MEF, the early IFN-β response depends on a signaling pathway involving IPS-1, TRAF3, and TBK1 whereas the late IFN-β response may also partially involve TRAF3. Unfortunately, because TRAF3$^{-/-}$ and TBK1$^{-/-}$ mice are lethal shortly after birth [50,51], we could not confirm this signaling pathway in mDC.

Recent studies with VSV-infected cells have suggested that TRAF6 regulates the IPS-1-dependent signal to induce type I IFN [52]. To evaluate the contribution of TRAF6 to induction of the IFN response after WNV infection, levels of mRNA and IFN-β secreted protein were assayed in TRAF6$^{-/-}$ MEF. In contrast to

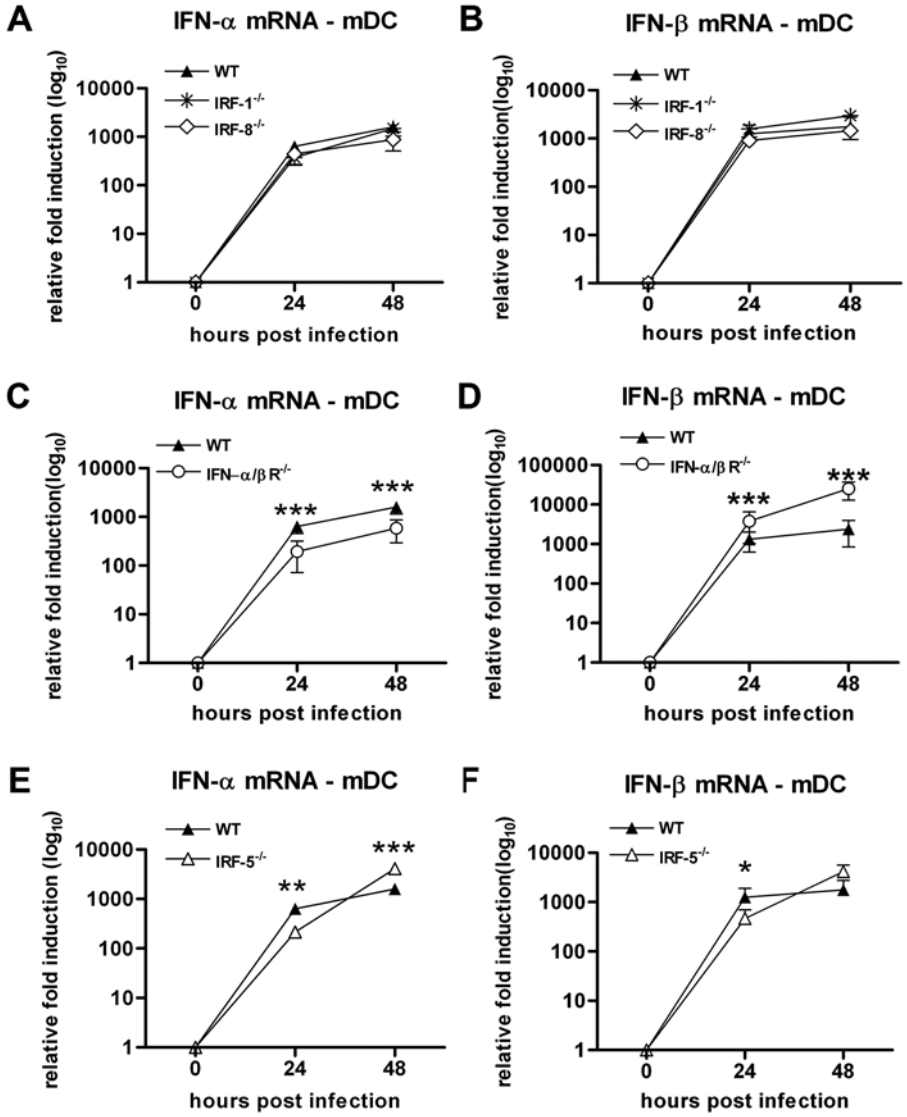

Figure 8. The IFN-β response in mDC is IRF-1, IRF-8, IFN-α/β-independent but partially IRF-5-dependent. mDC generated from wild type, (**A** and **B**) IRF-1$^{-/-}$, IRF-8$^{-/-}$, (**C** and **D**) IFN-α/βR$^{-/-}$, or (**E** and **F**) IRF-5$^{-/-}$ mice were infected at an MOI of 0.1 and levels of IFN-α (**A**, **C**, and **E**) and IFN-β (**B**, **D**, and **F**) mRNA were measured by qRT-PCR. Values are an average of triplicate samples generated from three independent experiments. Asterisks indicate values that are statistically significant (***, $P<0.0001$, **, $P<0.005$, *, $P<0.05$) compared to wild type.
doi:10.1371/journal.ppat.1000607.g008

that observed in TRAF3$^{-/-}$ MEF, levels of mRNA and secreted IFN-β in TRAF6$^{-/-}$ cells supernatants were equivalent to wild type cells at 24 hours post infection ($P>0.2$) but slightly reduced at 48 hours (~2-fold decrease, $P<0.0001$) (**Fig 11D**). TRAF6$^{-/-}$ MEF, however, exhibited reduced IFN-α mRNA levels and protein secretion (240-fold and 4-fold reduction, $P<0.0001$) despite a relatively normal early IFN-β response (**Fig 11A and 11C**). Thus, TRAF6 appears dispensable for the early IFN-β gene response but required for amplifying the late IFN-α and -β responses in MEF. Our experiments suggest that TRAF3 and TRAF6 have distinct and complementary functions in activating the type I IFN response in MEF after WNV infection.

Discussion

Early protection of the host against viral infections relies on the rapid detection of the pathogen and optimal activation of the type I IFN response. Here, using mice and primary cells lacking expression of both IRF-3 and IRF-7, we demonstrate that these transcriptional activators have essential non-redundant functions: DKO mice exhibited a more rapid lethality with enhanced tissue viral burden compared to mice lacking either IRF-3 or IRF-7. Associated with this profound virological phenotype, DKO mice had attenuated levels of systemic type I IFN. A combined deficiency of IRF-3 and IRF-7 however, showed heterogeneous cellular IFN-β but not -α responses. Whereas IFN-α was virtually abolished in all DKO cells tested, the IFN-β response was sustained in DKO Mϕ and mDC. The uncoupling of virus induction of IFN-β from IFN-α in DKO Mϕ and mDC establishes a cell-type specificity and IRF-3/IRF-7-independence of this pathway.

The combined absence of IRF-3 and IRF-7 largely abrogated the IFN-α and β responses in primary fibroblasts and cortical neurons. This data agrees with previous experiments showing loss of IFN-α and -β gene induction in DKO MEF infected with HSV-1, VSV, or EMCV [14]. In contrast, a deficiency of both IRF-3

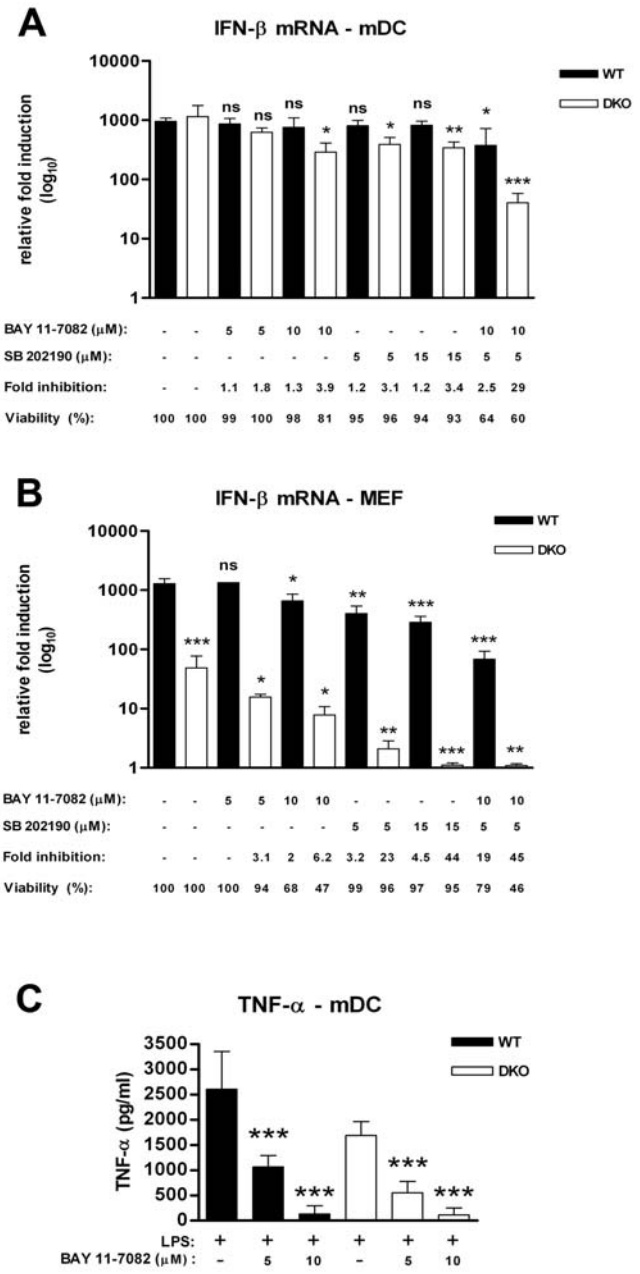

Figure 9. Pharmacological inhibition of NF-κB and p38 in wild type and DKO mDC and MEF. A–B. mDC (**A**) and MEF (**B**) generated from wild type and DKO mice were infected at an MOI of 0.1 in the presence of 1% DMSO or increasing concentrations of BAY 11-7082 (in 1% DMSO) and/or increasing concentrations of SB 202190 (in 1% DMSO). Levels of IFN-β mRNA were evaluated at the indicated times post-infection by qRT-PCR. Cell viability was analyzed using a cytotoxicity assay as described in the Materials and Methods. **C**. Efficiency of BAY 11-7082 in inhibiting NF-κB transcriptional activity. Wild type and DKO mDC were treated with 1% DMSO or 5 μM and 10 μM of BAY 11-7082 and stimulated with LPS (2 μg/ml) for 24 hours. Levels of secreted TNF-α were measured by ELISA. Values are an average of duplicate samples generated from three independent experiments. Asterisks indicate values that are statistically significant (***, $P<0.0001$, **, $P<0.005$, *, $P<0.05$); n.s. indicates differences that were not statistically significant.
doi:10.1371/journal.ppat.1000607.g009

and IRF-7 had a relatively modest effect on the IFN-β response in Mϕ and mDC. Thus, IFN-β induction after WNV infection in myeloid cells depends on IRF-3 and IRF-7-independent transcriptional signals. This result is consistent with data showing significantly reduced but not abrogated type I IFN levels in serum of DKO mice after WNV infection. Analogously, a recent study showed residual IFN-β activity in serum after MCMV infection in independently generated DKO mice [28]. In blood, plasmacytoid DC (pDC) are believed to be primary producers of type I IFN during infection by RNA viruses [53,54]; in pDC, IFN is induced after nucleic acid recognition by TLR7 and signaling through MyD88 to IRF-7 [14,55]. As pDCs require IRF-7 for IFN production, yet DKO mice still produce systemic levels of IFN after WNV infection, non-pDC cell population(s) must contribute to this response. This result agrees with recent data showing no alteration of systemic type I IFN production in TLR7$^{-/-}$ mice infected with WNV [18].

The current model for optimal IFN-β gene transcriptional depends on complete occupancy of the enhanceosome of the IFN-β gene promoter by the transcriptional factors IRF-3, IRF-7, NF-κB and ATF-2/c-Jun. Coordinate transcription factor binding enables recruitment of chromatin-remodeling proteins such as the co-activators GCN5 and CBP/p300 [23,24]. Our data with MEF lacking IRF-3 and IRF-7 show a requirement of all individual enhanceosome constituents in efficiently regulating the IFN-β response. Consistent with this, pharmacological inhibition of the other enhanceosome constituents, NF-κB and ATF-2/c-Jun in MEF expressing IRF-3 and IRF-7 also strongly reduced the efficacy of IFN-β gene transcription. Surprisingly, this model did not apply to mDC where only functional loss of all four enhancesome components strongly diminished IFN-β gene activation. Thus, in mDC, IFN-β expression after viral infection can be induced robustly without full occupancy of the enhanceosome by the canonical transcriptional regulators. Although we do not fully understand the molecular basis for the cell-type restriction of enhanceosome occupancy and IFN-β gene induction, it is possible that in myeloid cells other transcriptional regulators can substitute for the canonical complex members to activate IFN-β gene transcription. However, other individual IRF family members (e.g., IRF-1 or IRF-8), which are known to induce the IFN-β response after viral infection or engagement of PRR in some systems [36,56–58], did not have a dominant regulatory effect in the context of WNV infection. The role of IRF-2 and IRF-4 was not specifically tested as these factors have been reported as negative regulators of the type I IFN responses [59,60]. Nonetheless, we did observe a small yet transient reduction in the IFN-β response after WNV infection in IRF-5$^{-/-}$ mDC and had previously detected a similarly small (~2-fold) reduction in IFN-β transcription in single-deficient IRF-7$^{-/-}$ mDC [22]. In contrast, DKO mDC did not show altered IFN-β responses possibly because of the higher level of WNV infection in these cells.

IRF-5 was initially characterized as a transcription factor downstream of TLR-MyD88 signaling pathway that mediated induction of pro-inflammatory cytokines (e.g., IL-6 and TNF-α) excluding type I IFN [41]. More recent studies indicate that type I IFN induction in mDC after treatment with TLR4, TLR7, or TLR9 agonists is partially IRF-5-dependent [61,62]. IRF-5 is critical for immunity against some viruses, as IRF-5$^{-/-}$ mice have increased mortality and/or blunted systemic IFN production after infection with VSV, HSV, and NDV [38,42]. One group recently identified a new signaling pathway involving NOD2, RIP2 and IRF-5 in modulating IFN-α/β gene induction in response to *Mycobacterium tuberculosis* [63]. Although it remains unclear precisely how IRF-5 regulates the IFN-β gene response or interacts with the enhanceosome components, its expression could account for why induction of the IFN-β response does not require complete occupancy of canonical complex constituents in myeloid cells. The

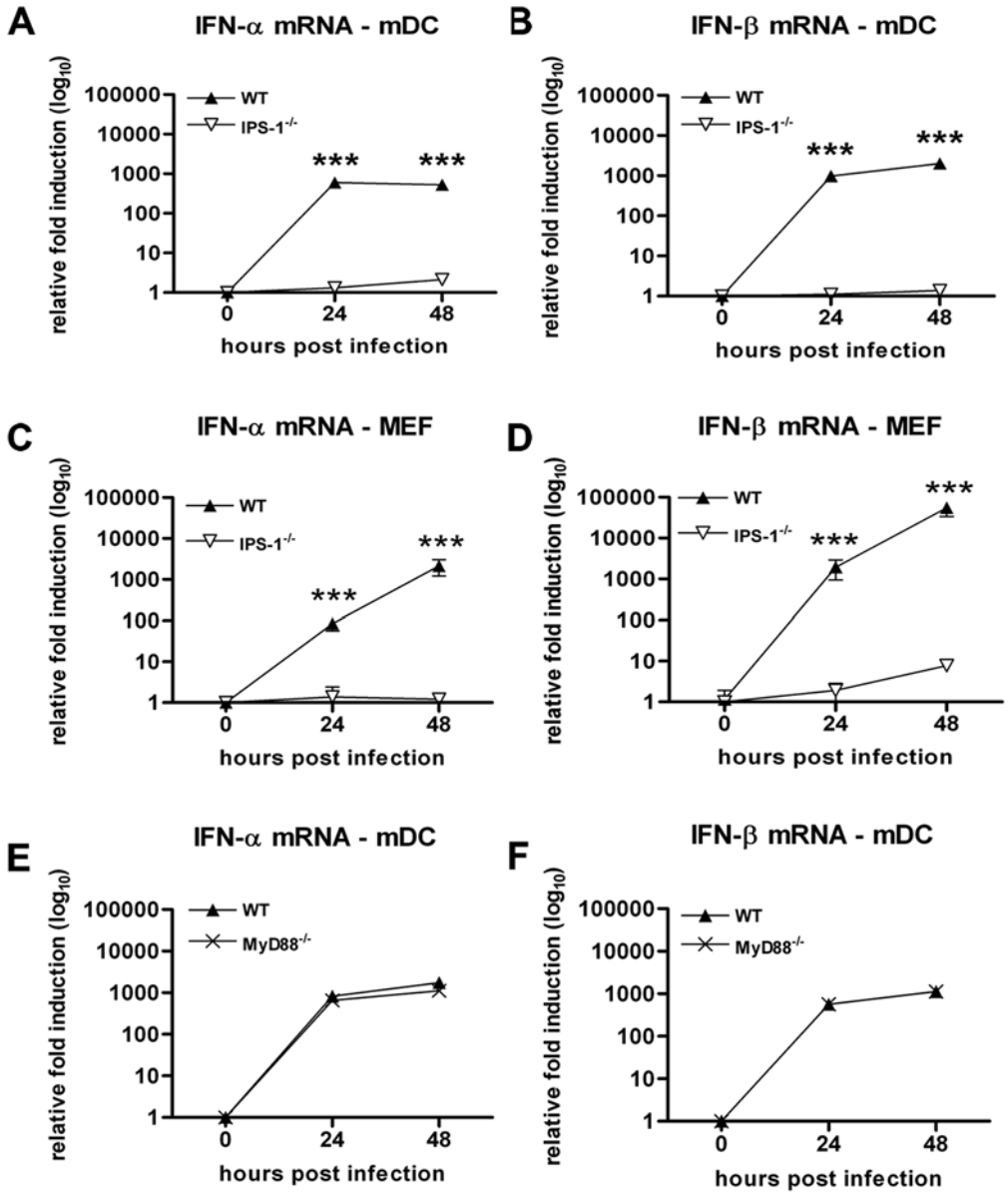

Figure 10. The IFN-β response in mDC and MEF is IPS-1-dependent but MyD88-independent. mDC and MEF generated from wild type, IPS-1$^{-/-}$ and MyD88$^{-/-}$, mice were infected at an MOI of 0.1 and levels of (**A**, **C**, and **E**) IFN-α and (**B**, **D**, and **F**) IFN-β mRNA were quantified by qRT-PCR. Values are an average of duplicate samples generated from three independent experiments. Asterisks indicate values that are statistically significant (***, $P<0.0001$).
doi:10.1371/journal.ppat.1000607.g010

generation of triple IRF-3, IRF-7 and IRF-5 knockout mice and cells may help to address this question. Alternatively, a differential level of histone acetylation of the IFN-β gene could exist in MEF and mDC. A more "relaxed" chromatin structure of the IFN-β gene in mDC might not require the coordinate recruitment of all chromatin-remodeling proteins; thus, full occupancy of the enhanceosome by transcription factors may not be a prerequisite for optimal activation of IFN-β gene transcription in this cell type.

Our results also establish that IFN-β gene activation in several cell types is largely IPS-1-dependent and likely occurs downstream of RIG-I and MDA5 recognition of WNV RNA. This data is consistent with studies in MEF, peritoneal exudates cells, and mDC with NDV, VSV, EMCV, influenza and Sendai viruses [1,16,64–66]. Similarly, a prior study with two related flaviviruses, Japanese encephalitis and Dengue viruses suggested that IFN-β gene induction in A549 lung carcinoma cells was through NF-κB and RIG-I/IRF-3-dependent pathways [67]. Our data also agrees with a previous study that observed no role for TLR3 in regulating the IFN-α/β response in mDC after WNV infection [17]. The IPS-1 dependence validates the primary role for RIG-I and/or MDA5 in sensing WNV. Although both RIG-I and MDA5 coordinately contribute to IFN and ISG induction in MEF after WNV infection [16], in mDC the RIG-I recognition pathway appears dominant ([68] and M. Suthar, S. Daffis, M. Diamond, and M. Gale, unpublished results).

Further dissection of the IPS-1-dependent signaling pathway in MEF showed a differential role of TRAF3 and TRAF6 in regulating IFN-β responses. Based on studies with deficient MEF, TRAF3 contributes dominantly to the early phase of IFN-β production, likely by recruiting TBK1. Consistent with this, others have shown

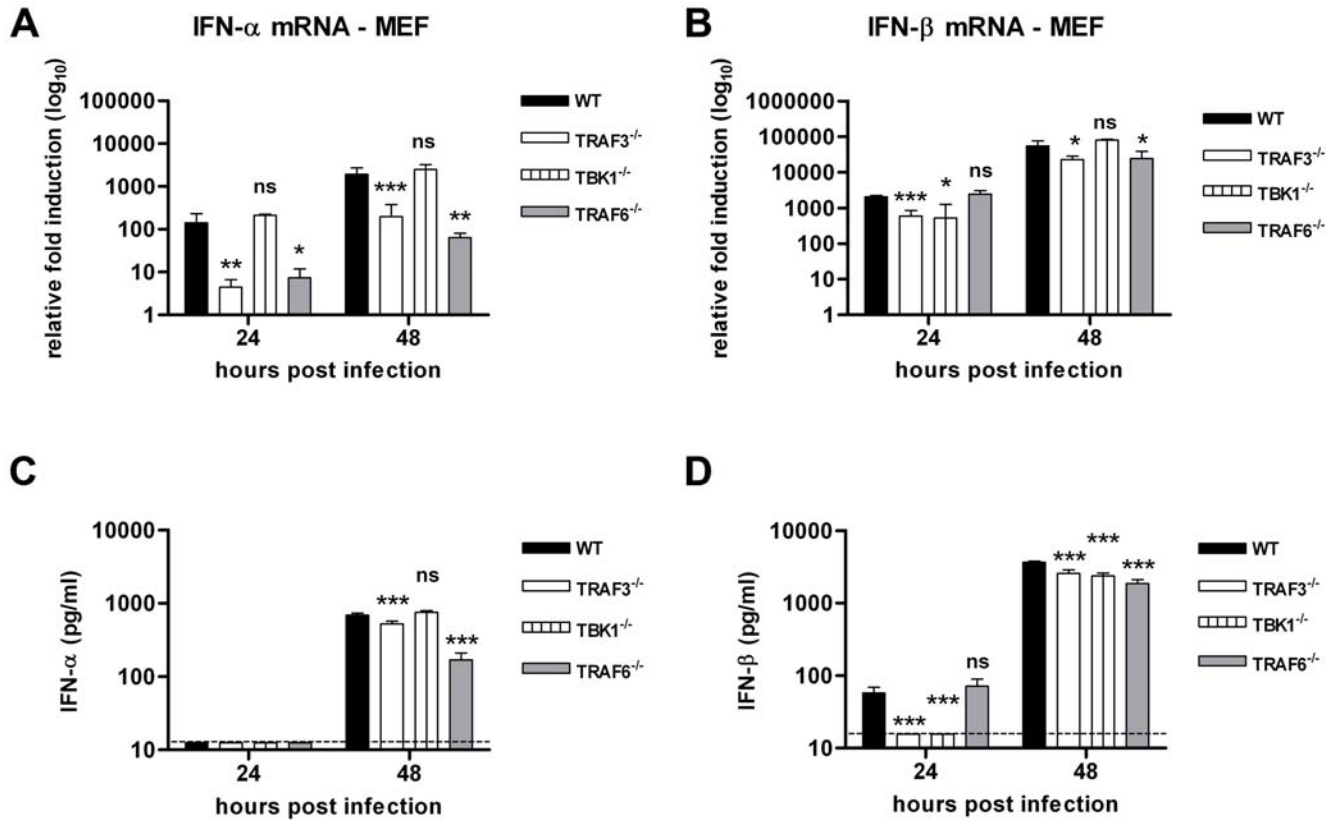

Figure 11. The early phase of the type I IFN regulation in MEF partially involves TRAF3 and TBK1 whereas the late phase requires TRAF6. TRAF3$^{-/-}$, TBK1$^{-/-}$ and TRAF6$^{-/-}$ MEF were infected at an MOI of 0.1 and levels of (**A** and **C**) IFN-α and (**B** and **D**) IFN-β mRNA and secreted protein were measured by qRT-PCR and ELISA. Since basal mRNA expression of the IFN-β gene in uninfected TBK1$^{-/-}$ and TRAF6$^{-/-}$ MEF was lower than that observed in congenic wild type cells, for these cells only, we compared IFN-β mRNA levels to the wild type MEF. Values are an average of duplicate samples generated from three independent experiments. Asterisks indicate values that are statistically significant (***, $P<0.0001$, **, $P<0.005$, *, $P<0.05$); n.s. indicates differences that were not statistically significant.
doi:10.1371/journal.ppat.1000607.g011

that TBK1$^{-/-}$ MEF infected with Sendai virus have a reduced IFN-β response [69]. These results also agree with our unpublished data in IRF-3$^{-/-}$ MEF; a deficiency of IRF-3, which is activated primarily by TRAF3 [49], results in a blunted IFN-α/β response. In contrast to TRAF3, TRAF6 had a more dominant function in sustaining the type I IFN positive feedback. Thus, after WNV infection, the type I IFN amplification loop appears mediated by signals downstream of the IFN-αβR receptor, which may include induction and/or activation of IRF-7 and TRAF6. Since TRAF3 and TRAF6 activate IRF-3, NF-κB, and p38 in MEF [49,52], induction of the late phase of type I IFN may require these signaling adaptor molecules to activate the four components (IRF-3, IRF-7, NF-κB and ATF-2/c-Jun) of the enhanceosome. Based on the data presented here and elsewhere [16], we propose a model for host detection of WNV, signaling through IPS-1 and key adaptor molecules, and transcriptional activation of the IFN-α and β genes at early and late times after infection of MEF (**Fig 12**).

In summary, our studies demonstrate that IRF-3 and IRF-7 coordinately play essential but differential roles in vivo in protecting against WNV pathogenesis primarily by regulating the IPS-1-dependent type I IFN responses through a cell type-dependent mechanism. These studies illuminate the cell-specific complexity of IFN induction and enhance our understanding of how an effective innate response becomes activated soon after viral infection. Greater insight into the molecular mechanisms of the earliest protective antiviral immune response against WNV may provide novel strategies for therapeutic intervention against many related and unrelated viral pathogens.

Materials and Methods

Viruses

The WNV strain (3000.0259) was isolated in New York in 2000 [70] and passaged once in C6/36 *Aedes albopictus* cells to generate a stock (5×10^7 PFU/ml) that was used in all experiments. Chikungunya virus (strain 142, gift of S. Higgs, UTMB) and EMCV (strain K) were propagated in C6/36 and L929, respectively.

Mouse experiments and quantitation of viral burden

C57BL/6 wild-type mice were commercially obtained (Jackson Laboratories, Bar Harbor, ME). IFN-αβ receptor (IFN-αβR)$^{-/-}$ congenic C57BL/6 mice were the kind gift of J. Sprent (La Jolla, CA). The congenic backcrossed IRF-3$^{-/-}$ [37], IRF-5$^{-/-}$ [41], and IRF-7$^{-/-}$ [14] mice were the kind gift of T. Taniguchi (Tokyo, Japan) and provided generously by colleagues in the United States (I. Rifkin, Boston, MA and K. Fitzgerald, Worcester, MA). The IRF-1$^{-/-}$ mice were obtained commercially (Jackson Laboratories). The IRF-8$^{-/-}$ mDC were obtained from bone marrow of IRF-8$^{-/-}$ mice [36] and were a generous gift of P. Tailor and K. Ozato (Bethesda, MD). The TRAF3$^{-/-}$ and TRAF6$^{-/-}$ MEF were kindly provided by G. Cheng (UCLA, Los Angeles, CA) and T. Mak (University of Toronto, Canada),

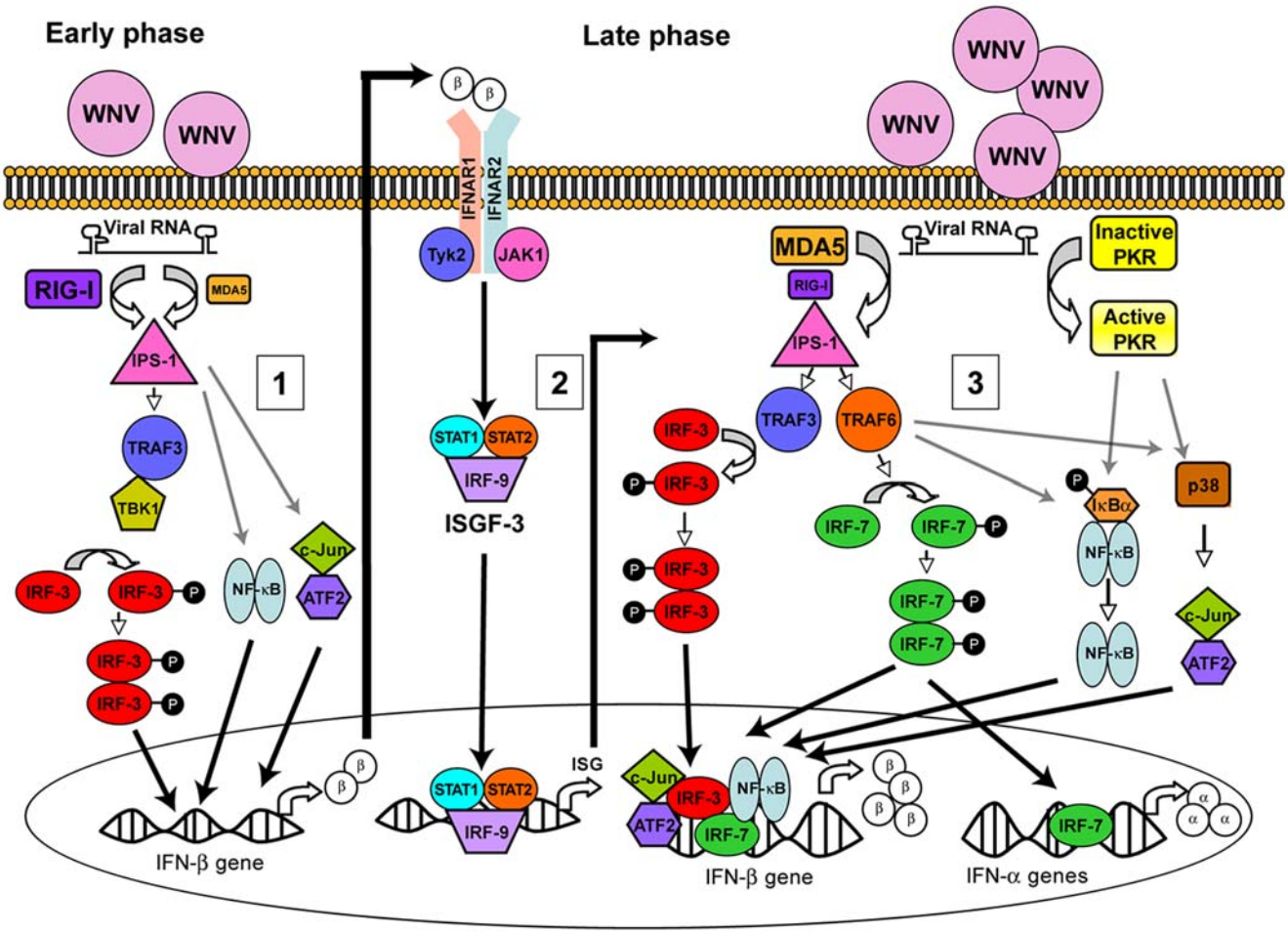

Figure 12. A model for detection of WNV and IFN-α/β gene activation in MEF. (**1**). The host through recognition of an as yet undefined viral RNA PAMP in the cytoplasm detects WNV. RIG-I acts as the primary PRR sensor for WNV during the early stages of infection. RIG-I activation promotes association with IPS-1, which leads to recruitment of TRAF3 and TBK1, and phosphorylation of IRF-3. NF-κB and ATF-2/c-Jun and the small amounts of constitutively expressed IRF-7 may also be activated via this IPS-1-dependent pathway. IRF-3, IRF-7 NF-κB, ATF-2/c-Jun translocate to the nucleus, bind the IFN-β gene promoter and promote transcription. Secretion of IFN-β by infected cells during this early phase results in autocrine and paracrine type I IFN signaling through binding of the IFN-αβR. (**2**). Activation of IFN-αβR results in phosphorylation of JAK1 and Tyk2, which activate STAT1 and STAT2 leading to formation of the heterotrimer ISGF3 (STAT1, STAT2 and IRF-9). Nuclear translocation and promoter binding of ISGF3 upregulates hundreds of different ISG, including IRF-7. (**3**). During a later phase of infection, detection of WNV in MEF also relies on MDA5 and PKR. Recruitment of TRAF3 and TRAF6 activates IRF-3 and IRF-7. NF-κB and ATF-2/c-Jun are also activated via an as yet undefined mechanism. Subsequently, IRF-3, IRF-7, NF-κB, and ATF-2/c-Jun translocate to the nucleus, bind the IFN-β gene promoter and induce optimal transcription. Induction of IFN-α genes occurs through TRAF6 and the transcriptional activation of IRF-7.
doi:10.1371/journal.ppat.1000607.g012

respectively. The TBK1 MEF were obtained from B. TenOever (Mount Sinai Hospital, NY). IRF-$3^{-/-}$× IRF-$7^{-/-}$ DKO mice were generated after large-scale crossing and recombination in the F1 generation because of the 1 cM linkage of the two loci. DKO mice were genotyped and bred in the animal facilities of the Washington University School of Medicine, and experiments were performed with approval of the Washington University Animal Studies Committee. Eight to twelve week-old age-matched mice were used for all in vivo studies. 10^2 PFU of WNV was diluted in Hanks balanced salt solution (HBSS) supplemented with 1% heat-inactivated fetal bovine serum (FBS) and inoculated by footpad injection in a volume of 50 µl.

Tissue viral burden and viremia

To monitor viral dissemination in vivo, mice were infected with 10^2 PFU of WNV by footpad inoculation and sacrificed at specific time points after inoculation. After extensive cardiac perfusion with PBS, organs were harvested, weighed, homogenized and virus was titrated by standard plaque assay as described [71]. Viral burden also was measured by analyzing WNV RNA levels using fluorogenic quantitative RT-PCR (qRT-PCR) as described [13].

Measurement of IFN activity

(a) L929 bioassay. Levels of biologically active IFN in serum were measured using an EMCV L929 cytopathic effect bioassay as described [13]. Results were compared with a standard curve using recombinant mouse IFN-α (PBL Laboratories) and confirmed as IFN-specific using a neutralizing mAb (MAR-1) against the IFN-αβR [72].

(b) IFN-α and β mRNA by qRT-PCR. Total RNA was isolated from uninfected or WNV-infected cells at specific time points using the RNeasy kit (Qiagen). IFN-α and -β mRNA levels were measured by qRT-PCR using previously established primer sets [21]. To analyze the relative fold induction of IFN-α and β

mRNA, 18S rRNA expression levels were determined in parallel for normalization using the Ct method [73].

(c) IFN-α and β ELISA. A commercial capture ELISA kit (PBL Laboratories) was used to measure levels of secreted IFN-α and β protein in supernatants or uninfected or WNV-infected cells.

Primary cell culture and viral infection

(a) Macrophages and dendritic cells. Bone marrow derived Mϕ and conventional mDC were generated as described previously [22]. Briefly, bone marrow cells were isolated from mice and cultured for seven days in the presence of macrophage colony-stimulating factor (M-CSF) (PeproTech, Inc.) to generate Mϕ, or interleukin-4 (IL-4) and granulocyte-macrophage colony-stimulating factor (GM-CSF) (PeproTech, Inc.) to generate mDC. Multi-step viral growth curves were performed after infection at a multiplicity of infection (MOI) of 0.01 for Mϕ or 0.001 for mDC. Supernatants were titrated by plaque assay on BHK21-15 cells. Quantitation of IFN-α and -β mRNA levels in Mϕ and mDC was assessed after infection at a MOI of 0.1.

(b) Fibroblasts. MEF were generated from wild type and deficient 14-day-old embryos and maintained in DMEM supplemented with 10% FBS. Cells were used between passages 2 and 4 for all experiments. Multi-step virus growth curves and IFN-α and β ELISA were performed after infection at an MOI of 0.001 and 0.1, respectively.

(c) Cortical neurons. Primary cortical neurons were prepared from wild type and deficient 15-day-old mouse embryos as described [13]. Cortical neurons were then cultured for four days with Neurobasal medium containing B27 and L-Glutamine (Invitrogen). Multi-step virus growth curves and IFN-α and β protein quantitation were performed after infection at an MOI of 0.001 and 0.1, respectively.

Toll-like receptor stimulation assays

mDC, generated as described above, were stimulated with TLR3 ligand (50 μg/ml poly(I:C)) or TLR4 ligand (2 μg/ml LPS) for 24 hours. Levels of IFN-α mRNA and IFN-β protein were measured by qRT-PCR as described above.

Western blots

Primary cells (10^6) were lysed in RIPA buffer (10 mM Tris, 150 mM NaCl, 0.02% sodium azide, 1% sodium deoxycholate, 1% Triton X-100, 0.1% SDS, pH 7.4), with protease inhibitors (Sigma) and 1 mM okadaic acid (Sigma). Samples (30 μg) were resolved on 10% SDS-polyacrylamide gels. Following transfer, membranes were blocked with 5% non-fat dried milk overnight at 4°C. Membranes were probed with the following panel of monoclonal or polyclonal antibodies anti-WNV (Centers for Disease Control), anti-tubulin, anti-STAT1, anti-PKR, (Santa Cruz Biotechnology), and anti-mouse ISG54 (gift from G. Sen, Cleveland, Ohio). Antibodies specific to RIG-I, MDA5, IRF-3 and IRF-7 have been described [65]. Blots were incubated with peroxidase-conjugated secondary antibodies (Jackson Immunoresearch) and visualized using ECL-Plus Immunoblotting reagents (Amersham Biosciences).

Pharmacological inhibition of NF-κB and p38/ATF-2

To evaluate the role of NF-κB and/or p38/ATF-2 in regulating the IFN-β gene expression in mDC, 2×10^5 cells were infected with WNV and treated with 1% DMSO (diluent control), 5 μM or 10 μM of BAY 11-7082 (Calbiochem) a specific inhibitor of NF-κB and/or 5 μM or 15 μM of SB 202190 (Calbiochem), a specific inhibitor of p38/ATF-2 for 24 h. Levels of IFN-β mRNA were measured by qRT-PCR as described above. As a positive control, 2×10^5 mDC were treated with 2 μg/ml LPS (List Biological Laboratories) for 24 h in the absence or in the presence of BAY 11-7082 and TNF-α production was monitored by ELISA (R&D Systems). Cytotoxicity of BAY 11-7082 and SB 202190 was evaluated using the Celltiter-96® Aqueous One Solution Cell proliferation Assay according to the manufacturer's instructions (Promega).

Statistical analysis

For in vitro experiments, an unpaired two-tailed T-test was used to determine statistically significant differences. For viral burden analysis, differences in log titers were analyzed by the Mann-Whitney test. Kaplan-Meier survival curves were analyzed by the log rank test. All data were analyzed using Prism software (GraphPad Software).

Acknowledgments

We thank M. Noll and K. O'Brien for technical help with generation of the DKO mice and M. Colonna for critical review of the manuscript. We also thank the generosity of our colleagues in obtaining deficient mice (T. Taniguchi) and primary cells (T. Mak, B. TenOever, G. Cheng, and K. Ozato) for these studies.

Author Contributions

Conceived and designed the experiments: SD MSS MG MSD. Performed the experiments: SD MSS KJS. Analyzed the data: SD MSS KJS MG MSD. Wrote the paper: SD MSS MG MSD.

References

1. Koyama S, Ishii KJ, Coban C, Akira S (2008) Innate immune response to viral infection. Cytokine 43: 336–341.
2. Stetson DB, Medzhitov R (2006) Antiviral defense: interferons and beyond. J Exp Med 203: 1837–1841.
3. Stetson DB, Medzhitov R (2006) Type I interferons in host defense. Immunity 25: 373–381.
4. Kumagai Y, Takeuchi O, Akira S (2008) Pathogen recognition by innate receptors. J Infect Chemother 14: 86–92.
5. Takeuchi O, Akira S (2007) Recognition of viruses by innate immunity. Immunol Rev 220: 214–224.
6. Takeuchi O, Akira S (2008) MDA5/RIG-I and virus recognition. Curr Opin Immunol 20: 17–22.
7. Honda K, Takaoka A, Taniguchi T (2006) Type I interferon [corrected] gene induction by the interferon regulatory factor family of transcription factors. Immunity 25: 349–360.
8. Honda K, Yanai H, Takaoka A, Taniguchi T (2005) Regulation of the type I IFN induction: a current view. Int Immunol 17: 1367–1378.
9. Honda K, Taniguchi T (2006) IRFs: master regulators of signalling by Toll-like receptors and cytosolic pattern-recognition receptors. Nat Rev Immunol 6: 644–658.
10. Lenschow DJ, Lai C, Frias-Staheli N, Giannakopoulos NV, Lutz A, et al. (2007) IFN-stimulated gene 15 functions as a critical antiviral molecule against influenza, herpes, and Sindbis viruses. Proc Natl Acad Sci U S A 104: 1371–1376.
11. Degols G, Eldin P, Mechti N (2007) ISG20, an actor of the innate immune response. Biochimie 89: 831–835.
12. Zhang Y, Burke CW, Ryman KD, Klimstra WB (2007) Identification and characterization of interferon-induced proteins that inhibit alphavirus replication. J Virol 81: 11246–11255.
13. Samuel MA, Whitby K, Keller BC, Marri A, Barchet W, et al. (2006) PKR and RNase L contribute to protection against lethal West Nile Virus infection by controlling early viral spread in the periphery and replication in neurons. J Virol 80: 7009–7019.
14. Honda K, Yanai H, Negishi H, Asagiri M, Sato M, et al. (2005) IRF-7 is the master regulator of type-I interferon-dependent immune responses. Nature 434: 772–777.
15. Fredericksen BL, Gale M, Jr. (2006) West Nile virus evades activation of interferon regulatory factor 3 through RIG-I-dependent and -independent pathways without antagonizing host defense signaling. J Virol 80: 2913–2923.
16. Fredericksen BL, Keller BC, Fornek J, Katze MG, Gale M, Jr. (2008) Establishment and maintenance of the innate antiviral response to West Nile

Virus involves both RIG-I and MDA5 signaling through IPS-1. J Virol 82: 609–616.
17. Daffis S, Samuel MA, Suthar MS, Gale M, Jr., Diamond MS (2008) Toll-like receptor 3 has a protective role against West Nile virus infection. J Virol 82: 10349–10358.
18. Town T, Bai F, Wang T, Kaplan AT, Qian F, et al. (2009) Toll-like Receptor 7 Mitigates Lethal West Nile Encephalitis via Interleukin 23-Dependent Immune Cell Infiltration and Homing. Immunity 30: 242–253.
19. Wang JP, Liu P, Latz E, Golenbock DT, Finberg RW, et al. (2006) Flavivirus activation of plasmacytoid dendritic cells delineates key elements of TLR7 signaling beyond endosomal recognition. J Immunol 177: 7114–7121.
20. Querec T, Bennouna S, Alkan S, Laouar Y, Gorden K, et al. (2006) Yellow fever vaccine YF-17D activates multiple dendritic cell subsets via TLR2, 7, 8, and 9 to stimulate polyvalent immunity. J Exp Med 203: 413–424.
21. Daffis S, Samuel MA, Keller BC, Gale M, Jr., Diamond MS (2007) Cell-specific IRF-3 responses protect against West Nile virus infection by interferon-dependent and -independent mechanisms. PLoS Pathog 3: e106. doi:10.1371/journal.ppat.0030106.
22. Daffis S, Samuel MA, Suthar MS, Keller BC, Gale M, Jr., et al. (2008) Interferon regulatory factor IRF-7 induces the antiviral alpha interferon response and protects against lethal West Nile virus infection. J Virol 82: 8465–8475.
23. Panne D (2008) The enhanceosome. Curr Opin Struct Biol 18: 236–242.
24. Panne D, Maniatis T, Harrison SC (2007) An atomic model of the interferon-beta enhanceosome. Cell 129: 1111–1123.
25. Thanos D, Maniatis T (1995) Virus induction of human IFN beta gene expression requires the assembly of an enhanceosome. Cell 83: 1091–1100.
26. Samuel MA, Diamond MS (2005) Alpha/beta interferon protects against lethal West Nile virus infection by restricting cellular tropism and enhancing neuronal survival. J Virol 79: 13350–13361.
27. Bourne N, Scholle F, Silva MC, Rossi SL, Dewsbury N, et al. (2007) Early production of type I interferon during West Nile virus infection: role for lymphoid tissues in IRF3-independent interferon production. J Virol 81: 9100–9108.
28. Steinberg C, Eisenacher K, Gross O, Reindl W, Schmitz F, et al. (2009) The IFN regulatory factor 7-dependent type I IFN response is not essential for early resistance against murine cytomegalovirus infection. Eur J Immunol 39: 1007–1018.
29. Marie I, Durbin JE, Levy DE (1998) Differential viral induction of distinct interferon-alpha genes by positive feedback through interferon regulatory factor-7. Embo J 17: 6660–6669.
30. Sato M, Hata N, Asagiri M, Nakaya T, Taniguchi T, et al. (1998) Positive feedback regulation of type I IFN genes by the IFN-inducible transcription factor IRF-7. FEBS Lett 441: 106–110.
31. Samuel MA, Diamond MS (2006) Pathogenesis of West Nile Virus infection: a balance between virulence, innate and adaptive immunity, and viral evasion. J Virol 80: 9349–9360.
32. Davis LE, DeBiasi R, Goade DE, Haaland KY, Harrington JA, et al. (2006) West Nile virus neuroinvasive disease. Ann Neurol 60: 286–300.
33. Martina BE, Koraka P, van den Doel P, Rimmelzwaan GF, Haagmans BL, et al. (2008) DC-SIGN enhances infection of cells with glycosylated West Nile virus in vitro and virus replication in human dendritic cells induces production of IFN-alpha and TNF-alpha. Virus Res 135: 64–71.
34. Hildner K, Edelson BT, Purtha WE, Diamond M, Matsushita H, et al. (2008) Batf3 deficiency reveals a critical role for CD8alpha+ dendritic cells in cytotoxic T cell immunity. Science 322: 1097–1100.
35. Schmitz F, Heit A, Guggemoos S, Krug A, Mages J, et al. (2007) Interferon-regulatory-factor 1 controls Toll-like receptor 9-mediated IFN-beta production in myeloid dendritic cells. Eur J Immunol 37: 315–327.
36. Tailor P, Tamura T, Kong HJ, Kubota T, Kubota M, et al. (2007) The feedback phase of type I interferon induction in dendritic cells requires interferon regulatory factor 8. Immunity 27: 228–239.
37. Sato M, Suemori H, Hata N, Asagiri M, Ogasawara K, et al. (2000) Distinct and essential roles of transcription factors IRF-3 and IRF-7 in response to viruses for IFN-alpha/beta gene induction. Immunity 13: 539–548.
38. Paun A, Reinert JT, Jiang Z, Medin C, Balkhi MY, et al. (2008) Functional characterization of murine interferon regulatory factor 5 (IRF-5) and its role in the innate antiviral response. J Biol Chem 283: 14295–14308.
39. Schoenemeyer A, Barnes BJ, Mancl ME, Latz E, Goutagny N, et al. (2005) The interferon regulatory factor, IRF5, is a central mediator of toll-like receptor 7 signaling. J Biol Chem 280: 17005–17012.
40. Barnes BJ, Moore PA, Pitha PM (2001) Virus-specific activation of a novel interferon regulatory factor, IRF-5, results in the induction of distinct interferon alpha genes. J Biol Chem 276: 23382–23390.
41. Takaoka A, Yanai H, Kondo S, Duncan G, Negishi H, et al. (2005) Integral role of IRF-5 in the gene induction programme activated by Toll-like receptors. Nature 434: 243–249.
42. Yanai H, Chen HM, Inuzuka T, Kondo S, Mak TW, et al. (2007) Role of IFN regulatory factor 5 transcription factor in antiviral immunity and tumor suppression. Proc Natl Acad Sci U S A 104: 3402–3407.
43. Kamthong PJ, Wu M (2001) Inhibitor of nuclear factor-kappaB induction by cAMP antagonizes interleukin-1-induced human macrophage-colony-stimulating-factor expression. Biochem J 356: 525–530.
44. Lappas M, Yee K, Permezel M, Rice GE (2005) Sulfasalazine and BAY 11-7082 interfere with the nuclear factor-kappa B and I kappa B kinase pathway to regulate the release of proinflammatory cytokines from human adipose tissue and skeletal muscle in vitro. Endocrinology 146: 1491–1497.
45. Ashwell JD (2006) The many paths to p38 mitogen-activated protein kinase activation in the immune system. Nat Rev Immunol 6: 532–540.
46. Kaisho T, Takeuchi O, Kawai T, Hoshino K, Akira S (2001) Endotoxin-induced maturation of MyD88-deficient dendritic cells. J Immunol 166: 5688–5694.
47. Liu H, Sidiropoulos P, Song G, Pagliari LJ, Birrer MJ, et al. (2000) TNF-alpha gene expression in macrophages: regulation by NF-kappa B is independent of c-Jun or C/EBP beta. J Immunol 164: 4277–4285.
48. Saha SK, Pietras EM, He JQ, Kang JR, Liu SY, et al. (2006) Regulation of antiviral responses by a direct and specific interaction between TRAF3 and Cardif. Embo J 25: 3257–3263.
49. Oganesyan G, Saha SK, Guo B, He JQ, Shahangian A, et al. (2006) Critical role of TRAF3 in the Toll-like receptor-dependent and -independent antiviral response. Nature 439: 208–211.
50. Xu Y, Cheng G, Baltimore D (1996) Targeted disruption of TRAF3 leads to postnatal lethality and defective T-dependent immune responses. Immunity 5: 407–415.
51. Bonnard M, Mirtsos C, Suzuki S, Graham K, Huang J, et al. (2000) Deficiency of T2K leads to apoptotic liver degeneration and impaired NF-kappaB-dependent gene transcription. Embo J 19: 4976–4985.
52. Yoshida R, Takaesu G, Yoshida H, Okamoto F, Yoshioka T, et al. (2008) TRAF6 and MEKK1 play a pivotal role in the RIG-I-like helicase antiviral pathway. J Biol Chem 283: 36211–36220.
53. Asselin-Paturel C, Trinchieri G (2005) Production of type I interferons: plasmacytoid dendritic cells and beyond. J Exp Med 202: 461–465.
54. Liu YJ (2005) IPC: professional type 1 interferon-producing cells and plasmacytoid dendritic cell precursors. Annu Rev Immunol 23: 275–306.
55. Diebold SS, Kaisho T, Hemmi H, Akira S, Reis e Sousa C (2004) Innate antiviral responses by means of TLR7-mediated recognition of single-stranded RNA. Science 303: 1529–1531.
56. Matsuyama T, Kimura T, Kitagawa M, Pfeffer K, Kawakami T, et al. (1993) Targeted disruption of IRF-1 or IRF-2 results in abnormal type I IFN gene induction and aberrant lymphocyte development. Cell 75: 83–97.
57. Ruffner H, Reis LF, Naf D, Weissmann C (1993) Induction of type I interferon genes and interferon-inducible genes in embryonal stem cells devoid of interferon regulatory factor 1. Proc Natl Acad Sci U S A 90: 11503–11507.
58. Tailor P, Tamura T, Ozato K (2006) IRF family proteins and type I interferon induction in dendritic cells. Cell Res 16: 134–140.
59. Honda K, Mizutani T, Taniguchi T (2004) Negative regulation of IFN-alpha/beta signaling by IFN regulatory factor 2 for homeostatic development of dendritic cells. Proc Natl Acad Sci U S A 101: 2416–2421.
60. Negishi H, Ohba Y, Yanai H, Takaoka A, Honma K, et al. (2005) Negative regulation of Toll-like-receptor signaling by IRF-4. Proc Natl Acad Sci U S A 102: 15989–15994.
61. Richez C, Yasuda K, Watkins AA, Akira S, Lafyatis R, et al. (2009) TLR4 ligands induce IFN-alpha production by mouse conventional dendritic cells and human monocytes after IFN-beta priming. J Immunol 182: 820–828.
62. Yasuda K, Richez C, Maciaszek JW, Agrawal N, Akira S, et al. (2007) Murine dendritic cell type I IFN production induced by human IgG-RNA immune complexes is IFN regulatory factor (IRF)5 and IRF7 dependent and is required for IL-6 production. J Immunol 178: 6876–6885.
63. Pandey AK, Yang Y, Jiang Z, Fortune SM, Coulombe F, et al. (2009) NOD2, RIP2 and IRF5 play a critical role in the type I interferon response to Mycobacterium tuberculosis. PLoS Pathog 5: e1000500. doi:10.1371/journal.ppat.1000500.
64. Kumar H, Kawai T, Kato H, Sato S, Takahashi K, et al. (2006) Essential role of IPS-1 in innate immune responses against RNA viruses. J Exp Med 203: 1795–1803.
65. Loo YM, Fornek J, Crochet N, Bajwa G, Perwitasari O, et al. (2008) Distinct RIG-I and MDA5 signaling by RNA viruses in innate immunity. J Virol 82: 335–345.
66. Koyama S, Ishii KJ, Kumar H, Tanimoto T, Coban C, et al. (2007) Differential role of TLR- and RLR-signaling in the immune responses to influenza A virus infection and vaccination. J Immunol 179: 4711–4720.
67. Chang TH, Liao CL, Lin YL (2006) Flavivirus induces interferon-beta gene expression through a pathway involving RIG-I-dependent IRF-3 and PI3K-dependent NF-kappaB activation. Microbes Infect 8: 157–171.
68. Gitlin L, Barchet W, Gilfillan S, Cella M, Beutler B, et al. (2006) Essential role of mda-5 in type I IFN responses to polyriboinosinic:polyribocytidylic acid and encephalomyocarditis picornavirus. Proc Natl Acad Sci U S A 103: 8459–8464.
69. Perry AK, Chow EK, Goodnough JB, Yeh WC, Cheng G (2004) Differential requirement for TANK-binding kinase-1 in type I interferon responses to toll-like receptor activation and viral infection. J Exp Med 199: 1651–1658.
70. Ebel GD, Dupuis AP, 2nd, Ngo K, Nicholas D, Kauffman E, et al. (2001) Partial genetic characterization of West Nile virus strains, New York State, 2000. Emerg Infect Dis 7: 650–653.
71. Diamond MS, Shrestha B, Marri A, Mahan D, Engle M (2003) B cells and antibody play critical roles in the immediate defense of disseminated infection by West Nile encephalitis virus. J Virol 77: 2578–2586.

72. Sheehan KC, Lai KS, Dunn GP, Bruce AT, Diamond MS, et al. (2006) Blocking monoclonal antibodies specific for mouse IFN-alpha/beta receptor subunit 1 (IFNAR-1) from mice immunized by in vivo hydrodynamic transfection. J Interferon Cytokine Res 26: 804–819.

73. Livak KJ, Schmittgen TD (2001) Analysis of relative gene expression data using real-time quantitative PCR and the 2(−Delta Delta C(T)) Method. Methods 25: 402–408.